Faculty of Engineering

Image Reconstruction Based on Combination of Inverse Scattering Technique and Total Variation Regularization Method

Nor Haizan Binti Jamali

Master of Engineering
2020

Image Reconstruction Based on Combination of Inverse Scattering Technique and Total Variation Regularization Method

Nor Haizan Binti Jamali

A thesis submitted

In fulfilment of the requirements for the degree of Master of Engineering

(Electronics Engineering)

Faculty of Engineering
UNIVERSITI MALAYSIA SARAWAK
2020

DECLARATION

I declare that the work in this thesis was carried out in accordance with the regulations of Universiti Malaysia Sarawak. Except where due acknowledgements have been made, the work is that of the author alone. The thesis has not been accepted for any degree and is not concurrently submitted in candidature of any other degree.

……

Signature

Name: Nor Haizan Binti Jamali

Matric No.: 15020056

Faculty of Engineering

Universiti Malaysia Sarawak

Date :

ACKNOWLEDGMENT

It is apparent that the progress and development of this project needs the support of many people. First of all, I would like to thank my supervisor behind the development of this research, Assoc. Prof. Ir. Dr Kismet Anak Hong Ping, and my co-supervisors, Dr Shafrida Binti Sahrani and Dr Dayang Azra Binti Awang Mat.

I would also like to thank my beloved family and friends for their love, care and support during my studies in Universiti Malaysia Sarawak. Lastly, thanks to all the lecturers and staffs of Electrical and Electronics (Telecommunication) Engineering Programme, Universiti Malaysia Sarawak.

Thank you very much.

ABSTRACT

In this research, Total Variation (TV) regularization method was incorporated with the Forward-Backward Time-Stepping (FBTS) algorithm to deal with the ill-posedness of the inverse scattering problem in the time domain. The effectiveness between FBTS without and with regularization method is compared and analyzed by numerical simulations and calculation of Mean Square Error (MSE). Finite-Difference Time-Domain (FDTD) scheme is used to calculate the inverse scattering signals in forward time-stepping and adjoint field in backward time-stepping to reconstruct the microwave properties. The Forward-Backward Time-Stepping - Total Variation (FBTS-TV) regularization algorithm is in a two-dimensional case and implemented in C++ language executed in single computing. The FBTS-TV regularization method shows a good performance of reconstructing relative permittivity and conductivity profiles of the unknown embedded object for its size, shape, and location. The image reconstruction in enhanced by smoothing irregular contours while preserved the edges, and hence produced a better estimation of the image's boundaries. A distinct improvement is shown in the reconstruction of the object's relative permittivity. In the case of reconstruction of a simple object for relative permittivity, FBTS-TV improved the FBTS algorithm by 15%.

Keywords: Inverse scattering, image reconstruction, microwave imaging, regularization, total variation regularization.

Pengimejan Berdasarkan Gabungan Kaedah Songsang Berselerak Bersama Kaedah Penyusunan Jumlah Variasi

ABSTRAK

Dalam kajian ini, kaedah penyusunan Total Variation (TV) *telah digabungkan bersama* Forward-Backward Time-Stepping (FBTS) *dalam lapangan masa bagi menangani masalah ketidaksempurnaan di dalam kaedah songsang berselerak. Keberkesanan kaedah* FBTS *tanpa dan dengan gabungan kaedah penyusunan telah dibandingkan serta dianalisis melalui kaedah simulasi berangka serta pengiraan ralat min kuasa dua. Teknik* Finite-Difference Time-Domain (FDTD) *digunakan bagi penggiraan isyarat tuju serta isyarat serakan dalam proses pengimejan. Algoritma bagi gabungan kaedah tersebut,* Forward-Backward Time-Stepping - Total Variation (FBTS-TV) *adalah dalam bentuk dua dimensi dan diprogramkan di dalam bahasa pengaturcaraan C++ menggunakan jenis pengkomputeran tunggal. Kaedah* FBTS-TV *telah menunjukkan prestasi yang baik dalam pembinaan semula sifat-sifat dielektrik gelombang mikro bagi objek yang tidak diketahui mengikut saiz, bentuk dan lokasinya. Mutu pengimejan telah ditingkatkan dengan melicinkan permukaan kontur yang menggerutu, sementara memelihara kawasan pinggir, dan disebabkan itu, sempadan imej dapat dianggarkan dengan lebih baik. Penambahbaikan yang jelas telah ditunjukkan bagi pembinaan semula objek dalam keterusan elektrikal. Bagi kes pembinaan semula sebuah objek mudah dalam keterusan elektrikal, kaedah* FBTS-TV *telah memberikan peningkatan sebanyak 15% berbanding kaedah* FBTS.

Kata kunci: *Kaedah penyusunan, kaedah penyusunan* Total Variation, *kaedah songsang berselerak, pembinaan semula imej*, *pengimejan gelombang mikro*.

TABLE OF CONTENTS

LIST OF TABLES

LIST OF FIGURES

LIST OF ABBREVIATIONS

ABC	Absorbing Boundary Condition
CPML	Convolutional Perfectly Matched Layer
CT	Computerized Tomography
FBTS	Forward-Backward Time-Stepping
FDTD	Finite-Difference Time-Domain
GSV	Generalized Cross-Validation
MRI	Magnetic Resonance Imaging
NDT&E	Non-Destructive Testing and Evaluation
OGG	Overset Grid Generation
PEC	Pulsed Eddy Current
PET	Positron Emission Tomography
PML	Perfectly Matched Layer
ROF	Rudin-Osher-Fatemi
SAR	Synthetic Aperture Radar
SVD	Singular-Value Decomposition
TSVD	Truncated Singular Value Decomposition
TV	Total Variation
TV	Total Variation
UAV	Unmanned Aerial Vehicle

CHAPTER 1

INTRODUCTION

1.1 Overview

Microwave imaging is a technique used to sense objects by means of analyzing microwave signals. Extensive researches have been conducted on microwave imaging and it had proven its potential utility and effectiveness for a wide range of applications such as in medical imaging, remote sensing of earth, and non-destructive testing and evaluation. For example, in remote sensing, Synthetic Aperture Radar (SAR); form of a radar system, has the capability to produce a high-resolution imagery of bio and the geophysical parameter of the Earth's surface [1-3]. Remote sensing also applied for forest biomass mapping [4], monitoring global land surface phenology [5] and mapping natural hazard and disaster [6].

In Non-Destructive Testing and Evaluation (NDT & E), high-frequency electromagnetic energy is utilized to determine material characterization and its structural integrity. Pulsed Eddy Current (PEC) is among the popular technique applied in NDT & E due to its effectiveness of quantifying defects in multilayer structures. Some applications involving NDT & E are identifying hidden defect characterization in some complex structures [7], and defect detection of riveted structures of aging aircraft [8].

Microwave imaging applications for medical purposes had pulled a great attention and continuously investigated by the researchers. Medical imaging is the visualization of a biological system for clinical diagnosis and medical intervention proposes. Medical imaging modalities examples are X-ray, Ultrasound, Computerized Tomography (CT), Positron Emission Tomography (PET) and Magnetic Resonance Imaging (MRI).

In microwave tomography, transmitting antenna is used to illuminate the biological part in microwave region and the scattered field data are then collected by receiving antennas. The scattered field information will be processed and analyzed to reconstruct the dielectric properties of the biological part. The dielectric properties concern is the relative permittivity, ε_r, the capacitance of a unit volume of matter and conductivity, σ, the conductivity of a unit volume of matter. Microwave tomography can be obtained through single-frequency, multi-frequency or time domain method [9-11]. Microwave tomography is preferable method compared to other conventional medical imaging modalities due to its non-ionizing detection, more comfortable for patients, inexpensive, no side effect for human body and potentially increases the sensitivity of cancer detection [12].

Recently, there is a positive growth in research on medical tomography for cancer detection due to the significant contrast of dielectric properties of healthy and malignant or abnormalities tissue at microwave frequencies. For the similar reason, a group of researchers focuses on microwave imaging technique for breast cancer detection [13-17]. Takenaka et al. [18] introduced Forward-Backward Time-Stepping (FBTS) to solve electromagnetic inverse scattering problems in the time domain. Time domain method in FBTS means allowing a broad spectrum of frequencies to be utilized in a single optimization, thus, this method will give more useful quantitative information of electrical parameter profiles and increase in accuracy for the reconstructed images. FBTS has shown a strong ability to reconstruct images providing the electrical properties of the objects together with its size, shape, a position of the scatters or objects. In recent studies, the reconstructed of breast imagery with FBTS technique had shown a significant disparity of the dielectric properties in which enabling the differentiation and recognition of normal and abnormal breast tissue.

It is reported that FBTS technique capable of detecting as small as 4 mm malignant tumor in its reconstructed image [19].

Another advancement of FBTS is a reconstruction of breast imagery in three-dimensional forms [20], and incorporating low pass filter with several cut-off frequencies in the FBTS algorithm to avoid nonlinearity problem [21].

In many cases, inverse problems are ill-posed due to noise in measurement data which cause misinterpretations of the solution. Ill-posed problems can be handled either by incorporating a priori information through the use of transformation or by applying appropriate numerical methods, called regularization techniques [22]. Regularization method can be applied to improve the conditioning and determine a useful approximation of the actual reconstruction image.

Some of the commonly known and used methods of regularization are Singular-Value Decomposition (SVD) as in [23-25], and Tikhonov regularization as in [26-27]. SVD and Tikhonov's regularization perform successfully in image enhancement, noise removal, and deblurring, however, these types of regularization tend to produce smoothed or over-smoothed solution which eliminates sharpness at object boundaries on the resulting solution.

The Total Variation (TV) regularization method was introduced by Rudin, Osher and Fatemi in [28], is a constrained optimization type of numerical method for image denoising while preserved the edge information. Unlike other conventional smoothing filters that have a greater tendency to blur the discontinuities, TV regularization is well suited for edge-preserving as it is not discriminating against smoothness in an image and tends to preserve edges of the reconstructed image [29]. Due to efficacy and robustness of TV regularization method, it has been considered to be utilized in image denoising, deblurring, inpainting, edge-preserving, and restoration. TV regularization method has been applied in image

denoising [30], reconstruction for images that missing some pixels due to impulsive noise [31], and reconstruction of super-resolution images [32]. There are also researches on a combination of regularization methods, for example, hybrid of Tikhonov and TV regularization method in [33-34] to compensate both methods' weaknesses thus improving the outcome.

1.2 Problem Statement

Breast imaging with FBTS had shown a great success due to its ability to determine and reconstruct images by providing useful quantitative information about the size, location, shape and the internal composition of the backscatters or objects in a test area [18-21]. FBTS shown the potential to detect malignancy and assessed internal compositions in a breast model [35]. A good and stable image reconstruction will aid in better medical analysis and diagnosis [14-15].

FBTS, an inverse scattering method in time domain is utilizing an iterative scheme based on conjugate gradient method, which is updating simultaneously the unknown field in the scattering domain and the unknown material contrast by minimizing a cost functional at each iteration [18]. The process of developing the reconstruction of the electrical properties is dependent greatly on its quantitative information produced by the calculation of error between the measured and simulated scattering field data. FBTS has strong non-linearity and ill-posed in nature causes the algorithm to get trapped in a local minimum leading to false estimation. False estimation in the scattering data calculation will give negative impact in the reconstruction output such as distortion and irregularities in the reconstructed images. A regularization method is needed to improve the quality and stability of the FBTS algorithm [35].

Ill-posed problems can be handled either by incorporating a priori information through the use of transformation or by incorporating an appropriate numerical method, called regularization method [36]. The regularization method will give constraints on the reconstructed image that lead to more accurate estimation. In this research, the Total Variation (TV) regularization scheme will be incorporated in the FBTS inverse scattering algorithm to improve the reconstructed image by giving information such as its shapes and location, smoothing the uninterested structures, and reconstructing sharp edges in the enclosed region that should give a better estimation of the image's boundaries.

1.3 Objectives

The goal of this research is to develop a low cost and safe microwave imaging system that detect the presence of objects buried in inhomogeneous medium and also to identify the electric properties of the objects. The project will involve the following objectives:

a) To formulate edge preserving with Total Variation (TV) regularization method.
b) To analyze the effect of Total Variation Regularization with different parameter settings such as regularization parameter, number of antenna, and center frequency.
c) To incorporate the Total Variation Regularization scheme with the time-domain inverse scattering technique for edge-preserving image reconstruction.

1.4 Scope of Project

This research was conducted to investigate and formulate Total Variation Regularization, which is one of a regularization method, and incorporated it with FBTS in two-dimensional transverse magnetic case, in order to improve the quality of the

reconstructed image. It is assumed that the media is nondispersive with constant permittivity and conductivity over changes in frequency.

Thus, the study is conducted for less complex reconstruction algorithm which is for two electrical profile parameters of relative permittivity, ε_r , and conductivity, σ. For the reconstructed image, it is assumed that the position, shape, and size of the object could be detected. The research will consider free space as background medium. The development of numerical simulation is completed using the C++ programming language in single computing, while the demonstration of the obtained data is accomplished by MATLAB R2010a software. Besides that, the study aims to determine the effect of Total Variation Regularization with different parameter settings such as scaling, orientation, and central frequencies.

1.5 Thesis Outline

Chapter 1 presents the introductory statements of the study that include a brief introduction to the research, problem statements, objectives, and scopes of this research.

Chapter 2 describes the research of related literature and studies such as microwave imaging system, Maxwell's equation, the Forward-Backward Time-Stepping, the Finite-Difference Time-Domain, ill-posed problem in image reconstruction, and regularization method in image reconstruction such as the Truncated Singular Value Decomposition, Tikhonov Regularization and Total Variation Regularization.

Chapter 3 provides explanations of methods to be use in this research, which include Forward-Backward Time-Stepping method, and TV regularization method to be utilize in this research.

Chapter 4 presents and discusses the findings of numerical experiments, which demonstrate the performance of the method proposed. The comparison of reconstruction of a simple object with and without regularization presented. Furthermore, the efficacy simple object reconstructed tested for a higher optimization and the impact of utilizing different regularization parameter value has been evaluated. Reconstructions of a simple object with multiple configurations of antennas are tested and analyzed for its performance. Besides that, reconstruction of multiple circular and square shape objects with varying sizes has been studied and presented. MSE statistic used for measuring the method effectiveness.

Chapter 5 concludes the whole research and provides some recommendations for future works and improvement of this research.

CHAPTER 2

LITERATURE REVIEW

2.1 Microwave Imaging

Microwave imaging is a continually evolving science to estimate hidden or embedded objects in a structure or media with the usage of electromagnetic information in the microwave regime. Researchers in microwave imaging always make used of numerical modeling and hardware to improve its detection of the embedded object. The information on electromagnetic properties is acquired by measuring scattered electric field via transceivers. The analysis of the electric field permits the location and identification of the unknown objects. Microwave imaging has a huge potential for a wide range of applications such as in remote sensing of the earth [1-4], biomedical imaging and diagnostic [13-17], non-destructive testing and evaluation [7-8], underground surveillance [37], and through-wall imaging [38].

One of the microwaves imaging application is in remote sensing. Remote sensing is a great tool to observe the earth due to its capability to operate unmanned and durability to be under any weather circumstances for day or night. The radiated electromagnetic energy from its transmitting antenna will focus on a target. As the electromagnetic energy hit the target, it will be reflected or create backscatter in which are detected by the receiving antenna. The received electromagnetic energy of the target will be analyzed and observed via signal processing [1-2].

In Synthetic Aperture Radar (SAR), it synthesizes a large aperture antenna from the antenna scanning. A miniature SAR system operated on a small dimension of Unmanned Aerial Vehicle (UAV) platform that generating 5m x 5m spatial resolutions has been

reported in [3]. Several techniques have been applied to improve the performance and efficacy of the SAR such as adding filter-based deconvolution [39], advancement in signal processing technique [40] and enhanced target discrimination algorithm [41].

In [39], two SAR based methods, piecewise and wiener filter were introduced to improve the conventional SAR imaging in term of images' focus and object's position inside of layered structures. In [40], Orthogonal Matching Pursuit is incorporated with compressed sensing algorithm to reduce the computational time and providing a high resolution images. In [41], the proposed method had shown a good performance for discriminating between target and the clutter in SAR images while improving the K-center one-class classification based on Hausdorff distance measurement.

Near-field method always related to biomedical imaging due to the evidence of dielectric contrast to detect and differentiate anomalies in the human body. The purpose of medical imaging is to reconstruct the spatial distribution of the dielectric properties of the interested domain. An electromagnetic source is used to illuminate an unknown material, and then the totals of the scattering field are measured and are inverted to determine its shape, location, and size. The inverse scattering problem is a nonlinear problem due to nonlinearity function of the scattering properties.

Biomedical imaging produces the visualization of a biological system for clinical diagnosis and medical intervention proposes. It modalities include X-ray, Ultrasound, Computerized Tomography (CT), Positron Emission Tomography (PET) and Magnetic Resonance Imaging (MRI). Recently there has been renewed interest in breast cancer detection [13-17]. The sensing of the breast cancer is possible due to the significant contrast of dielectric properties of healthy and malignant or abnormalities tissue at microwave frequencies.

Figure 2.1 shows the classification of the biomedical imaging system of active, passive and hybrid methods. In passive microwave imaging, the received power level or energy from the object is used to build up the microwave image of the respected environment. In an active microwave imaging, the biological object is detected by probing it with an electromagnetic radiation. The electromagnetic radiation will illuminate the object and with the measured scattered radiation, an estimated image of the internal dielectric properties can be gained. Active microwave imaging divided into microscopy and tomography. Unlike in active microwave imaging, the hybrid methods measure the heated biological object by detecting the scattered radiation through ultrasound transducers. Hybrid method can be classified into microwave with thermal acoustic and microwave with ultrasound.

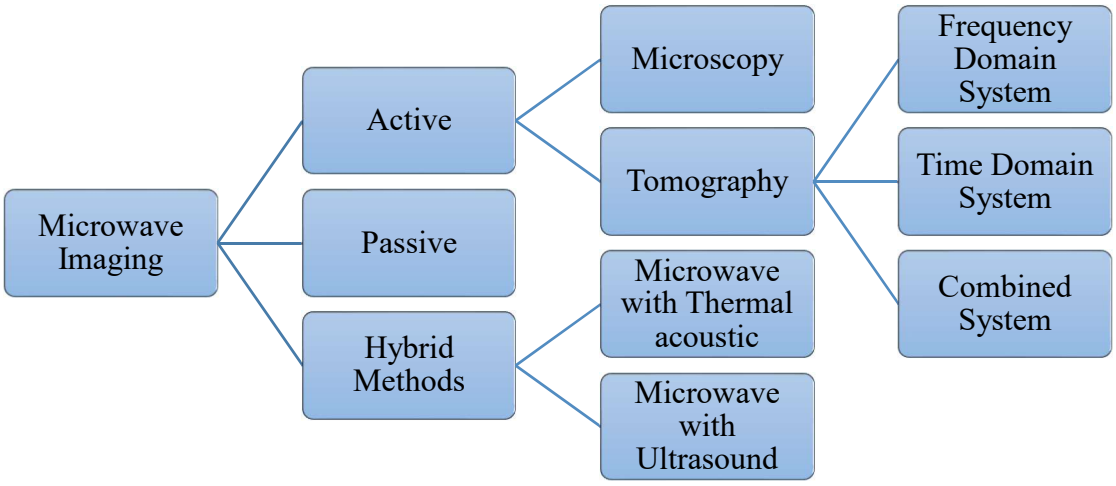

Figure 2.1: Biomedical Imaging System [42]

There are two main methods to tomography, the frequency domain, and time domain. In the frequency domain, the estimated detection of an object is evaluated according to the progression to the response of different frequencies while in the time domain, the progression is evaluated according to the state of time. The tomography in frequency domain

requires less imaging hardware and lower computational power than in time domain. However, the advantage of time domain over frequency domain is the measurement in time domain covers a large frequency band which, provide more information of the objects and therefore will produce a better reconstruction [10].

Studies in [43] shown that microwave imaging in the time domain has the advantages over frequency domain in deep-tissue fluorescence imaging of turbid media, in which it gives the better distinction of the reconstruction of the target under test. Data acquisition in time domain analysis is reported more feasible [44] and it gives higher efficiencies than in the frequency domain [45].

2.2 Maxwell's Equations

James Clerk Maxwell was first to determine the speed of propagation of electromagnetic waves is the same as the speed of light. Maxwell took a set of known experimental laws such as Faraday's Law and Ampere's Law and incorporated them into a symmetric coherent set of equations known as Maxwell's Equations.

Maxwell's equations represent the basic ways to state the fundamentals of electricity and magnetism. A flow of current will produce a magnetic field. A varies in current flow influence the magnetic field which also gives rise to an electric field. Electromagnetic waves can be demonstrated in time domain form or frequency domain form.

Figure 2.2 shows an electromagnetic wave composed of oscillating magnetic and electric fields. The electric field and magnetic field of an electromagnetic wave are perpendicular to each other and to the direction of the wave. In vacuum, the electromagnetic wave travel with a constant velocity of 3×10^8 ms^{-1}.

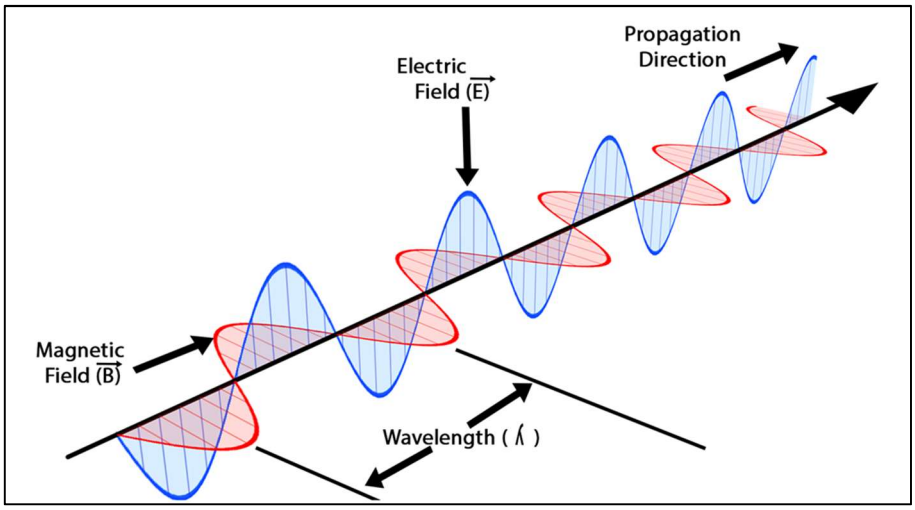

Figure 2.2: Electromagnetic Wave [46]

2.2.1 Time Domain Form

This research considering time domain form modeling, thus the differential equations or time-varying Maxwell's equations are shown as below. Common Maxwell's equation for the differential form of Faraday's Law, Ampere-Maxwell's equation, Gauss's Law for the electric field and magnetic field, respectively [47]:

$$\nabla \times \boldsymbol{E}(t) = -\frac{\partial \boldsymbol{B}(t)}{\partial t} \tag{2.1}$$

$$\nabla \times \boldsymbol{H}(t) = \boldsymbol{J}(t) + \frac{\partial \boldsymbol{D}(t)}{\partial t} \tag{2.2}$$

$$\nabla \cdot \boldsymbol{D}(t) = \rho(t) \tag{2.3}$$

$$\nabla \cdot \boldsymbol{B}(t) = 0 \tag{2.4}$$

where

$\boldsymbol{E}$: Electric field (Volts/meter)

$\boldsymbol{B}$: Magnetic flux density (Webers/meter^2)

$\boldsymbol{H}$: Magnetic field (Amperes/meter)

$\boldsymbol{J}$: Electric current density (Amperes/meter^2)

$\boldsymbol{D}$: Electric flux density (Coulombs/meter^2)

ρ : Electric charge density (Coulomb/m^3)

The relation of electric and magnetic flux densities, $\boldsymbol{D}$ and $\boldsymbol{B}$ to the field intensities $\boldsymbol{E}$ and $\boldsymbol{H}$ can be shown by the simplest form of constitutive relationships as shown in Equation (2.5) to (2.7) [47].

$$\boldsymbol{J}(t) = \sigma(t) \cdot \boldsymbol{E}(t) \tag{2.5}$$

$$\boldsymbol{D}(t) = \varepsilon(t) \cdot \boldsymbol{E}(t) \tag{2.6}$$

$$\boldsymbol{B}(t) = \mu(t) \cdot \boldsymbol{H}(t) \tag{2.7}$$

where

ε : Electrical permittivity (Farads/meter)

μ : Magnetic permeability (Henrys/meter)

σ : Electric conductivity (Siemens/meter)

2.2.2 Frequency Domain Form

The mathematical expression for frequency domain form modelling can be simplified by reducing convolutions to simple expression through transformation of Equation (2.1) to (2.7). The differential form of Faraday's Law, Ampere-Maxwell's equation, Gauss's Law for the electric field and magnetic field in frequency domain, respectively [47]:

$$\nabla \times \boldsymbol{E} = -j\omega \boldsymbol{B} \tag{2.8}$$

$$\nabla \times \boldsymbol{H} = \boldsymbol{J} + j\omega \boldsymbol{D} \tag{2.9}$$

$$\nabla \cdot \boldsymbol{D} = \rho \tag{2.10}$$

$$\nabla \cdot \boldsymbol{B} = 0 \tag{2.11}$$

as well as the three constitutive relationships:

$$\boldsymbol{J}(t) = \sigma \boldsymbol{E} \tag{2.12}$$

$$\boldsymbol{D}(t) = \varepsilon \boldsymbol{E} \tag{2.13}$$

$$\boldsymbol{B}(t) = \mu \boldsymbol{H} \tag{2.14}$$

By substituting Equation (2.12) to (2.14) into Equation (2.9) to (2.11), the new differential forms of Faraday's Law, Ampere-Maxwell's equation, Gauss's Law for the electric field and magnetic field in frequency domain are as follows.

$$\nabla \times \boldsymbol{E} = -j\omega\mu \boldsymbol{H} \tag{2.15}$$

$$\nabla \times \boldsymbol{H} = \sigma \boldsymbol{E} + j\omega\varepsilon \boldsymbol{E} \tag{2.16}$$

$$\nabla \cdot \boldsymbol{D} = \nabla \cdot \varepsilon \boldsymbol{E} = \rho \tag{2.17}$$

$$\nabla \cdot \boldsymbol{B} = \nabla \cdot \mu \boldsymbol{H} = 0 \tag{2.18}$$

2.3 Forward-Backward Time-Stepping (FBTS)

The Forward-Backward Time-Stepping (FBTS) was first introduced by Takenaka et al. [18] is a method of microwave imaging to solve the inverse scattering problem in the time domain. Previous studies of FBTS have shown that the method is applicable to medical imaging such as in breast cancer detection. In [19-20], [26], [48], and [55], FBTS method

has been utilized to reconstruct breast composition and differentiate the contrast between normal and malignant breast tissue.

A simple case of one-dimensional reconstruction has been reported in [49], the case has been extended to a two-dimensional reconstruction as mentioned in [19] and [48]. Further addition of the case is in three-dimensional reconstruction as reported in [20] and [26]. Most of the researches more focused in two-dimensional cases compare to three-dimensional due to the increment of its computational cost. In [19], FBTS has been proved its ability to sense a malignant tissue of 4 mm sized in the two-dimensional dielectric reconstruction in breast imaging. Besides the application of FBTS in medical imaging, there were also investigations of FBTS applied in Borehole radar application [50] and buried object detection [51].

FBTS method is a quantitative reconstruction technique which aims to provide the distributions of the unknown electrical properties for a target object within the region of interest. The unknown target object is considered embedded in free space. The electrical properties include the permittivity, permeability, electric conductivity, and magnetic conductivity. The useful information of the electrical properties will contribute to the reconstruction of an object as for its shape, size and location.

FBTS utilized Finite-Difference Time-Domain (FDTD) to compute and solve the direct and adjoint microwave scattering problems. Through FBTS a large amount of information about the dielectric parameters obtained as it consuming a broad spectrum of frequencies in a single optimization. This allows for more accurate and precise quantitative reconstruction of the electrical properties.

Figure 2.3 shows the simple configuration of an active microwave tomography set up in FBTS. The scattering objects are by definition have different properties from the

background environment. In this research, the scattering objects are anticipated as a collection of an induced source, as the target object in the region of interest is illuminated by short-pulsed waves. In its initial state, the background of FBTS is assumed free of the scattering objects.

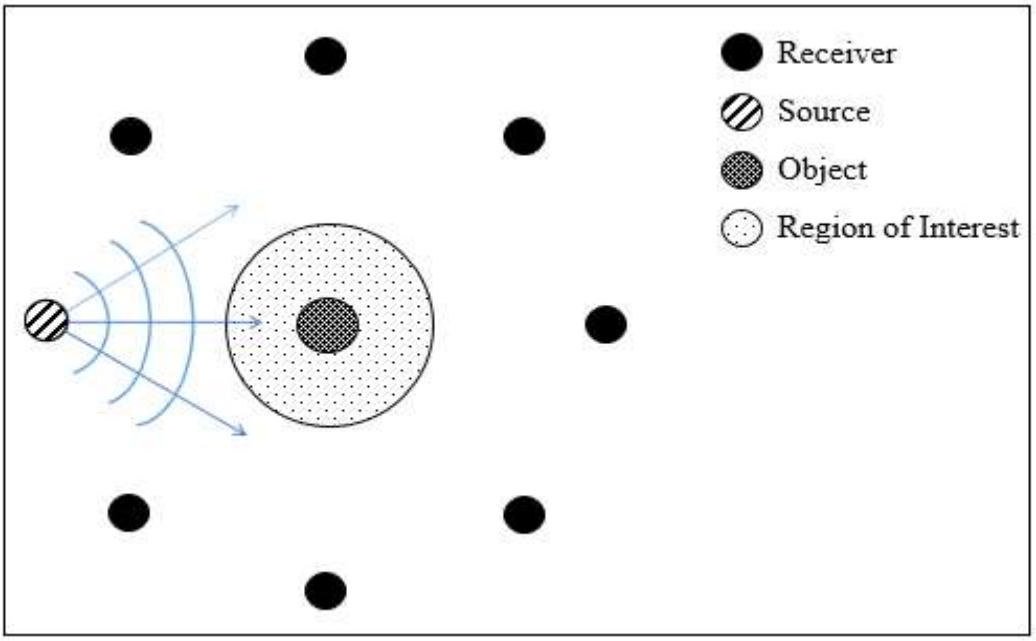

Figure 2.3: Simple setup of FBTS with 8-Elements circular arrays and tabulation of antennas [19]

For the forward time stepping, the transmitting antenna acted as a source, will transmit short pulsed waves to the target object. The incident wave as it has interacted with the target object will be transferred to other directions, which are known as scattering objects. The scattering objects will be collected by other antennas that acted as a receiver to be analyzed.

For the backward time stepping, the difference between measured and simulated microwave scattering measurements for each transmitter and receiver combination is propagated back toward the target object. The errors between those measurements are

minimized by an optimizing technique. As FBTS is a gradient-based optimization method, the cost function is minimized iteratively by using the Conjugate Gradient Method. During each of the optimization process, the step size, and direction are estimated and updated for next iteration.

Research in FBTS is continually progressing with incorporating the method with other enhancement technique to improve its efficacy in reconstructions development, such as integrating the method with the filtered inversion algorithm [21], [52], a regularization technique [27], [53-54], frequency hopping technique [55], and iterative multiscaling technique [50],[56]. There are studies to improve FBTS computational time and reduce reconstruction costs such as time delay pulses [57], source group method [58], and parallel computing [59].

Some of the researches have focused on increasing the quality and resolution of the reconstructed objects or structures of different sizes, specifically with the high contrast content. It is shown in [54] and [60-61], the sensing of the imaging objects was correlated with the chosen spectral frequency.

Large objects can be sensed at a lower spectral frequency [54]. However, imaging a smaller object or high contrast structure at a lower spectral frequency is always ineffective. In order to increase the sensing performance for the smaller object, the spectral frequency should be tuned higher. Selecting a suitable spectral frequency for the imaging will give a good tradeoff of the reconstructed resolution and hence providing a better approximation of the objects' sizes [60-61].

Frequency Hopping method incorporated with FBTS has been proposed in [55] utilizing a multiple spectral frequencies to improve the reconstructions accuracy of extremely dense breast composition. Exploiting a priori data into the reconstruction

algorithm should also enhanced the reconstruction of small objects or high contrast structures [61].

2.4 Finite-Difference Time-Domain (FDTD)

The Finite-Difference Time-Domain (FDTD) is a popular method and has been applied widely in the modeling of electromagnetic wave scattering. FDTD method was first proposed by K. Yee [47], and later on, has been improved by other researchers. FDTD has been chosen due to its simplicity of data decomposition and acquisition. FDTD also has the capabilities to solve complicated problems however, it is generally computationally intensive [57].

The fundamental of FDTD for solving the electromagnetic problem is to discretize in time and space, Maxwell's equations with central difference approximation. FDTD determines the allocation in space between the electric and magnetic fields components and the marching in time for the evolution of the procedure [62].

Several studies have been published implementing FDTD to solve the inverse scattering problem such as in reconstruction of shapes and material distributions of unknown cylinders [63], microwave imaging for human head modeling [64], electromagnetic wave propagation modeling in one-dimensional, two-dimensional and three-dimensional cases [65-66], through the wall radar imaging with time reversal method [67] and analysis of electromagnetic fields with Overset Grid Generation (OGG) method [68].

In the FBTS algorithm, the forward and adjoint fields are calculated numerically by utilizing the FDTD method. The FDTD model used in FBTS to solve the forward and adjoint fields is shown in Figure 2.4. The utilization of FDTD method in FBTS has been reported

in [20-21], [48-59]. The first numerical computation is to determine the numerical forward fields, and the second is the adjoint fields.

From Figure 2.4, for each transmitter reaction in the FDTD model, the forward electrical fields are gained and used to solve the direct problem. The difference between the calculated and measured electrical fields at the measured point is computed and assumed as error signals. The adjoint electrical fields are solved by propagating the error signals reversed in time [62].

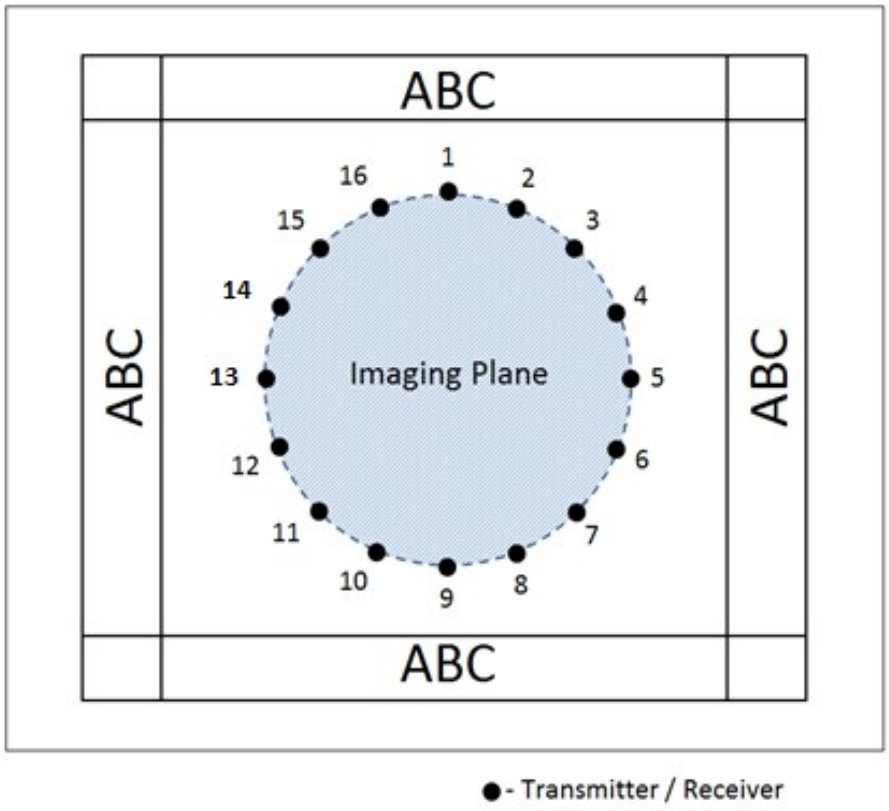

Figure 2.4: The FDTD Model [58]

2.4.1 Stability

The electromagnetic wave propagating in free space should not propagate faster than the speed of light, 3×10^8 ms^{-1}. The cell size, Δx and time step, Δt should be chosen carefully to maintain the FDTD method running unconditionally stable and without the constraint of Courant stability condition shown in Equation (2.19) [61].

$$\Delta t \leq \frac{\Delta x}{\sqrt{n} \cdot c_o} \tag{2.19}$$

where n is the dimension of the simulation and c_o is the speed of light in free space.

2.4.2 TM_Z Polarization

Considering the electric field propagation is in TM_Z polarization where the magnetic field is transverse to the z-direction. The Maxwell's equations satisfied for TM_Z polarization are as shown in Equation (2.20) to (2.22) [47].

$$\mu \frac{\partial \overrightarrow{\boldsymbol{H}_x}}{\partial t} + \frac{\partial \overrightarrow{\boldsymbol{E}_z}}{\partial y} = 0 \tag{2.20}$$

$$\mu \frac{\partial \overrightarrow{\boldsymbol{H}_y}}{\partial t} + \frac{\partial \overrightarrow{\boldsymbol{E}_z}}{\partial x} = 0 \tag{2.21}$$

$$\varepsilon \frac{\partial \overrightarrow{\boldsymbol{E}_z}}{\partial t} - \frac{\partial \overrightarrow{\boldsymbol{H}_y}}{\partial x} + \frac{\partial \overrightarrow{\boldsymbol{H}_x}}{\partial y} + \sigma \overrightarrow{\boldsymbol{E}_z} = 0 \tag{2.22}$$

where

$\boldsymbol{E}$: Electric field (Volts/meter)

$\boldsymbol{H}$: Magnetic field (Amperes/meter)

ε : Electrical permittivity (Farads/meter)

μ : Magnetic permeability (Henrys/meter)

σ : Electric conductivity (Siemens/meter)

Consequently, the unknown dielectric properties can be estimated by minimizing the cost functional shown in Equation (2.23) [62].

$$F(\varepsilon, \vec{E}_z) = \frac{1}{2}\sum_{n=1}^{N}\sum_{m=1}^{M}\int_0^T \left\| \vec{E}_z^{n,m} - \overrightarrow{E'}_z^{n,m} \right\|^2 dt \tag{2.23}$$

where ε is the dielectric properties of the scatter $\vec{E}_z^{n,m}$ and $\overrightarrow{E'}_z^{n,m}$ represent the measured and the calculated field at *m*-th measurement position for the *n*-th incident wave.

2.4.3 Boundary Condition

The application FDTD method of solving electromagnetic wave interaction if simulated in open region where the spatial domain of the computation field is unbounded in one or more coordinate direction will generate an infinite number of data in a computer. Therefore the computational domain should be limited in size or in enclosed geometry.

The boundary condition allows the simulation of electromagnetic fields interacting in an unbounded region on a computer with finite memory. The computational field should be adequate to enclose the structure of interest with a suitable boundary condition thus preventing any reflection where the mesh ended. There are three types of boundary conditions; reflective, periodic and absorbing [69].

The reflective boundary condition is the simplest condition whereas the field, in particular, is set equal to zero. The ways to implement reflective boundary condition are to

collide with the same wave propagating in inverse direction or multiplying the field by a really small value. However, it can be only used in a test program [69].

The periodic boundary condition is generally used for periodic structure modeling in the direction of one of the axis. The conditions can be implemented by setting the field on one boundary equal to the field on opposite boundary. The condition is simpler when applied one-dimensional case compared two or three-dimensional cases. Reflective and Periodic boundary condition are always applied for one-dimensional cases.

The most flexible boundary condition, the absorbing condition is applying a conductive layer on the boundaries of the computational domain which is more than one cell. An absorbing boundary condition (ABC) is shown in Figure 2.4. A type of ABC, Perfectly Matched Layer (PML) was introduced in [69], is used for the computational domain to truncate simulation boundaries and preventing spurious reflection from the edge of the problem space.

PML works by setting the impedance in a way to match perfectly in the problem space. By matching the impedance, the outgoing reflections from the grid boundaries are absorbed and reflections are prevented to enter the lossy region. Through PML computation, it is reported in [70], a small amount of numerical reflection obtained at the environment boundary which can be rectified by tuning the magnitude of the layer's parameter.

2.4.4 FDTD Source

FDTD utilized a source excitation to radiate energy from a point of its grid to another for the computational modeling. The source excitation for FDTD is in transient with consideration of the time signature and bandwidth which will dictate the frequency band of

the propagating electromagnetic wave. The examples of sources are the Gaussian pulse, Blackman-Harris window, point source dipoles, and Plane wave [71].

Sources in FDTD can be classified into the soft and hard source. Soft source permit the updating of the electromagnetic field at the source location and penetrable at the source location. The hard source is enforcing a field like excitation function at a certain location of the simulation domain to vary with a predefined function of time. The waves cannot pass through the hard source and are reflected off it.

The soft source is a better choice as a wave source in FDTD due to more accuracy in radiating energy from a punctual source to the FDTD grid and when transmitted at high frequencies [69]. An exact method of controlling the direction of wave propagation in the soft and hard source has been reported in [72].

The Gaussian pulse is commonly used as a wave source in FDTD computation and has been utilized as in [73-74]. A graph of a Gaussian pulse in Figure 2.5 has shown a symmetrically bell-shaped character that quickly falls towards plus and minus infinity. Equation (2.24) shows the general equation for a Gaussian pulse, where $\mathrm{A} = 1.0$, t_0 is the time delay, $T_S = (0.646 / 0.45)^{-9} = 1.4356$ ns is the half width of the pulse [71].

$$f(t) = \mathrm{A}e^{-\frac{(t-t_0)^2}{0.29T_S}} \tag{2.24}$$

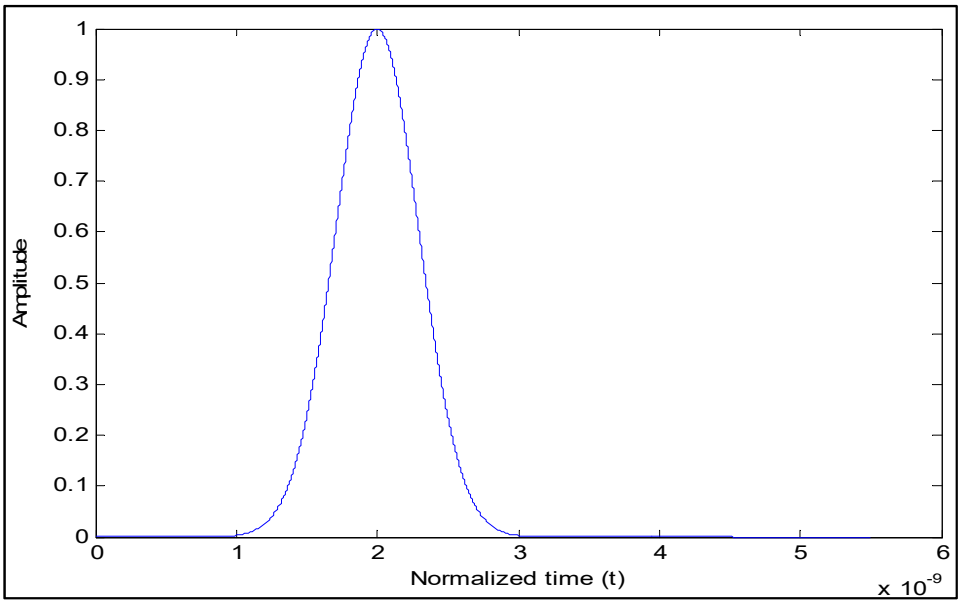

Figure 2.5: The Gaussian pulse at center frequency of 2 GHz referring to Equation (2.24) [71]

2.5 Ill-Posed Problem in Image Reconstruction

There are a considerable amount of studies and application of inverse problems in science and engineering where mathematical methods are preferably used. Hadamard [75] defined a linear and well-posed problem should satisfy three requirements; existence, uniqueness, and stability.

Existence in the sense of Hadamard's definition implied that there exists a solution to the problem, uniqueness is where there is at most one solution to the problem, and stability when the solution depends continuously on the data.

If the problem did not fulfill one or more of those requirements, the problem is said to be ill-posed [76], and the inverse problem is typically ill-posed. In operator language, let $A: X \rightarrow Y$ be an operator from normed space X into a normed space Y. The equation $Ax = y$

is said to be well posed if A is bijective and the inverse operator $A^{-1}: Y \rightarrow X$ is continuous. Otherwise the equation is called ill-posed.

In the early vision, a satisfactory theoretical framework of regularization of in certain class has been discussed and developed for providing a natural way to the solution [77-80]. As was stated in [78], the three equivalent conditions that constraints the solution of the inverse problem. The first condition, the quasi-solution and the second condition, the discrepancy principle are classified in a constrained optimization problem. The third condition is an unconstrained optimization problem.

i. Find x that minimizes $\|Ax - y\|$ that satisfied $\|Px\| < c_1$ whereas c_1 is a positive scalar constant.
ii. Find x that minimizes $\|Px\|$ that satisfied $\|Ax - y\| < c_2$ whereas c_2 is a positive scalar constant.
iii. Find x that minimizes $\|Ax - y\|^2 + \lambda\|Px\|^2$, whereas λ is a regularization parameter ($\lambda = {}^{c_2}/_{c_1}$),

For the conditions, x is the solution, y is the observation, A and P are the linear operators, and $\|\cdot\|$ is a kind of norm operator depending on a specific physical scenario. Thus, in general, the solution of the ill-posed problem through regularization method can be formulated as Equation (2.25) [78].

$$arg\min_x \|Ax - y\|^2 + \lambda\|Px\|^2 \tag{2.25}$$

The regularization method depends on parameter $\lambda \geq 0$, is the penalty term of Equation (2.25). For a large enough λ, the regularized solution of the ill-posed problem is stable from noise or perturbations. As λ goes to zero, the solution becomes less regularized

and more to originated solution. Thus, the regularization parameter λ controls the tradeoff between solution stability and nearness of the regularized solution to the non-regularized solution [79]. The role of regularization parameter has been outlined in [80-81]. The expressions of image reconstruction problems will be described in Section 2.5.1 by referring to [82].

2.5.1 Image Reconstruction Problems

For image reconstruction, it is crucial to recover the desired image, $f(x, y)$ from the related observed image $g(x, y)$, which is always inaccurate. The distortion model in linear integral equation is shown in Equation (2.26) [82].

$$g(x, y) = \int_{-\infty}^{\infty} \int_{-\infty}^{\infty} h(x, y; \acute{x}, \acute{y}) f(\acute{x}, \acute{y}) d\acute{x} d\acute{y} \tag{2.26}$$

where $h(x, y; \acute{x}, \acute{y})$ is the kernel or response function of the distorting system. Assuming the observed image is observed as continuous model, the data are often discrete.

Thus for N_g observations, Equation (2.26) can be expressed as Equation (2.27), where $h_i(\acute{x}, \acute{y}) = h(x_i, y_i; \acute{x}, \acute{y})$ denotes the kernel corresponding to the *i*-th observation [82].

$$g_i(x_i, y_i) = \int_{-\infty}^{\infty} \int_{-\infty}^{\infty} h_i(\acute{x}, \acute{y}) f(\acute{x}, \acute{y}) d\acute{x} d\acute{y} \qquad 1 \leq i \leq N_g \tag{2.27}$$

The assumed unknown image $f(x, y)$ expressed in term of discrete and finite set of parameters for N_f observations, is shown in Equation (2.28) [82].

$$f(x,y) = \sum_{j=1}^{N_f} f_j \emptyset_j(x,y) \tag{2.28}$$

The $\emptyset_j(x,y)$ is the basis function to be set of unit height boxes corresponding to an array of square pixels. By substituting Equation (2.28) into Equation (2.27), the discrete relationship between the observations g_i and the unknown image coefficient f_j yields Equation (2.29) [82].

$$g_i = \sum_{j=1}^{N_f} H_{ij} f_j \qquad 1 \le i \le N_g \tag{2.29}$$

where H_{ij} is given by

$$H_{ij} = \int_{-\infty}^{\infty} \int_{-\infty}^{\infty} h_i(\acute{x},\acute{y}) \emptyset_j(\acute{x},\acute{y}) d\acute{x} d\acute{y} \qquad 1 \le i \le N_g, \;\; 1 \le j \le N_f \tag{2.30}$$

Hence, accumulating all the observations g_i and the unknown image coefficient f_j into a single matrix equation can be written as Equation (2.31) [82].

$$g = Hf \tag{2.31}$$

where the length of N_g vector g, the length of N_f vector f and $N_g \times N_f$ matrix H follow naturally from Equation (2.28) to Equation (2.30).

However, measured data is always degraded by inevitable noise, q therefore shown in Equation (2.32) [82].

$$g = Hf + q \tag{2.32}$$

2.6 Regularization Method in Image Reconstruction

Regularization theory has often been considered for the solution of an inverse problem in dealing with ill-posedness as it provides stability and increment in the solution's accuracy. The inclusion of prior knowledge to stabilize solution is the purpose of regularization method. The solution is the constraint in a kind of way as to avoid the oscillatory nature of noise dominated solution. This allow better reasonable estimation of the solution. The expressions of the truncated Singular Value Decomposition (SVD), Tikhonov and Total Variation regularization will be described in Section 2.6.1 by referring to [82].

2.6.1 Truncated Singular Value Decomposition Regularization

The singular value decomposition of a $N_g \times N_f$ matrix H is usually referred to as the SVD is given as following equation [82].

$$H = USV^T = \sum_{k=1}^{p} \sigma_k u_k v_k^T \tag{2.33}$$

where U is an $N_g \times N_g$ matrix, V is an $N_f \times N_f$ matrix, and S is an $N_g \times N_f$ diagonal matrix, with the value $\sigma_1, \sigma_2, \ldots, \sigma_p$ arrange on its main diagonal and zeros where $p = \min(N_g, N_f)$. The orthogonal columns u_i of U are called left singular vectors, the σ_i are called the singular values, and orthogonal columns v_i of V are called the right singular vectors. The general solution of SVD can be expressed as follows [82]:

$$\hat{f}^+ = \sum_{k=1}^{r} \frac{u_i^T g}{\sigma_i} v_i \tag{2.34}$$

The calculation of the entire SVD is can be computationally expensive for a solution to a larger problem. A way to solve this issue is to remove the irrelevant values from solution by simply truncating the small singular values to zero. This numeric filtering method is called truncated SVD or TSVD. The solution of regularized TSVD can be expressed in Equation (2.35) [82].

$$\hat{f}_{tsvd}(\lambda) = \sum_{k=1}^{r} w_{i,\lambda} \frac{u_i^T g}{\sigma_i} v_i \tag{2.35}$$

where $w_{i,\lambda}$ is a set of weightage parameter given by,

$$w_{i,\lambda} = \begin{cases} 1 & i \leq k(\lambda) \\ 0 & i > k(\lambda) \end{cases} \tag{2.36}$$

where the $k(\lambda) = [\lambda^{-1}]$, thus $[x]$ denote x rounded to the next smaller integer. The solution of TSVD also can be expressed as follows [82].

$$\hat{f}_{tsvd}(\lambda) = argmin\|f\|_2 \quad \text{subject to} \quad min\|g - H_k f\|_2 \tag{2.37}$$

Much work on improving the potential of TSVD has been carried out [83-85] with the aim to increase accuracy from the standard TSVD method. The application of TSVD as a regularization method in solving an ill-posed problem is been described in detail in [83].

According to in [84], TSVD performance of the solution approximation is depending on satisfaction of a discrete Picard condition. TSVD analysis has been used in the study of microwave inverse scattering for breast imaging. In the study [86], TSVD was applied to systematically evaluate the quality of the information contained in simulated scattering data with respect to system design and problem formulation.

2.6.2 Tikhonov Regularization

One of the well-known regularization methods, Tikhonov regularization, also known as ridge regression in statistics and is ℓ_2 norm regularization method was developed by Andrey Tikhonov [87]. The estimation of Tikhonov regularization solution can be achieved by minimization problem of Equation (2.38) [82].

$$\hat{f}_{TK}(\alpha) = ag\min_{f}\|g - Hf\|_2^2 + \alpha^2\|Lf\|_2^2 \tag{2.38}$$

The first term of $\hat{f}_{TK}(\alpha)$ is the same ℓ_2 norm for least-squares method which represent the fidelity to data while the second term is representing the regularization which contained the prior knowledge of expected solution. The Tikhonov regularization parameter α controls the weight given to the minimization of side constraint.

The regularization parameter α can be determined by employing a standard parameter selection method such as the Discrepancy Principle, Generalized Cross-Validation (GSV), and the L-Curve criterion. The role of such parameter selections has been described and compared in [88].

The Discrepancy Principle emphasized on adding a posteriori knowledge about the perturbation or noise as in Equation (2.32) in order to choose the practical regularization parameter. On the other hand, the GSV does not requiring the knowledge of the noise properties but is based on minimizing the set of prediction errors. Another popular parameter selection method in Tikhonov regularization is the L-Curve criterion.

The L-Curve criterion in Figure 2.6 is based on a plot of the norm of the regularized solution versus the residual norm for a range of values of regularization parameter in a log scale. The optimal regularization parameter is at the corner between the horizontal and vertical line of the plot which defines the balance between under and over-smoothing of the

solution. A detail investigation of the application of the L-Curve criterion for Tikhonov regularization parameter has been described and demonstrated in [88]. A new criterion of choosing the practical regularization parameter has been introduced in [89], known as the U-Curve which is comparable to the L-Curve criterion.

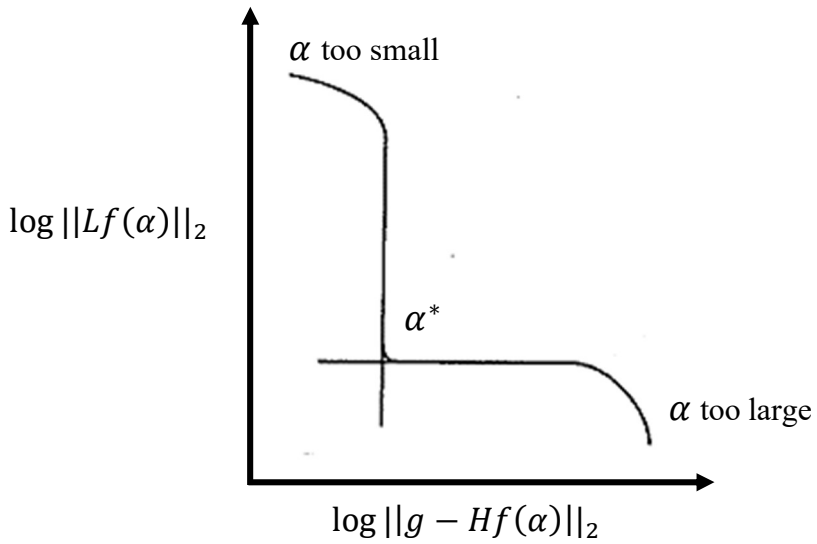

Figure 2.6: A standard L-Curve for Tikhonov Regularization [82]

Several studies have revealed that Tikhonov regularization is robust and provided a more efficient solution of an ill-posed problem. Tikhonov regularization has been applied to be an analysis tool to dynamic elastoplasticity problem [90], solving the image restoration problem with good results and faster convergence [91], and as a low-pass filter to refine two-dimensional surface defect image in inversion process in the frequency domain [92].

2.6.3 Total Variation Regularization

Total Variation (TV) minimizing function regularization was first introduced by L. Rudin, S.J. Osher, and E. Fatemi in [28] to use in image processing, particularly for regularizing the restoration of noisy images. The proposed method is also known as the ROF model. Other regularization methods like TSVD and Tikhonov assume the solution to be smoothed and continuous however the TV regularization is different. The ROF model has the ability for denoising image while recovers sharp discontinuities or edges of the image. The principle idea in TV regularization is to minimize the total $TV(f)$ in the image, where

$$TV(f) = \sum_{i=1}^{N_f} |[Df]_i| \tag{2.39}$$

where D is a discrete approximation to gradient operator. According to the ROF model in [28], the constrained minimization that need to be solved is shown in Equation (2.40).

$$\hat{f}_{TV}(\lambda) = arg\min_f \|g - Hf\|_2^2 + \lambda^2 \sum_{i=1}^{N_f} |[Df]_i| \tag{2.40}$$

The parameter λ is the nonnegative regularization parameter ($\lambda \geq 0$) which represents the tradeoff between the noise sensitivity and closeness to the observed image. The formulation of TV regularization shown in Equation (2.40) seems similar to Tikhonov regularization as shown in Equation (2.38).

However in TV regularization, it penalized only the total amount of gradient in the image and not its distribution, thus the regularization should containing localized steep gradient information. Consequently, the important attributes of an image, which is the edges of an image, can be preserved.

The research to date has tended to focus on utilizing TV regularization method in image processing. TV regularization method has been preferred to be incorporated into image reconstruction due to its potential to suppress noise while preserving edges in the image. It has been reported in [93], a fast computational compressive radar imaging based on TV regularization has improved the quality of reconstructed images. A comparative study between the performance of linear and nonlinear microwave imaging with adaptive of TV regularization method has been carried out [94]. Throughout the study, TV regularization method to minimize the cost function for the nonlinear case had outperformed the linear case. TV regularization has been very useful image restoration and is very efficient for denoising, deblurring, inpainting, and segmentation shown in Figure 2.7.

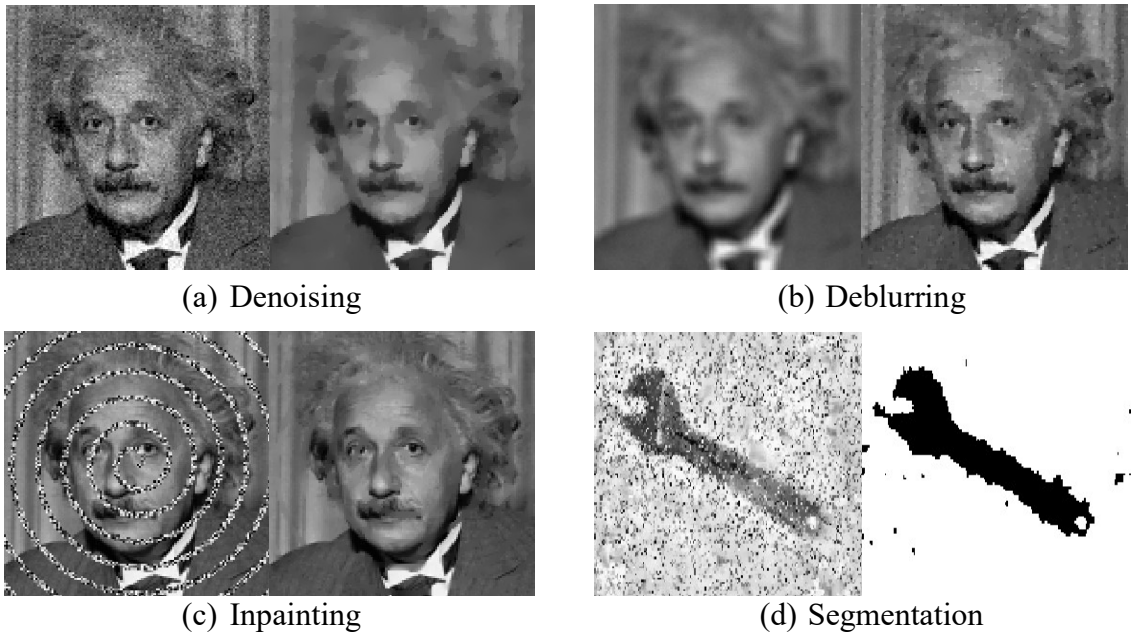

(a) Denoising (b) Deblurring

(c) Inpainting (d) Segmentation

Figure 2.7: TV regularization method tasks in image processing [95]

Image denoising is one of the fundamental problem in digital image restoration. Image denoising refers to the noise removal or recovery of a digital image that has been contaminate with noise such as additive white Gaussian noise (AWGN), speckle noise,

Poisson noise and impulse noise. The presence of noise during formation or transmission process is unavoidable. Image denoising is crucial to preserve useful information of the digital image and enhanced the image's quality [96, 97].

Image deblurring is the problem to recover a clear digital image that has degraded with blurring artifact and noise due to instrument and/or atmospheric factor. The blur processes described in continuous coordinate because the blurring takes place in continuous space. Therefore, blur always observed as the convolution of point spread function (PSF) which determined the quality of the deblurred image, and formulated as an inverse problem. Deblurring needed to deconvolve PSF of the blurred image with a hypothetical that the input image is sharp [97].

Image inpainting in image restoration is reconstructing the missing region of a digital image, which has corrupted, or deteriorate with plausible content so that the image will be more close resemblance with the original image. In inpainting task, an algorithm produced to predict the values of the missing pixel by the knowledge of pixels adjacent to the missing region [98, 99].

Image segmentation is the process of segregating a digital image into multiple segments or regions to enable the computational analysis of the image. Typical task in image segmentation includes locating objects, reconstruction its boundaries such as lines, edges and curves, and separating foreground from background of a digital image [100].

2.7 Summary

Chapter 2 describes the research of related literature and studies such as microwave imaging system, Maxwell's equation, the FBTS, the FDTD, ill-posed problem focusing on the image reconstruction problems, and regularization method in image reconstruction such as the TSVD, Tikhonov regularization and Total Variation regularization method. In this research, the Total Variation regularization method is functioning as image denoising. The summary of related comparative studies to this research as shown in Table 2.1. The gist of the studies presented in the focus or objectives, the method proposed by the researchers, the results gained from the proposed method and the conclusion.

Table 2.1: Summary of related comparative studies

Authors / Years	Focus / Objectives	Methods	Results	Conclusion
Liu, G., & Zhang, Y. (2010) [26]	Reconstruction of a three-dimensional breast cancer imaging based on FBTS and a regularization method.	Forward-Backward Time-Stepping with the Tikhonov's regularization method to improve the quantitative reconstruction of a simple three-dimensional nondispersive breast model.	The presented algorithm is convergent. • The reconstruction for electrical properties of skin tissue has shown an improvement. • The location and shape of the tumors has successfully reconstructed. • However, the estimation of ε_r values is poorer than in the σ case.	The presented method is feasible for early-stage breast cancer detection. The accuracy of the proposed method could be improve by adjusting the regularization parameter.
Wei, N. S., *et al.* (2015) [55]	Reconstruction of a two-dimensional extremely dense breast composition in utilizing inverse scattering technique integrated with frequency-hopping method.	Forward-Backward Time-Stepping with frequency hopping method. • Estimating the large region of breast composition at lower central frequency while improve the resolution at higher central frequency.	• The composition of the extremely dense breast significantly improved compared to reconstruction using a single central frequency.	The reconstruction of the extremely dense breast significantly improved.
Yong, G., *et al.* (2015) [101]	Preliminary study for reconstruction of a two-dimensional embedded object based on FBTS and an edge-preserving regularization method.	Forward-Backward Time-Stepping with an edge-preserving regularization method to enhance the quantitative reconstruction of electrical properties in terms of convergence and stability of the optimization technique.	• By incorporating an edge-preserving regularization method, the estimation of the object location, size and shape has been improve. • The rough surface of the reconstructed object has smoothed while preserving the discontinuity. • The efficacy of the proposed method has been verify with Mean Square Error (MSE).	The integration on an edge-preserving method with the FBTS has shown a potentially improved reconstruction of the electrical properties.

Table 2.1 continued

Authors / Years	Focus / Objectives	Methods	Results	Conclusion
Yong, G., *et al.* (2017) [54]	Profile reconstruction is utilizing FBTS with the integration of automated edge-preserving regularization method for object detection.	Forward-Backward Time-Stepping with an edge-preserving regularization method extended with the dynamic values of regularization parameters in each iteration process. The efficacy of the proposed method was verified by the calculation of Mean Square Error (MSE).	• The paper had shown a comparison of the reconstruction profile of dielectric properties by the proposed method with and without the regularization method, and with Tikhonov regularization method. • The proposed method yields the reconstruction with the lowest calculation of MSE in the case of relative permittivity. • However, in the case of conductivity reconstruction, FBTS without regularization outperform the proposed method.	The proposed method successfully increased the reconstruction quality and accuracy. The weighting parameters were automated and dynamically produced for each iteration process.
Elizabeth, M. A *et al.* (2017) [102]	Incorporating Chebyshev low pass filter with FBTS to filter the noisy environment as improvement of two-dimensional breast reconstruction quality.	The proposed method was presented via numerical simulations. Researchers add -3dB Gaussian noise in the measured field dataset. Chebyshev filter was applied at different order, k (k = 2, 3, 4 and 5) to determine and reconstruct breast image at the lowest loss.	Noises made in the measurement dataset are always impulsive and are in high frequency. • Chebyshev second order (k=2) is gives the best performance of the reconstruction. • Introducing a low pass filter at range of 1.5GHz to 2.65GHz eliminates any impulsive data in reconstruction region. • However, the reconstruction also suffer from loss some of it information due to the filter application.	The proposed filter has been sufficiently removing noise for the simple homogenous breast model.

CHAPTER 3

METHODOLOGY

3.1 Overview

In this research, the Total Variation (TV) regularization scheme will be incorporated in the FBTS inverse scattering algorithm to improve the reconstructed image by giving information such as its shapes and location, smoothing the uninterested structures, and also reconstructing sharp edges in the enclosed region that should give a better estimation of the image's boundaries. The algorithm was implemented in the C++ language while the reconstructed image is presented using MATLAB. The mathematical background of the TV method, and the parameters involved in the research will be discussed in this chapter.

3.2 Forward-Backward Time-Stepping Method

The Forward-Backward Time-Stepping (FBTS) method is applied to reconstruct images providing the electrical parameter profiles of the objects together with its size, shape, and position of the scatters or objects. This method achieved by solving the inverse scattering problem in the time domain, therefore allowing a broad spectrum of frequencies to be utilized in a single optimization. In return, a great amount of information of the electric parameter profiles of the objects obtained with FBTS method.

In FBTS, the nonlinear inverse scattering data are formulated in the time domain by applying Finite-Difference Time-Domain (FDTD) scheme. The FDTD scheme is used to calculate the scattering signals in forward time-stepping and adjoint field in backward time-stepping. The grid size for the FDTD configured at 1 mm x 1 mm. Convolution Perfectly

Matched Layer (CPML) applied in the FDTD solution space to outline simulation boundaries and preventing reflection of the signal in the environment. The particular of CPML applied considered as in [30]. Figure 3.1 shows a typical configuration of an active microwave tomography set up for FBTS inverse scattering problem.

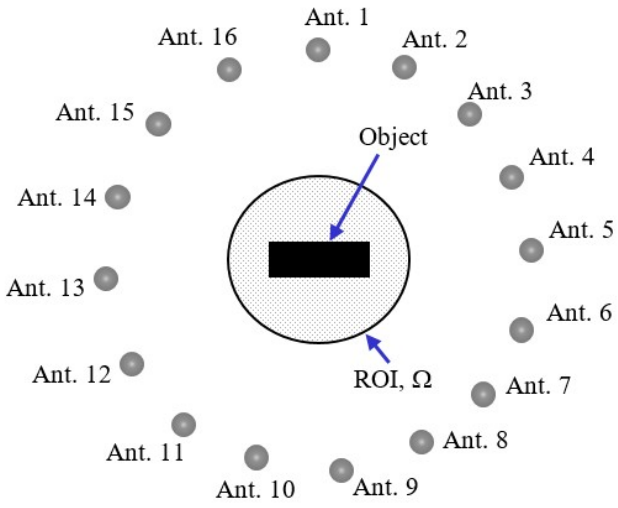

Figure 3.1: Configuration of the problem in two-dimensional [102]

The assumption is that an unknown scatters or object is embedded in a free space region of interest (ROI), and illuminated successively by *M* short-pulsed waves generated by current sources $\boldsymbol{s}_m(\boldsymbol{r}, t)$ located at $\boldsymbol{r} = \boldsymbol{r}_m^t(m = 1,2, \ldots\ldots, M)$. The antennas act as transmitter and receiver sequentially whereas only a transmitter transmits a signal at a time as shown in Figure 3.2. The other remaining antennas will act as a receiver collecting scattering signals as shown in Figure 3.3.

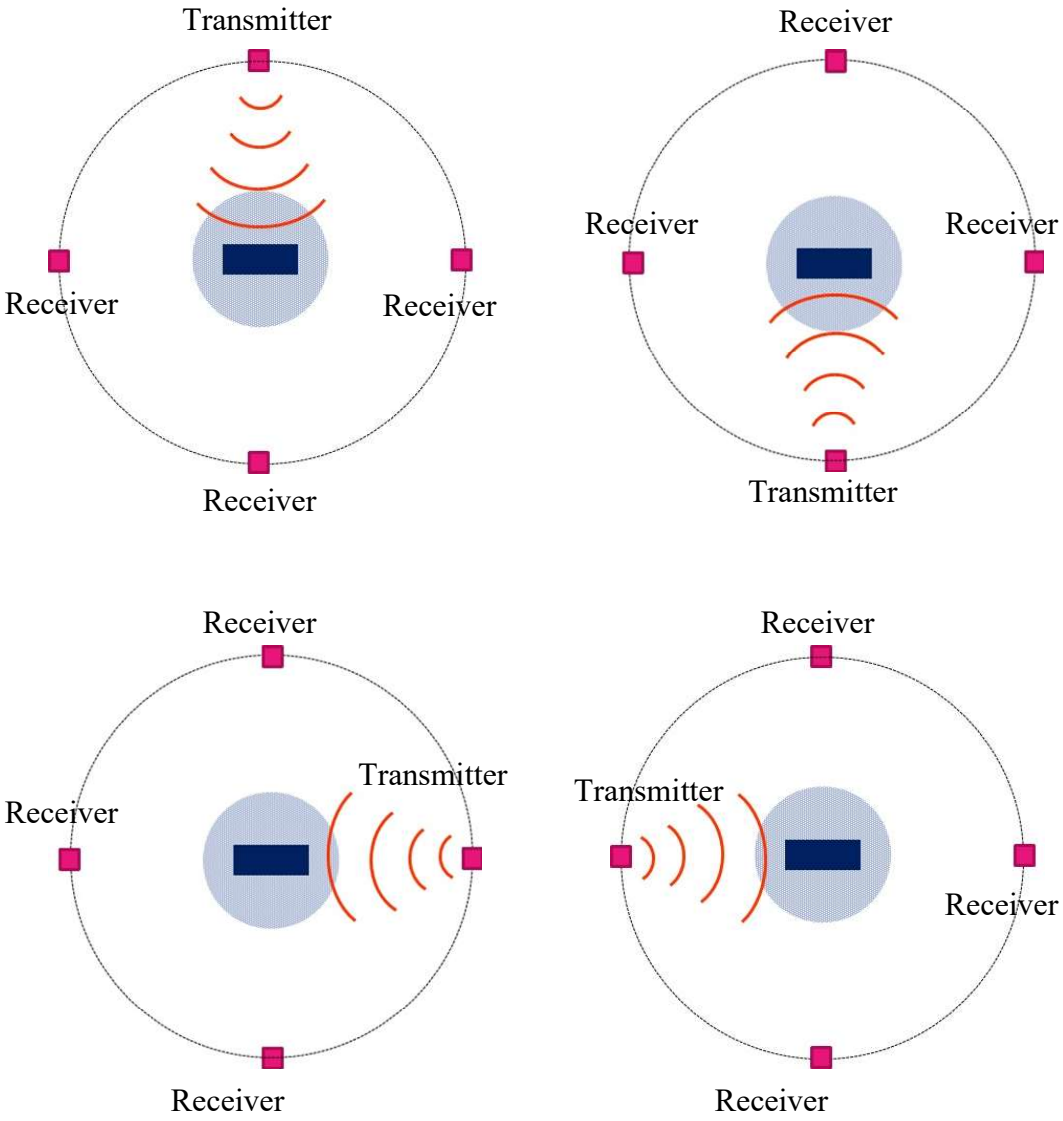

Figure 3.2: Forward Problem for the Estimated Object with Forward Time-Stepping

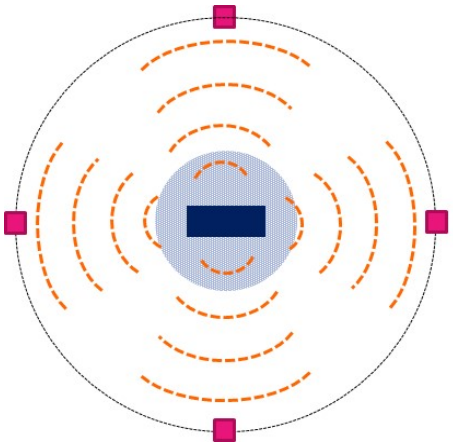

Figure 3.3: Adjoint Field by Residual Sources with Backward Time-Stepping

The reconstruction of the electrical parameter profiles obtained from the knowledge of the transient field data measured at several observation points or antennas, $\boldsymbol{r} = \boldsymbol{r}_n^t (n = 1,2, \ldots\ldots, N)$ for each illumination. For initial condition, the currents are assumed to be generated at time $t = 0$ and there is no electromagnetic field before time, $t = 0$. The total electromagnetic fields $\mathbf{v}_m(\mathbf{r}, t)$ for the m^{th} current sources $\boldsymbol{s}_m(\mathbf{r}, t)$ satisfy the following Maxwell's equation while L is given by,

$$L\mathbf{v}_m = \mathbf{s}_m \tag{3.1}$$

Under zero initial condition for

$$\mathbf{v}_m(\mathbf{r}, 0) = 0 \tag{3.2}$$

The optimization problem formulated in the form of cost functional to be minimized and stated as Equation (3.3).

$$Q(p) = \int_0^{cT} \sum_{m=1}^{M} \sum_{n=1}^{N} K_{mn}(t) \left|\mathbf{v}_m(\mathbf{p}; \mathbf{r}_n^r, t) - \tilde{\mathrm{v}}_m(\mathbf{r}_n^r, t)\right|^2 d(ct) \tag{3.3}$$

where $\mathbf{p}$ is a medium parameter vector function, $K_{mn}(t)$ is a nonnegative weighting function which takes a value of zero at time $t = T$ (T is the time duration of the measurement), and $\mathbf{v}_m(\mathbf{p}; \mathbf{r}_n^r, t)$ and $\tilde{\mathrm{v}}_m(\mathbf{r}_n^r, t)$ are the calculated electromagnetic fields for an estimated medium parameter vector $\mathbf{p}$ and the measured electromagnetic fields due to the m^{th} source excitation. M is the number of transmitters and N is the number of receivers.

Each optimization requires a complete dataset of all antennas transmitting and receiving scattering signals. A sinusoidal modulated Gaussian pulse is used as a source signal as shown in Figure 3.4. The source signal centered at 2 GHz frequency and its bandwidth is 1.3 GHz. The number of search steps, nsteps is 2380. The frequency range

chosen to give an optimal performance of the reconstructed image, which balanced for both image resolution, and convergence of the proposed algorithm.

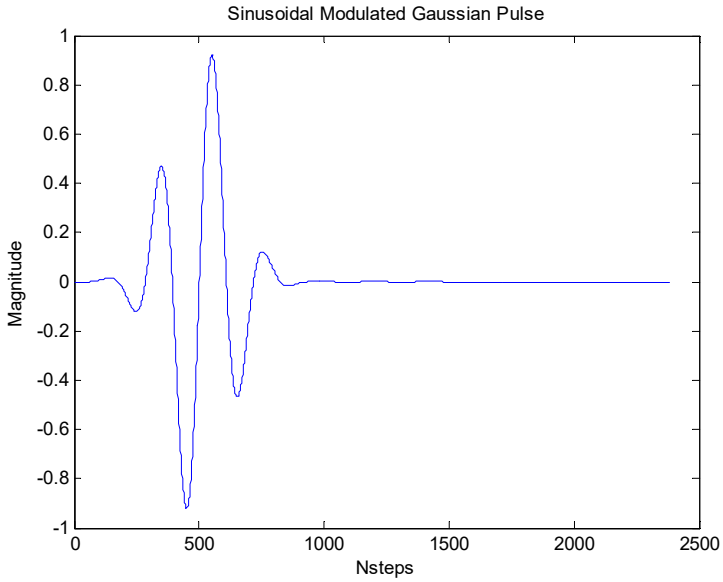

Figure 3.4: Sinusoidal Modulated Gaussian Pulse for Center Frequency of 2 GHz

Figure 3.5 shows the received signal at an antenna when there is no object embedded in the ROI. The amplitude of the receiving signal is lower than the illuminating source signal showing attenuation happens as the signal propagate through time as measurement taken.

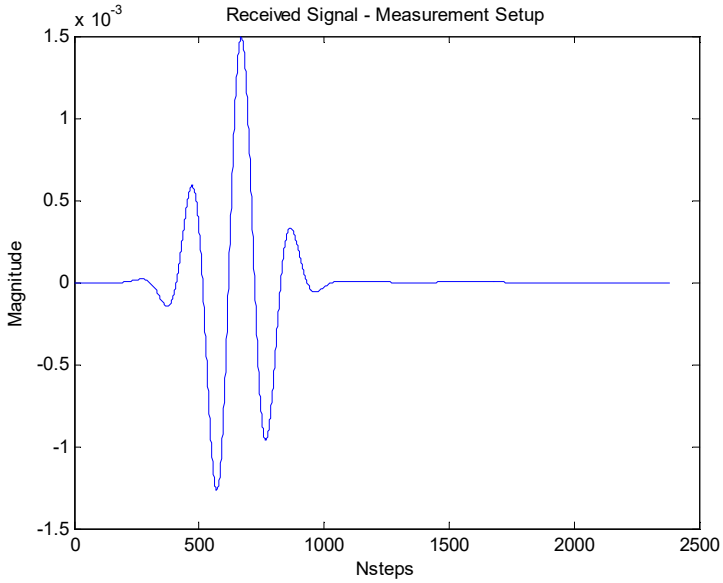

Figure 3.5: The Receiving Signal without Object in ROI

The substance of the FBTS method is the formulation of cost functional that compares error between measured and simulated microwave scattering measurement. The measurement of measured and simulated microwave scatters are summed for each transmitter-receiver combination and integrated over a time period from $t = 0$ to $t = T$.

By taking the Frechet derivative of Equation (3.3), the gradient of the functional of ε_r and σ is given by Equation (3.4).

$$g_{\varepsilon_r}(\mathbf{r}) = \int_0^T \sum_{m=1}^{M} \sum_{i=1}^{2} w_{mi}\,(\mathbf{p};\mathbf{r},t)\,\frac{d}{dt} v_{mi}(\mathbf{p};\mathbf{r},t)dt$$

$$g_{\sigma}(\mathbf{r}) = \int_0^T \sum_{m=1}^{M} \sum_{i=1}^{2} w_{mi}\,(\mathbf{p};\mathbf{r},t)\,\frac{d}{dt} v_{mi}(\mathbf{p};\mathbf{r},t)dt \tag{3.4}$$

where $w(\mathbf{p};\mathbf{r},t)$ is the calculated adjoint field and $v(\mathbf{p};\mathbf{r},t)$ is the calculated electromagnetic field in the reconstruction region, $\mathbf{r}$. The adjoint field $w(\mathbf{p};\mathbf{r},t)$ is obtained from the received residual scattered signals $[\mathbf{v}_m(\mathbf{p};\mathbf{r}_n^r,t) - \tilde{\mathrm{v}}_m(\mathbf{r}_n^r,t)]$ being reversed in time.

This is executed through FDTD method with backward stepping at $t = T$. The term $i = 1$ till $i = 2$ represents the calculated summation of the gradient of w_{mi} and v_{mi} in x and y directions. The gradient terms in Equation (3.4) allow the conjugate gradient method to be applied to minimize the error functional in Equation (3.3) in which providing the estimation of the electrical parameter profile, $\mathbf{p}$.

The flow chart of Forward-Backward Time-Stepping given in Figure 3.6. In predefined setting where information can be controlled and set up for the algorithm execution such as for antenna setting, initial guess for optimization technique, frequency scaling, synthetic data setting, and source signal setting will be discussed in Section 3.3.1.

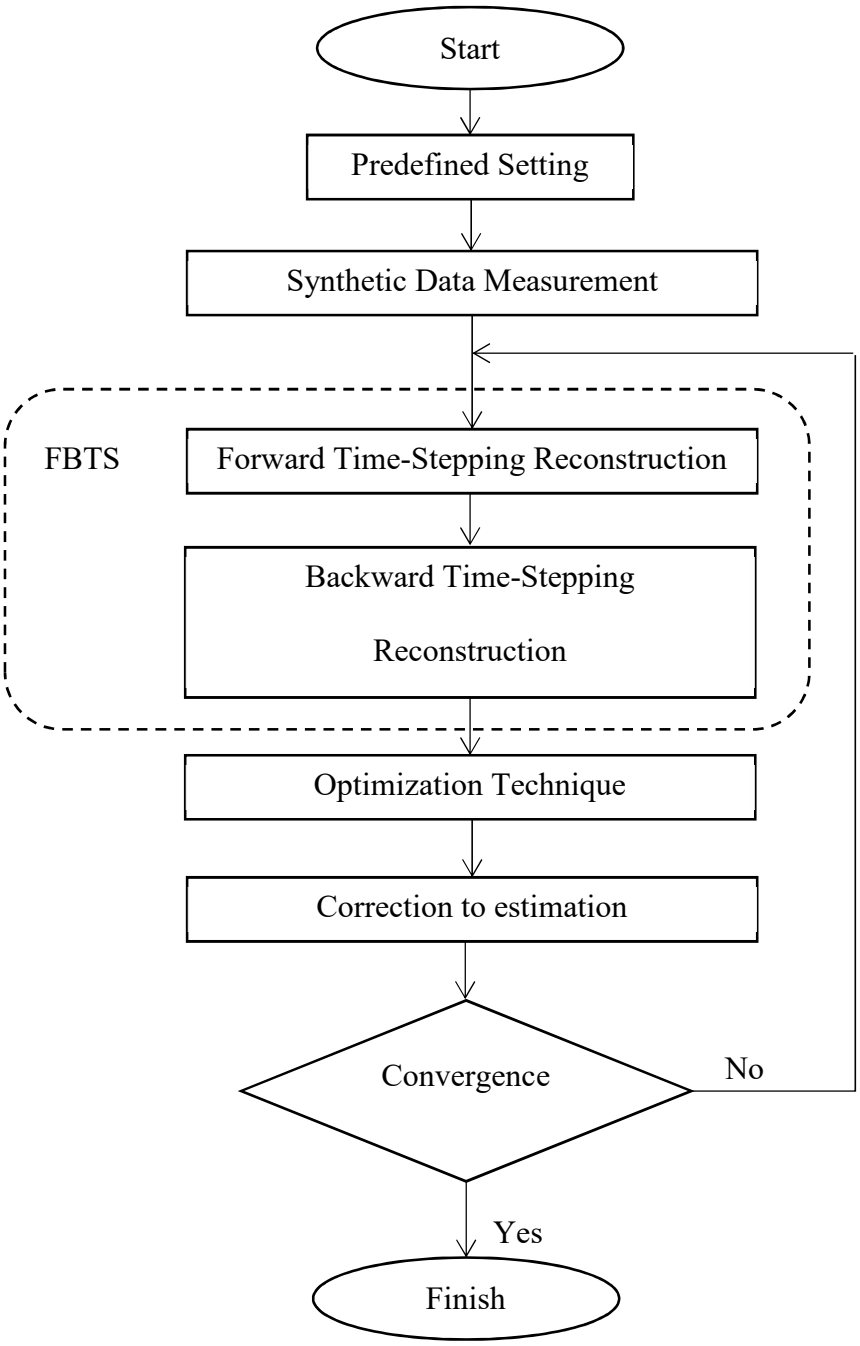

Figure 3.6: Forward-Backward Time-Stepping Flow Chart

The test is carried out for 100 iterations, and it is sufficiently yield optimum performance of the algorithm, ensured that only a minimal decrement in the error functional observed for the following iterations. The simple object is a rectangle shaped object embedded inside the ROI with the length of 40 mm and width of 16 mm surrounded by

number of antennas as shown in Figure 3.1. While the ROI is a circular shape with 80 mm of diameter for all cases. Increasing the ROI size will increase the number of computed pixels thus the computational time. The object is assumed to be unknown shape and located in center of the ROI.

The relative permittivity of 21.45 and the conductivity of 0.45 S/m is determined for the electrical properties of the object. As for the ROI, the relative permittivity was set to be 9.98 and conductivity is 0.18 S/m. Due to nonlinearity of the inverse problem, the optimization technique, conjugate gradient method does not always find its global minimum and its result is dependent on a proper initial guess [10].

A proper initial guess will avoid optimization to be trap in local minimum. The initial guess chosen for relative permittivity is 13.7 and the conductivity is 0.20 S/m for all cases. The conjugate gradient method applied to the minimization of the cost functional as in Equation (3.3). For each step of iteration, forward scattering problem and adjoint fields are solved numerically utilizing finite-difference time-domain method.

3.3 FBTS-TV Regularization Method

The Total Variation (TV) regularization method incorporated in the FBTS inverse scattering algorithm to improve the reconstructed image by giving information such as its shapes and location, and reconstructing sharp edges in the enclosed region that should give a better estimation of the image's boundaries.

The cost functional of FBTS-TV regularization method to be minimize stated as in Equation (3.5), [18].

$$
\begin{aligned}
F(\mathbf{p}) &= Q(\mathbf{p}) + Q_{TV}(\mathbf{p}) \\
&= \int_0^T \sum_{m=1}^{M} \sum_{n=1}^{N} K_{mn}(t) |\mathbf{v}_m(\mathbf{p}; \mathbf{r}_n^r, t) - \tilde{\mathrm{v}}_m(\mathbf{r}_n^r, t)|^2 dt \\
&\quad + \lambda_{\varepsilon_r} \int_\Omega \sqrt{|\nabla \varepsilon_r(\mathbf{r})|^2 + \alpha_{\varepsilon_r}} d\mathbf{r} + \lambda_\sigma \int_\Omega \sqrt{|\nabla \sigma(\mathbf{r})|^2 + \alpha_\sigma} d\mathbf{r}
\end{aligned} \tag{3.5}
$$

where $Q_{TV}(\mathbf{p})$ is total variation regularization terms, λ_{ε_r} , λ_σ regularization parameters, α_{ε_r} and α_σ small parameters, Ω an estimation region surrounding unknown objects and the medium parameter of vector function is given by [18],

$$
\mathbf{p}(\mathbf{r}) = (\varepsilon_r(\mathbf{r}), \sigma(\mathbf{r})) \tag{3.6}
$$

The gradient of the second term $Q_{TV}(\mathbf{p})$ is derived as followed [18], [101].

$$
\begin{aligned}
Q_{TV}(\mathbf{p}) &= \lambda_{\varepsilon_r} Q_{TV_{\varepsilon_r}}(\varepsilon_r) + \lambda_\sigma Q_{TV_\sigma}(\sigma) \\
Q_{TV}(\varepsilon_r) &= \int_\Omega \sqrt{|\nabla \varepsilon_r(\mathbf{r})|^2 + \alpha_{\varepsilon_r}}\, d\mathbf{r} \\
Q_{TV}(\sigma) &= \int_\Omega \sqrt{|\nabla \sigma(\mathbf{r})|^2 + \alpha_\sigma}\, d\mathbf{r}
\end{aligned} \tag{3.7}
$$

The Frechet differential of $Q_{TV_{\varepsilon_r}}(\mathbf{p})$ is given by [18],

$$
\begin{aligned}
Q'_{TV_{\varepsilon_r}}(\varepsilon_r) h_{\varepsilon_r} &= -\int_\Omega h_{\varepsilon_r} \nabla . \left(\frac{\nabla \varepsilon_r(\mathbf{r})}{\sqrt{|\nabla \varepsilon_r(\mathbf{r})|^2 + \alpha_{\varepsilon_r}}} \right) d\mathbf{r} \\
&= -\int_\Omega h_{\varepsilon_r} \left[\frac{\partial}{\partial x} \left(\frac{\frac{\partial \varepsilon_r}{\partial x}}{\sqrt{\left(\frac{\partial \varepsilon_r}{\partial x}\right)^2 + \left(\frac{\partial \varepsilon_r}{\partial y}\right)^2 + \alpha_{\varepsilon_r}}} \right) \right. \\
&\quad \left. + \frac{\partial}{\partial y} \left(\frac{\frac{\partial \varepsilon_r}{\partial y}}{\sqrt{\left(\frac{\partial \varepsilon_r}{\partial x}\right)^2 + \left(\frac{\partial \varepsilon_r}{\partial y}\right)^2 + \alpha_{\varepsilon_r}}} \right) \right] dxdy
\end{aligned} \tag{3.8}
$$

The Frechet differential of $Q_{TV_\sigma}(\mathbf{p})$ is given by [18],

$$
\begin{aligned}
Q'_{TV_\sigma}(\sigma)h_\sigma &= -\int_\Omega h_\sigma \nabla.\left(\frac{\nabla\sigma(\mathbf{r})}{\sqrt{|\nabla\sigma(\mathbf{r})|^2+\alpha_\sigma}}\right)d\mathbf{r} \\
&= -\int_\Omega h_\sigma\left[\frac{\partial}{\partial x}\left(\frac{\frac{\partial\sigma}{\partial x}}{\sqrt{\left(\frac{\partial\sigma}{\partial x}\right)^2+\left(\frac{\partial\sigma}{\partial y}\right)^2+\alpha_\sigma}}\right)\right. \\
&\left.+\frac{\partial}{\partial y}\left(\frac{\frac{\partial\sigma}{\partial y}}{\sqrt{\left(\frac{\partial\sigma}{\partial x}\right)^2+\left(\frac{\partial\sigma}{\partial y}\right)^2+\alpha_\sigma}}\right)\right]dxdy
\end{aligned}
\tag{3.9}
$$

where $h=(h_{\varepsilon_r}(x,y),h_\sigma(x,y))$ is the differential of the parameter vector $\mathbf{p}$. The gradient of $Q_{TV}(\varepsilon_r)$ with respect to ε_r and $Q_{TV}(\sigma)$ with respect to σ given by Equation (3.10) and Equation (3.11) which also gives the information about the discontinuities in the reconstructed image. Therefore, the gradient magnitude of the $Q_{TV}(\varepsilon_r)$ with respect to ε_r is given by [26],

$$
\begin{aligned}
g_{TV_{\varepsilon_r}}(x,y) &= \nabla.\left(\frac{\nabla\varepsilon_r(\mathbf{r})}{\sqrt{|\nabla\varepsilon_r(r)|^2+\alpha_{\varepsilon_r}}}\right) \\
&= -\left(\frac{\partial}{\partial x}\left(\frac{u_{\varepsilon_r x}}{\sqrt{{u_{\varepsilon_r x}}^2+{u_{\varepsilon_r y}}^2+\alpha_{\varepsilon_r}}}\right)\right. \\
&\left.+\left(\frac{u_{\varepsilon_r y}}{\sqrt{{u_{\varepsilon_r x}}^2+{u_{\varepsilon_r y}}^2+\alpha_{\varepsilon_r}}}\right)\right)
\end{aligned}
\tag{3.10}
$$

The gradient of the $Q_{TV}(\sigma)$ with respect to σ is given by [26],

$$g_{TV_\sigma}(x,y) = \nabla.\left(\frac{\nabla\sigma(\mathbf{r})}{\sqrt{|\nabla\sigma(r)|^2+\alpha_\sigma}}\right) = -\left(\frac{\partial}{\partial x}\left(\frac{u_{\sigma x}}{\sqrt{{u_{\sigma x}}^2+{u_{\sigma y}}^2+\alpha_\sigma}}\right) + \left(\frac{u_{\sigma y}}{\sqrt{{u_{\sigma x}}^2+{u_{\sigma y}}^2+\alpha_\sigma}}\right)\right) \tag{3.11}$$

3.3.1 FBTS Simulation Primary Setup

The image reconstruction of a two-dimensional numerical model as explained in Section 3.2 considered to demonstrate the efficacy of FBTS technique. The resolution 1 mm x 1 mm is determined for the grid size of two-dimensional Finite-Difference Time-Domain (FDTD). Gaussian pulse with center frequency of 2 GHz, and 1.3 GHz of bandwidth applied as the signal source. The measured scattering data accumulated through numerical simulation and considering for TM_Z polarization, where the magnetic field is transverse to the z-direction. Absorbing boundary condition, CPML has been use to terminate the grid as shown in Figure 3.7.

In Figure 3.7, an example of eight arrays of antennas is surrounding the Region of Interest (ROI) where each of the antennas will act as a transmitter and receivers sequentially. The behavior of the antenna has been explain in Section 3.2. In FDTD-CPML set up, the background is using free space which the relative permittivity, ε_r, and conductivity, σ are fixed to ε_r = 1.0 and σ = 0.0, respectively.

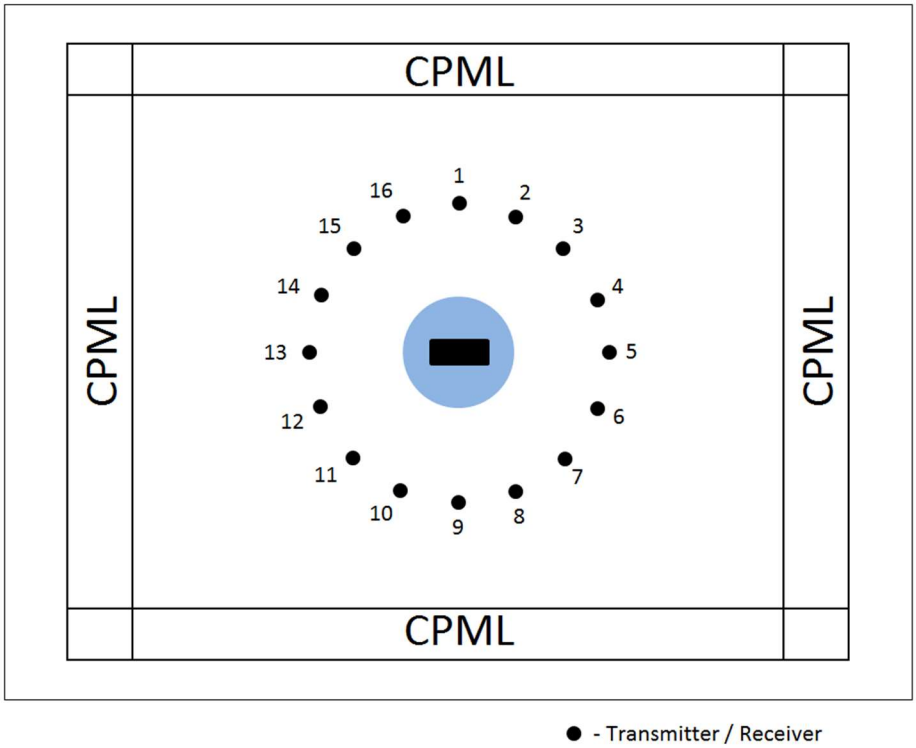

Figure 3.7: Two-Dimensional FDTD-CPML Set up in Object Reconstruction

The distance between the opposite antennas is 170 mm. The region of interest (ROI) is a circular shape with 40 mm of diameter. For the electrical properties of the object, the relative permittivity, ε_r is 21.45 and the conductivity, σ is 0.45 S/m. As for the ROI, the relative permittivity, ε_r was set to be 9.98 and conductivity, σ is 0.18 S/m. The initial guess chosen for relative permittivity, ε_r is 13.7 and the conductivity, σ is 0.20 S/m. The electrical properties values of the ROI, embedded objects, and initial guess remained the same for all simulations. The value of the regularization parameters, λ in this research was determined by means of numerical experiments as stated in Section 3.2. The individual values of λ are $\lambda_{\varepsilon_r} = 0.05$ for relative permittivity regularization parameter and $\lambda_{\sigma} = 0.006$ for conductivity regularization parameter. The value of small parameters is $\alpha_{\varepsilon_r} = \alpha_{\sigma} = 1.0 \times 10^{-24}$. These parameters set up are summarized as in Table 3.1 and be applied for all simulations.

Table 3.1: Simulation set up for object detection in free space

Object		Initial Guess		ROI Region		Background	
ε_r	σ (S/m)	ε_r	σ (S/m)	ε_r	σ (S/m)	ε_r	σ (S/m)
21.45	0.45	13.7	0.20	9.98	0.18	1.00	0.00
λ_{ε_r}		λ_σ		α_{ε_r}		α_σ	
0.05		0.0006		1.0×10^{-24}		1.0×10^{-24}	

The accuracy of the algorithm quantified by measuring the Mean Square Error (MSE). The MSE calculated as stated in Equation (3.12). $U(x, y)$ is the actual profile, $\acute{U}(x, y)$ is the reconstructed profile, and $M \times N$ is the dimension of the image.

$$MSE = \frac{1}{MN} \sum_{x=1}^{M} \sum_{y=1}^{N} \left[U(x, y) - \acute{U}(x, y)\right]^2 \tag{3.12}$$

3.3.2 Selection of Optimal Lambda Parameter and Small Parameter in TV Regularization Method

Determining an optimal value of regularization parameter is essential as it is an important criterion and should be determine carefully for a good solution. The regularization parameters, λ_{ε_r} and λ_σ in Equation (3.5) are the smoothing agent for the TV gradient, if it is too large for the solution, the reconstructed image will be over-smoothed. Applying a small-scale value of the parameters will give no effect of regularization for the reconstruction image. In this research, the value of λ_{ε_r} and λ_σ were considered by means of numerical experiments with references as in [28-30].

The ratio of the actual image over the reconstruction image are calculated in term of Improvement in Signal-to-Noise Ratio (ISNR) metric. A larger ISNR value indicates a greater quality of the reconstructed image, as it also yields a low Mean Square Error (MSE). The reconstructions executed for 100 iterations involving varying lambda values while other measurement set up remains the same.

The data obtained plotted into ISNR versus λ. The value of were λ_{ε_r} and λ_{σ} were determined by taking the highest peak value of the ISNR versus λ plot. Figure 3.9 and Figure 3.10 illustrate the plotted within the scale limit in order to ease finding the peak value, the optimal λ_{ε_r} and λ_{σ}. The regularization parameters in this research are λ_{ε_r}= 0.05 and λ_{σ} = 0.006. These parameters values, λ_{ε_r} and λ_{σ} were assumed applicable only for noise less environment.

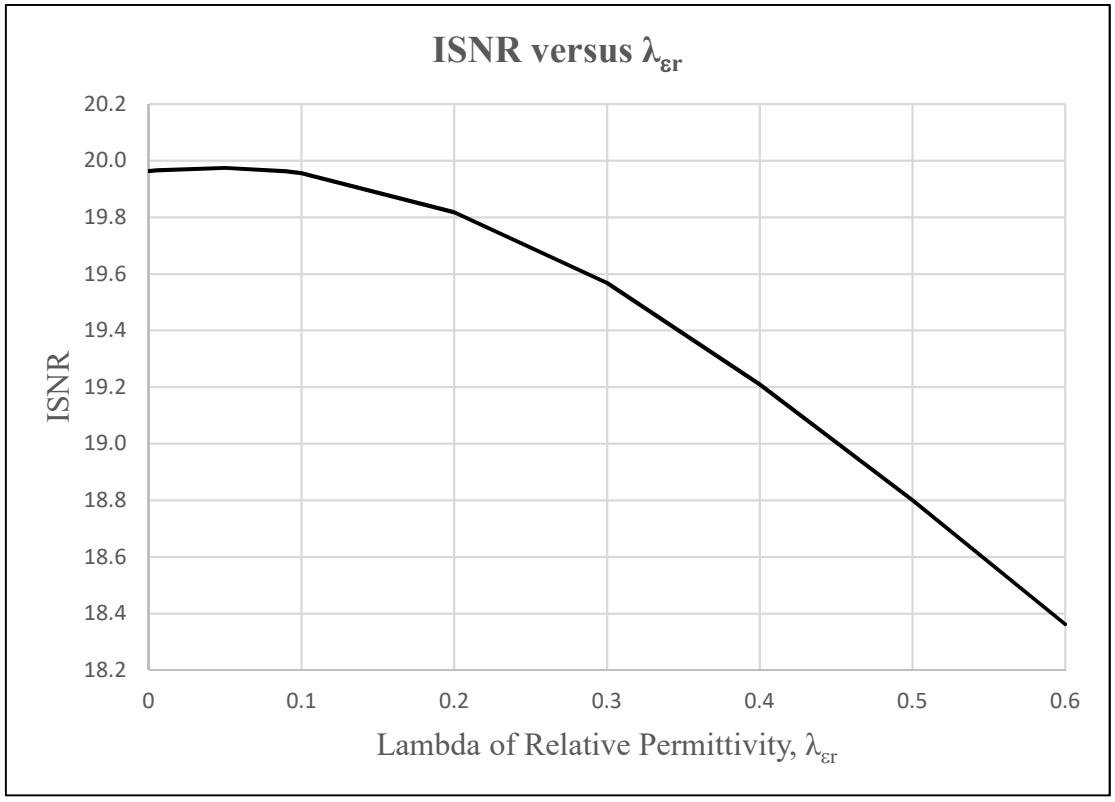

Figure 3.8: Selection of the Optimal Value of λ_{ε_r}

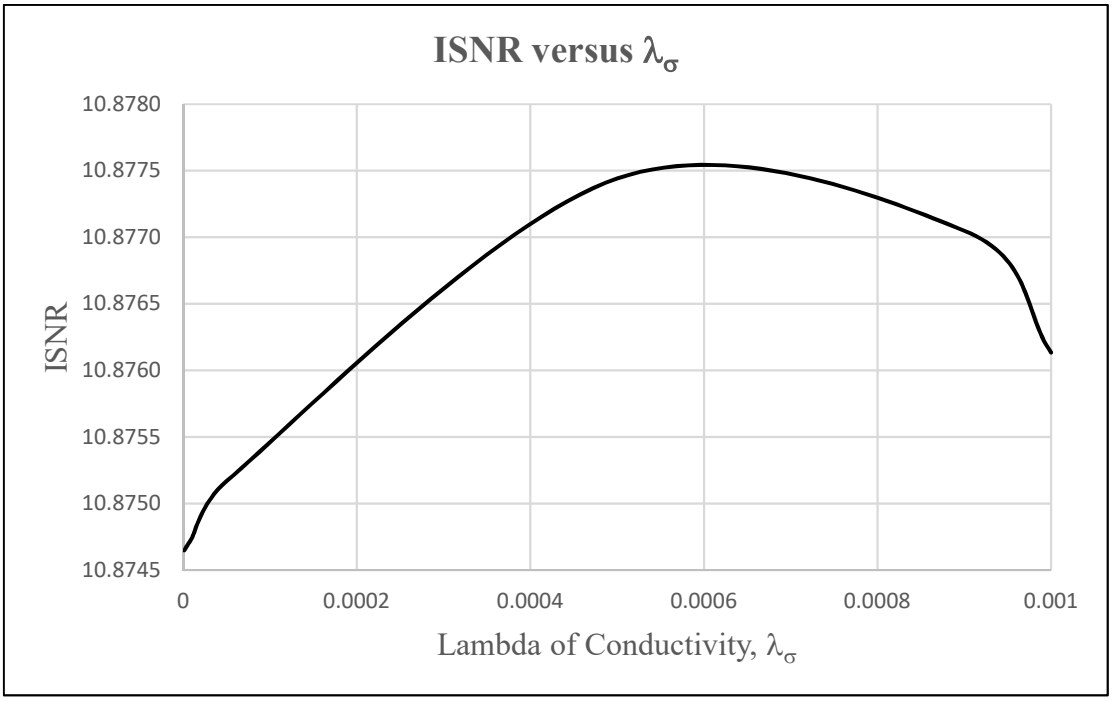

Figure 3.9: Selection of the optimal value of λ_σ

Other parameters that need to take into consideration is the small parameters, α_{ε_r} and α_σ. As the TV gradient is not differentiable at zero, the small parameters α_{ε_r} and α_σ with positive constant value are added in Equation (3.5). These parameters function are to avoid division by zero. The small parameters value should be small enough and not affect the TV gradient. In this research, the value of the small parameters is 1×10^{-24}.

3.3.3 FBTS-TV Regularization Flow Chart

The process flow of FBTS with TV regularization method represented as in Figure 3.11. Electrical properties obtained from FBTS method will be determined as initial condition for TV method. Throughout TV method calculation, new values of electrical parameters profiles are produced in which will be utilized in image reconstruction of ε_r and

σ will improve the correction to the estimation in optimization technique by giving a new values of gradient.

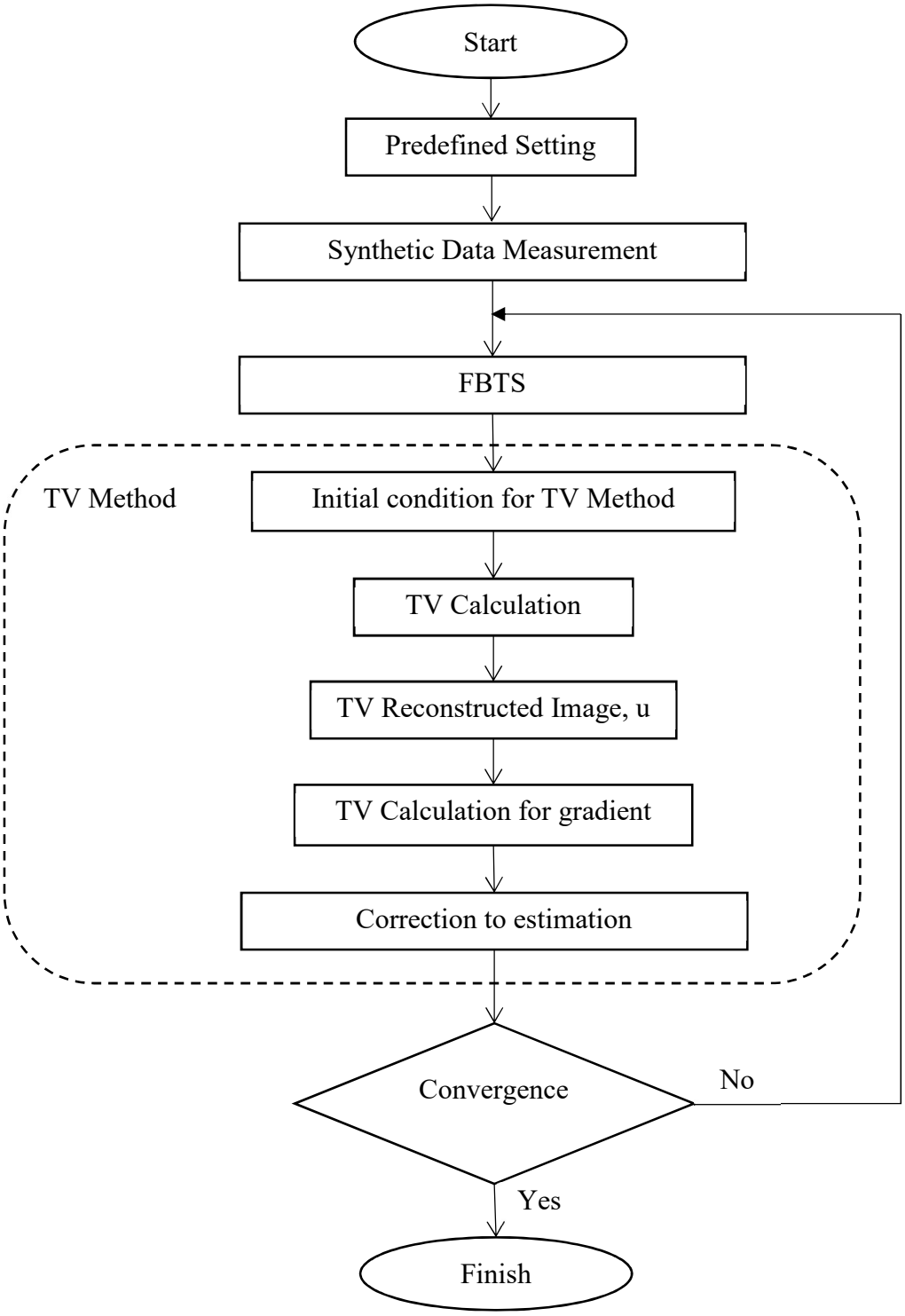

Figure 3.10: FBTS-TV Regularization Method Flow Chart

The gradient of conjugate gradient method, which has been utilize for FBTS, considered incorporating of TV method as in Equation (3.13). The weightage parameter β added to balance the TV gradient term [26].

$$g_{\varepsilon_r} = \int_0^T \sum_{m=1}^{M} \sum_{i=1}^{2} w_{mi}(\mathbf{p};\mathbf{r},t) \frac{d}{dt} v_{mi}(\mathbf{p};\mathbf{r},t) dt + \beta g_{TV_{\varepsilon_r}}$$
$$g_{\sigma} = \int_0^T \sum_{m=1}^{M} \sum_{i=1}^{2} w_{mi}(\mathbf{p};\mathbf{r},t) \frac{d}{dt} v_{mi}(\mathbf{p};\mathbf{r},t) dt + \beta g_{TV_{\sigma}} \quad (3\text{-}13)$$

3.4 Summary

Chapter 3 discusses the methods to be carried out in the research, which include FBTS method, and FBTS-TV regularization method. FBTS-TV method in Section 3.3 subdivided into the simulation primary setup, selection of optimal regularization parameters and small parameters, and flow chart of FBTS-TV method.

CHAPTER 4

RESULTS, ANALYSIS AND DISCUSSION

4.1 Overview

In this research, the Total Variation (TV) regularization method will be incorporate with Forward-Backward Time-Stepping (FBTS) inverse scattering technique to improve the reconstructed image by giving information such as its shape and location, and reconstructing sharp edges in the enclosed region that should give a better estimation of the image's boundaries. Numerical simulations carried out to investigate the effectiveness and any improvement of the reconstructed image of FBTS-TV regularization method. The image reconstruction considered of a two-dimensional numerical model. The analysis and discussion done based on the results obtained from the simulations.

4.2 Reconstruction of a Simple Object in Free Space by FBTS and FBTS-TV Regularization Method

Reconstruction of a simple object involving FBTS and FBTS-TV regularization simulation setup have been carried out to investigate the effectiveness and any improvement of the reconstructed image as regularization method applied to the FBTS system. The primary setup as explained in Section 3.3.1 is applied and presented. A simple object added into the ROI. The object is a rectangle shaped object with the length of 40 mm and width of 16 mm. The object placed at the center of the ROI. The ROI is a circular shape with 80 mm

of diameter. Figure 4.1 shows the actual profile of relative permittivity and conductivity of the embedded object through the accumulation of synthetic data.

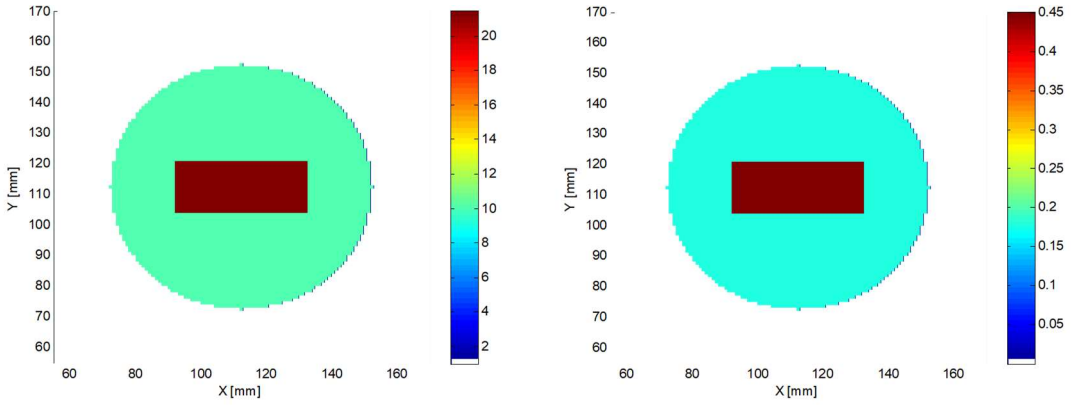

(a) (b)

Figure 4.1: Actual profile of the embedded object (a) relative permittivity (b) conductivity

4.2.1 Reconstruction of a Simple Object in Free Space with FBTS and FBTS-TV Regularization Method after 100th Iteration

The tests were been carry out in free space with 100 iterations and using 16 antennas. Figure 4.2 shows the reconstructed image of relative permittivity and conductivity of the embedded object by FBTS without applying regularization method. The results show that with FBTS simulation, both of the relative permittivity and conductivity been successfully reconstructed. However, the reconstructed ROI and embedded object have some vibrations, uneven surfaces, and smoothed edges. The uneven surfaces of the object is production of high total variations due to ill-posed in nature of solving inverse scattering problem. TV regularization method applied to improve FBTS image reconstruction. Figure 4.3 shows the reconstructed image of relative permittivity and conductivity of the embedded object by FBTS incorporating TV regularization method. The embedded object is reconstructed more firm and fewer vibrations which make the object detection more accurate. The uneven

surfaces appeared more flatten and smoothed as TV regularization method is implemented. TV regularization method regularize the high variations, smoothed out the surface and handle proper edges in the reconstructed object.

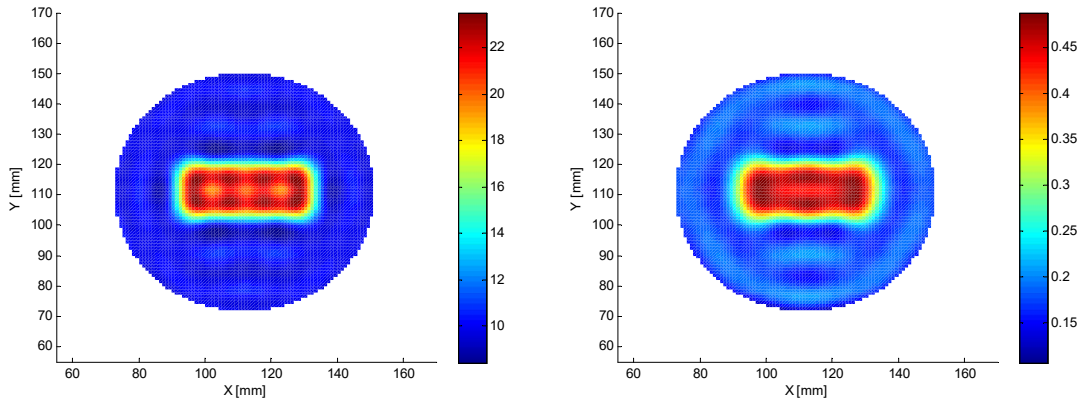

(a) (b)

Figure 4.2: Reconstruction of (a) relative permittivity (b) conductivity (by using FBTS method)

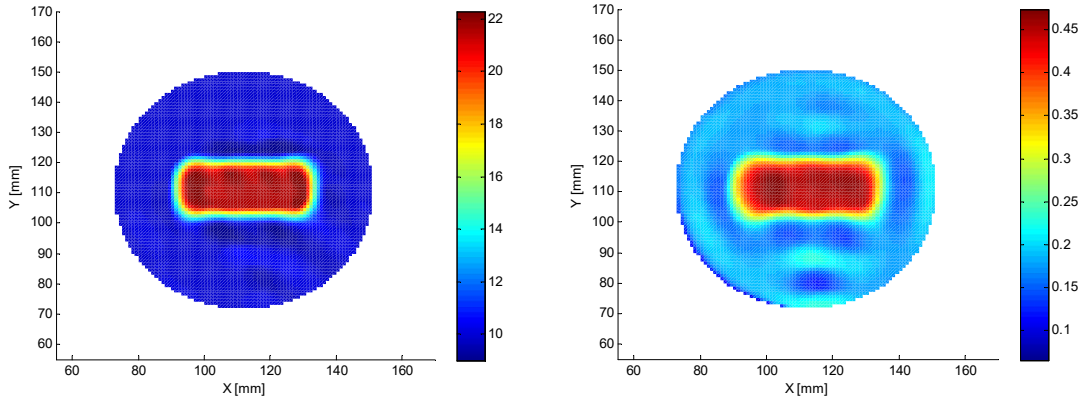

(a) (b)

Figure 4.3: Reconstruction of (a) relative permittivity (b) conductivity (by using FBTS-TV regularization method)

Figure 4.4 shows the cross-sectional view of comparing image reconstructed by FBTS with and without TV regularization method along the x-axis at y = 110 mm. From cross-sectional view, it is clear that the reconstructed image of relative permittivity and conductivity with TV regularization method is smoothed of irregular surface and more

accurate, thus resembling the actual image comparing to without using regularization method.

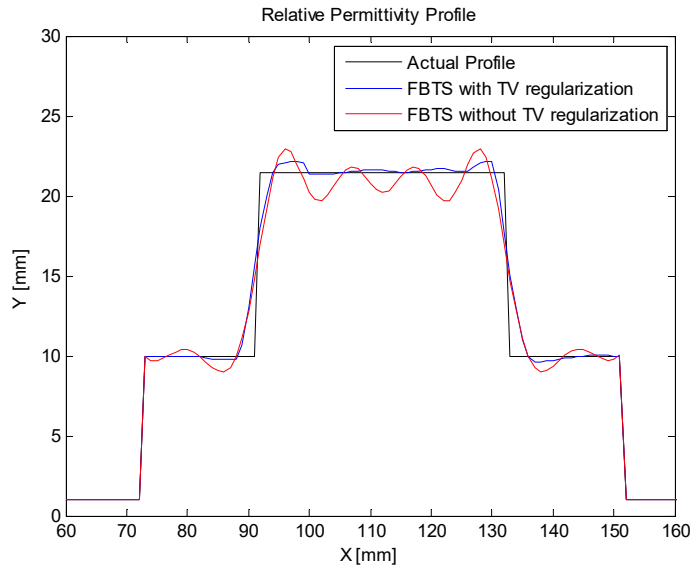

(a)

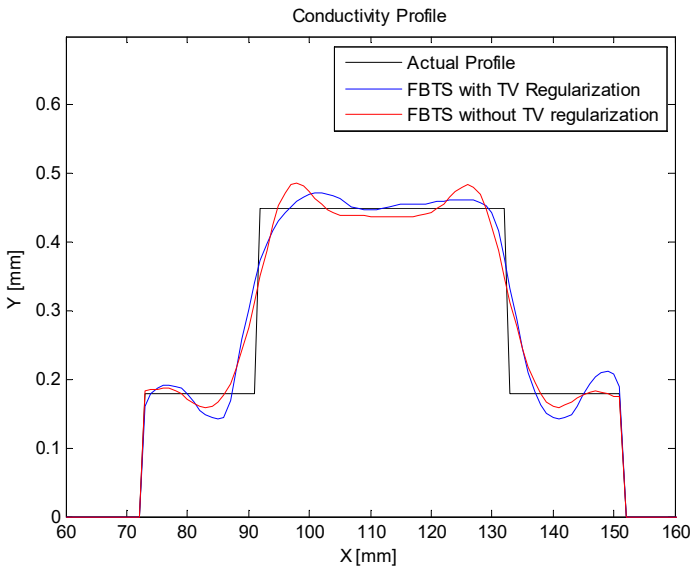

(b)

Figure 4.4: Reconstruction of (a) relative permittivity (b) conductivity (by using FBTS with and without TV regularization method) at cross sectional, y = 110 mm

Reconstruction of relative permittivity utilizing FBTS with regularization method, 1.3221 has a lower MSE value compare to the reconstruction without TV regularization method, 1.5488. The lower value of MSE indicated a better production of image

reconstruction which is by utilizing TV regularization method because TV regularization gave the proper side constraints that lead to more stabilized solution. Conductivity reconstruction utilizing FBTS with regularization method also give a good result and shown a small value of MSE. Table 4.1 shows the MSE value of the performance of FBTS incorporated with and without TV regularization method after the 100^{th} iteration. The algorithm is executed until 100 iterations because the solution has met convergence criterion.

Table 4.1: The MSE value of reconstruction by using FBTS with and without TV Regularization Method

MSE Value	ε_r	σ
Without TV regularization	1.5488	0.0011
With TV regularization	1.3221	0.0012

The MSE value for reconstruction of relative permittivity without TV regularization method is 1.5488 while with TV regularization method is 1.3221. The percentage of improvement for the reconstruction of relative permittivity with TV regularization method over the reconstruction of relative permittivity without TV regularization is 14.64%. The MSE value for reconstruction of conductivity without TV regularization method is 0.0011, and with TV regularization, method is 0.0012. The percentage of the reconstruction of conductivity with TV regularization method over the reconstruction of conductivity without TV regularization is -9.10%. The negative value shown a slight degradation for reconstruction of conductivity when regularization applied. The degradation for reconstruction of conductivity expected due to the cost functional as stated in Equation (3.5) is more sensitive to relative permittivity variations than in conductivity variations.

4.2.2 Reconstruction of a Simple Object in Free Space with FBTS-TV Regularization Method after 200th Iteration

Reconstruction of a simple object of FBTS-TV regulation with similar simulation setup as in Section 3.3.1 has been carry out to investigate for any improvement in reconstruction due to a higher number of iteration. The actual profile of relative permittivity and conductivity are as shown in Figure 4.1. Reconstructions of relative permittivity and conductivity through FBTS-TV regularization method are as shown in Figure 4.5. Based on the results, it is observed that reconstruction of relative permittivity and conductivity shown the presence of an object in the ROI accurately. The embedded object is reconstructed more firm and the uneven surface observed more flat and smoothed, therefore, it is easily differentiated from the background.

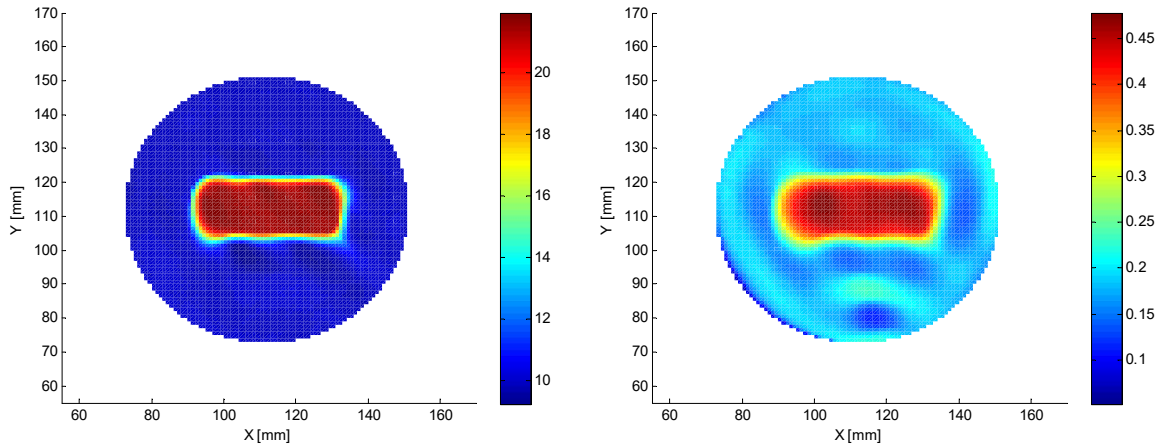

(a) (b)

Figure 4.5: Reconstruction of (a) relative permittivity (b) conductivity (by using FBTS-TV regularization method) after 200th iteration

In Figure 4.6 the cross-sectional view is taken along the x-axis at y = 110 mm to compare the actual object with reconstruction image. For reconstruction of relative permittivity, it is proven that the reconstruction has been successfully assembled as it actual

object. There is an improvement in the reconstruction of the conductivity compared than in 100th iteration. The reconstruction at 200th iteration in Figure 4.6 had shown a more even and fewer vibrations surface for both relative permittivity and conductivity comparing than in Section 4.2.1, due to increment of optimization processes in finding optimal or nearly optimal solution for FBTS-TV method.

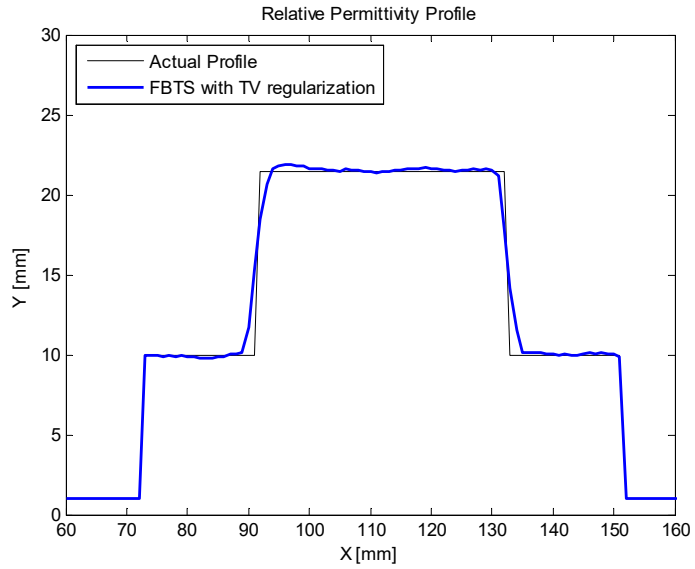

(a)

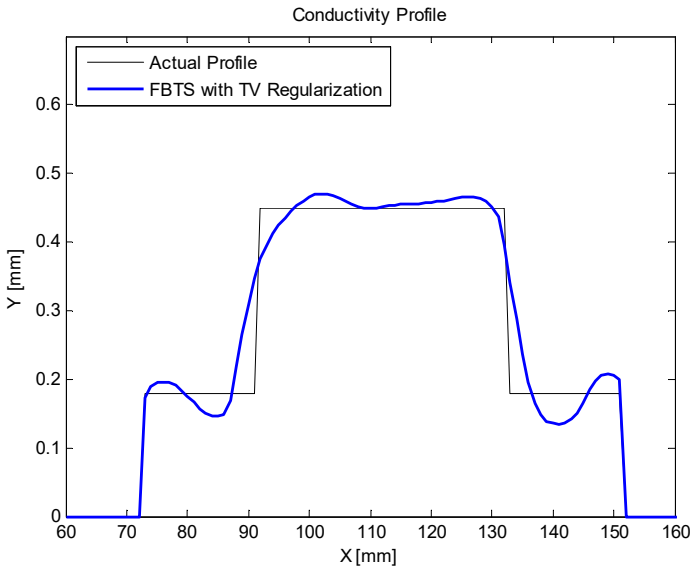

(b)

Figure 4.6: Reconstruction of (a) relative permittivity (b) conductivity (by using FBTS with TV regularization method) at cross sectional, y = 110 mm

The MSE value for FBTS-TV regularization through 200th iteration of reconstructing relative permittivity and conductivity shown as in Figure 4.7. MSE value for FBTS with TV regularization method of relative permittivity decreased proportionally with iteration as expected. The smallest value of MSE yields at 198th iteration, whereas the MSE value of relative permittivity is 0.9982 and conductivity is 0.0012, respectively. Throughout this simulation, the reconstruction of relative permittivity and conductivity is improving along the increment of the number of iteration.

After 198th iteration, the MSE value for relative permittivity and conductivity increased, hence concluded the best performance of the TV regularization algorithm is at 198th iteration and does not need further iterations thereafter.

Both of the plots showed a rapid decrement of MSE value until the 40th iteration. However, for conductivity, MSE value increased from the beginning of iteration and then rapidly decreased starting from the fifth iteration. It observed that the reconstruction relative permittivity and conductivity are progressing positively to shape up as the actual object starting from the 20th iteration. Figure 4.8 shows the Normalized Error Functional of the FBTS-TV regularization method through 200th iteration. This shows that the iteration of FBTS-TV regularization method is convergence enough for all simulations.

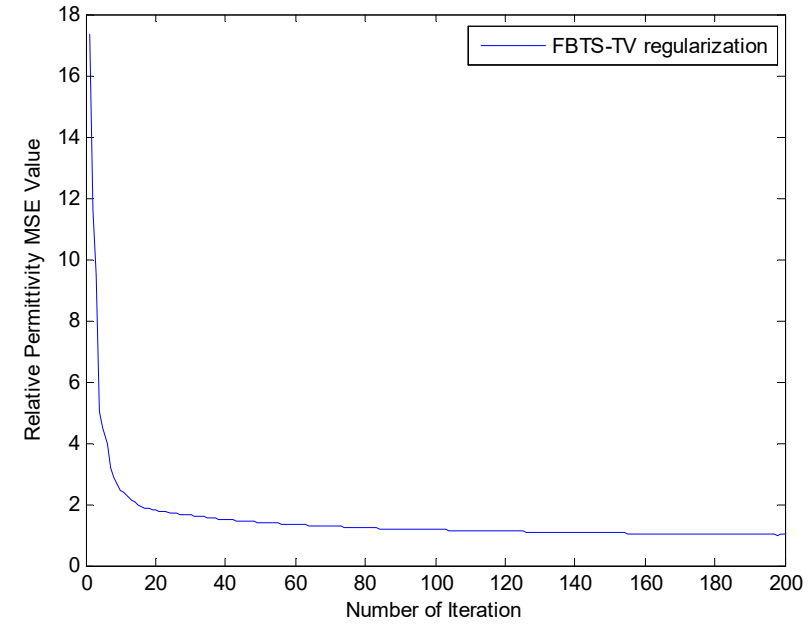

(a)

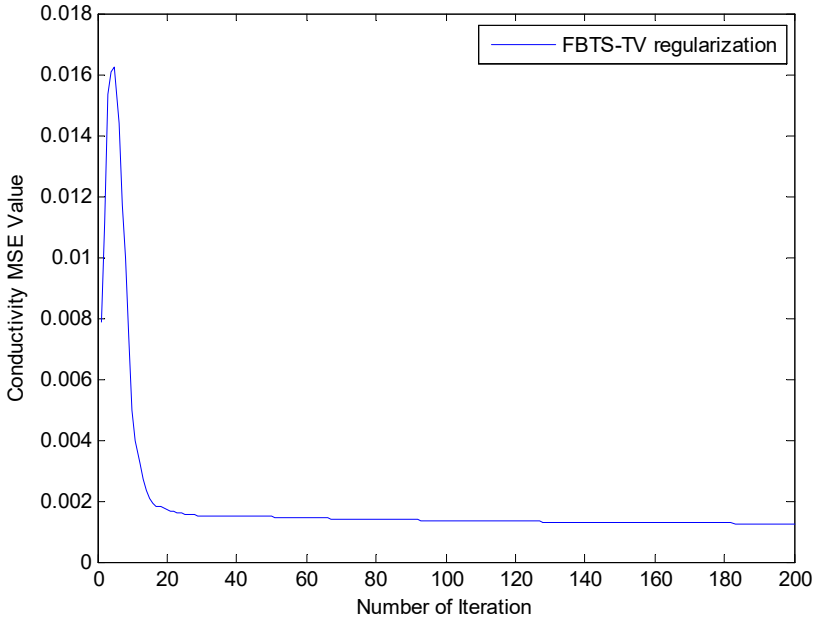

(b)

Figure 4.7: MSE calculation for reconstruction of (a) relative permittivity (b) conductivity (by using FBTS-TV regularization method) versus number of iteration

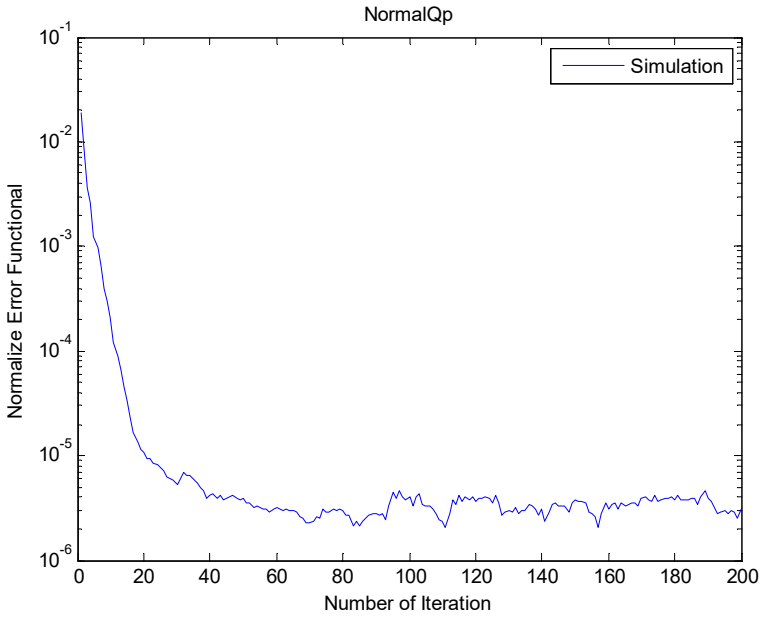

Figure 4.8: Normalized Error Functional versus number of iteration of FBTS-TV regularization method

4.2.3 Reconstruction of a Simple Object in Free Space with FBTS-TV Regularization Method with Different Regularization Parameter, λ Selection

Reconstruction of a simple object of FBTS-TV regulation with similar simulation setup as in Section 3.3.1 has been carry out to investigate for any improvement in reconstruction with the different value of the regularization parameters. The tests were carry out in free space with 100 iterations and using 16 antennas. The efficacy of the FBTS-TV depends on the selection of its non-negative regularization parameter, the optimal lambda, λ. Thus, the selection of λ should be carefully chosen. The regularization parameter compromises the level of irregularities of the reconstruction with the closeness reconstruction toward the actual object. The regularization parameters involved in this section are λ_{ε_r} for relative permittivity and λ_{σ} for conductivity reconstruction. The actual profile of relative permittivity and conductivity as shown in Figure 4.1.

Figure 4.9 shows the relative permittivity reconstruction with three different values of regularization parameters, λ_{ε_r}; 0.005, 0.05 and 0.5. The cross-sectional view of the relative permittivity reconstructions for those varying regularization parameters are taken along the x-axis at y = 110 mm is shown in Figure 4.10.

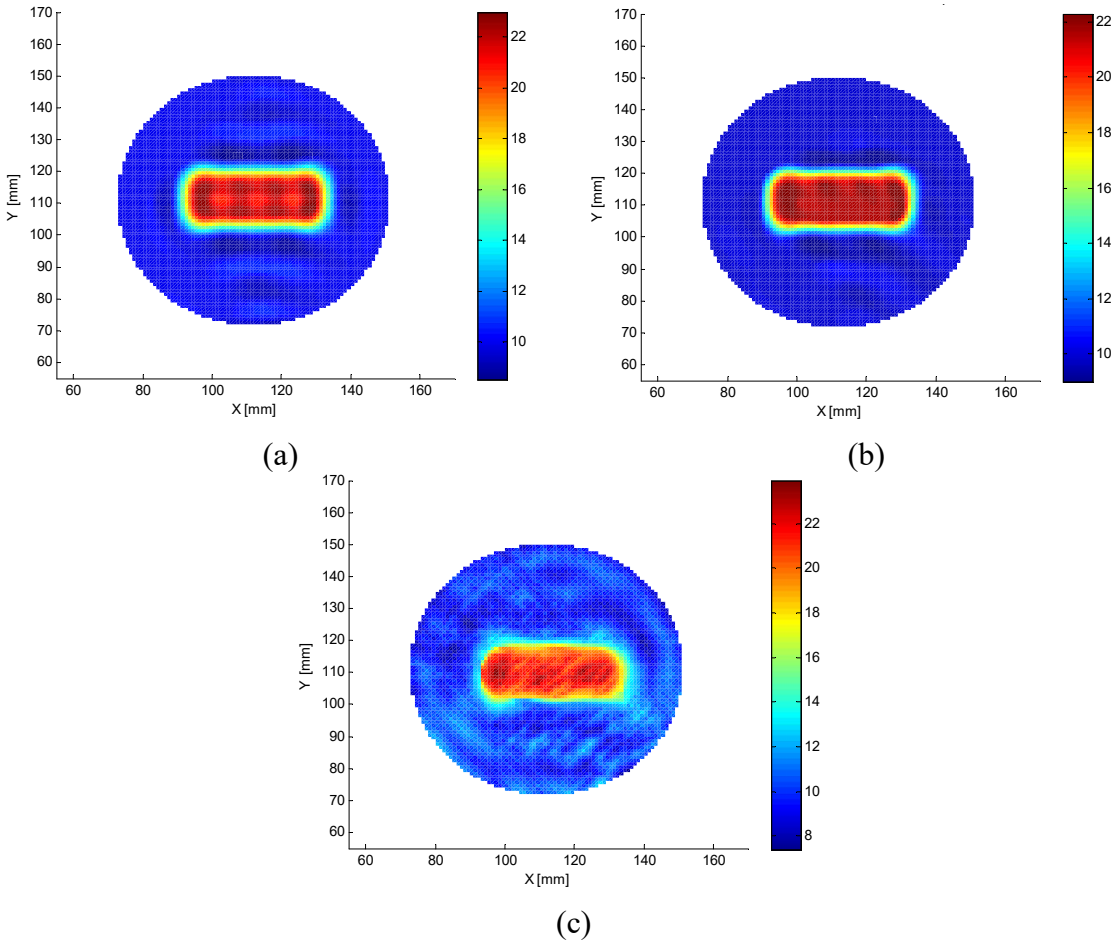

Figure 4.9: Reconstruction of relative permittivity (by using FBTS-TV regularization method) with λ_{ε_r} values (a) 5×10^{-3} (b) 5×10^{-2} (c) 5×10^{-1}

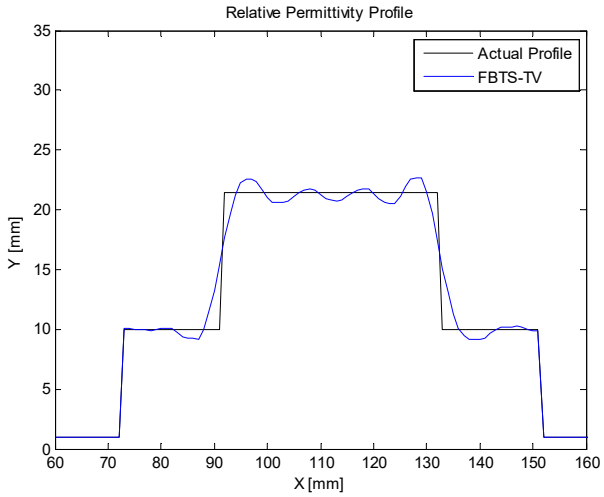

(a)

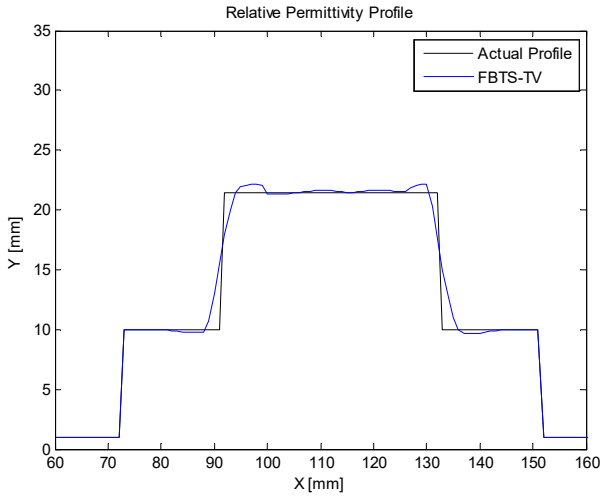

(b)

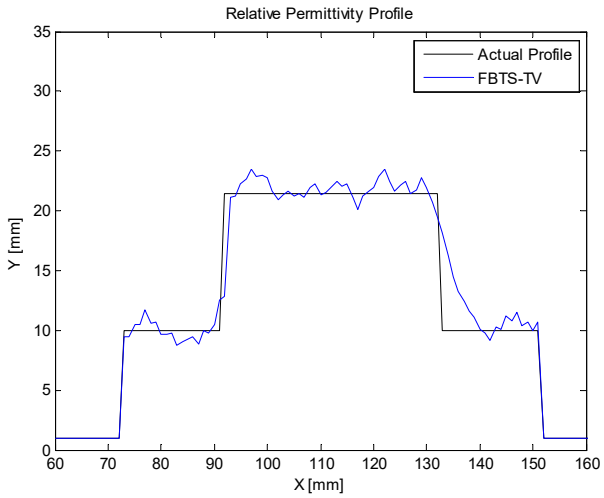

(c)

Figure 4.10: Reconstruction of relative permittivity (by using FBTS-TV regularization method) with λ_{ε_r} values (a) 5×10^{-3} (b) 5×10^{-2} (c) 5×10^{-1} at cross sectional, y = 110 mm

It is observed from Figure 4.9 and 4.10, for the case of relative permittivity reconstruction, when the value of λ_{ε_r} increased the irregularities of the reconstruction is also increased. Hence, for the reconstruction of relative permittivity with $\lambda_{\varepsilon_r} = 5 \times 10^{-1}$, the object suffers from many irregularities that make the reconstructed corrupted and failed to recognize.

However, for a smaller value of $\lambda_{\varepsilon_r} = 5 \times 10^{-3}$, the image reconstruction of the relative permittivity resembled the FBTS reconstruction without regularization as shown in Figure 4.2(a), as if there is no regularization applied. Reconstruction of relative permittivity for $\lambda_{\varepsilon_r} = 5 \times 10^{-2}$ yields a better performance as it gave a tradeoff between a very irregular reconstruction and non-regularized reconstruction.

Figure 4.11 shows the image reconstruction of conductivity with three different values of λ_σ; 6×10^{-6}, 6×10^{-4} and 6×10^{-3}. The cross-sectional view of the conductivity reconstructions for those varying regularization parameters are taken along the x-axis at y = 110 mm is shown in Figure 4.12. In Figure 4.11 and Figure 4.12, varying the regularization parameters, λ_σ gave impact to the conductivity reconstruction. In the case of conductivity reconstruction, the regularization parameter, λ_σ controls how much smoothing is performed, a higher value of the λ_σ will give a higher degree of smoothing. For the higher value of $\lambda_\sigma = 6 \times 10^{-3}$, conductivity reconstruction of the object is over-smoothed and do not preserve the interesting edges. Selection of a small value of $\lambda_\sigma = 6 \times 10^{-6}$ in return gives a no regularization effect to the conductivity reconstruction and it is similar as FBTS reconstruction as shown in Figure 4.2(b).

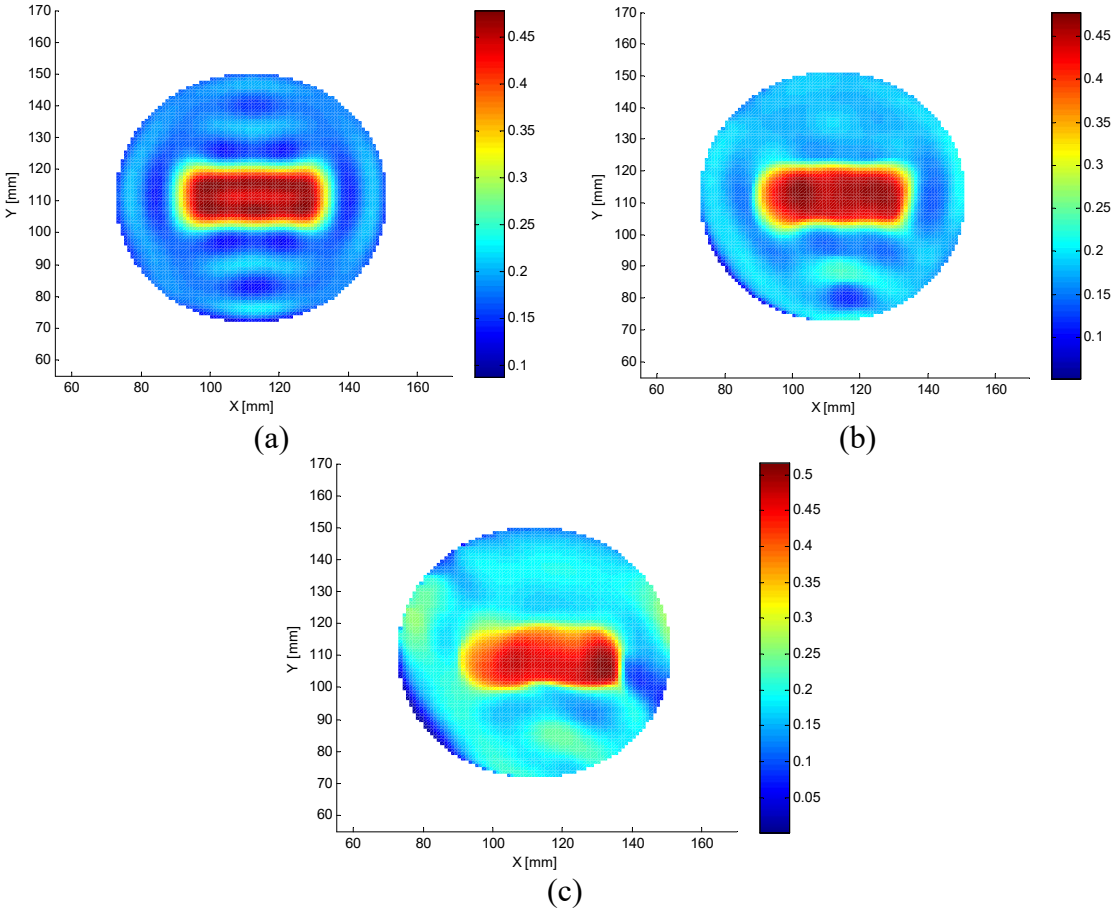

Figure 4.11: Reconstruction of conductivity (by using FBTS-TV regularization method) with values λ_σ values (a) 6×10^{-6} (b) 6×10^{-4} (c) 6×10^{-3}

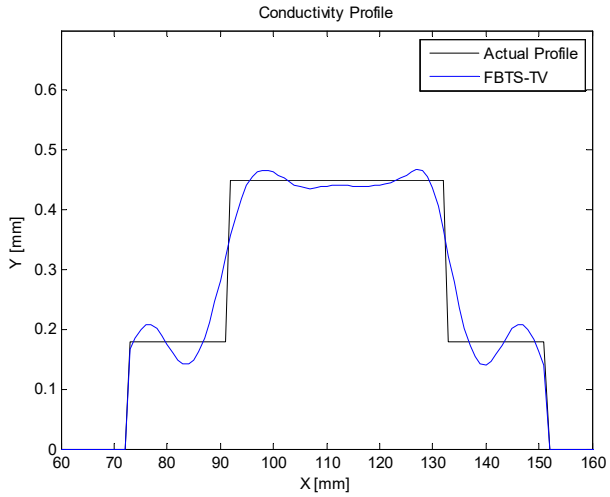

(a)

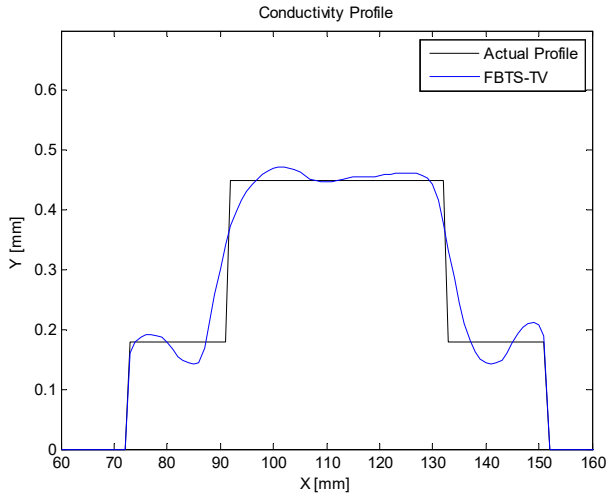

(b)

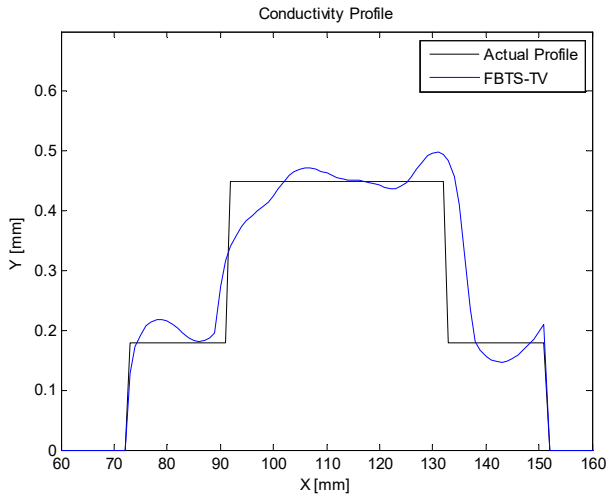

(c)

Figure 4.12: Reconstruction of conductivity (by using FBTS-TV regularization method) with values λ_σ values (a) 6×10^{-6} (b) 6×10^{-4} (c) 6×10^{-3} at cross sectional, y = 110 mm

Regularization parameter of $\lambda_\sigma = 6 \times 10^{-4}$ is preferable to give optimal quality of reconstruction because it provides a compromised solution between over-smoothed and no regularization of the conductivity reconstruction.

Table 4.2 shows the MSE calculation for reconstruction by using FBTS-TV regularization method for different values of regularization parameters. From Table 4.2, as compared for all regularization parameter values, relative permittivity reconstruction with regularization parameter $\lambda_{\varepsilon_r} = 5 \times 10^{-2}$ gives the smallest MSE value, 1.3221. Reconstruction of conductivity showed no improvement as the regularization parameter increased from $\lambda_\sigma = 6 \times 10^{-6}$ to $\lambda_\sigma = 6 \times 10^{-4}$ however, worsen if the parameter is too high, as in the case $\lambda_\sigma = 6 \times 10^{-3}$. The degradation of conductivity reconstruction at the higher regularization parameter, $\lambda_\sigma = 6 \times 10^{-3}$ due to the fact it is a high sensitivity field, whereas a small difference by the parameter will fluctuate data measurement. The reconstruction of both relative permittivity and conductivity suffer the most degradation when higher value of regularization parameter is applied. For the highest regularization parameter $\lambda_{\varepsilon_r} = 5 \times 10^{-1}$ the MSE value is 2.9383 and for $\lambda_\sigma = 6 \times 10^{-3}$ the MSE value is 0.0037.

Table 4.2: The MSE value for reconstruction of relative permittivity and conductivity (by using FBTS-TV regularization method) with different regularization parameter values

λ_{ε_r}	MSE Value	λ_σ	MSE Value
5×10^{-3}	1.5565	6×10^{-6}	0.0012
5×10^{-2}	1.3221	6×10^{-4}	0.0012
5×10^{-1}	2.9383	6×10^{-3}	0.0037

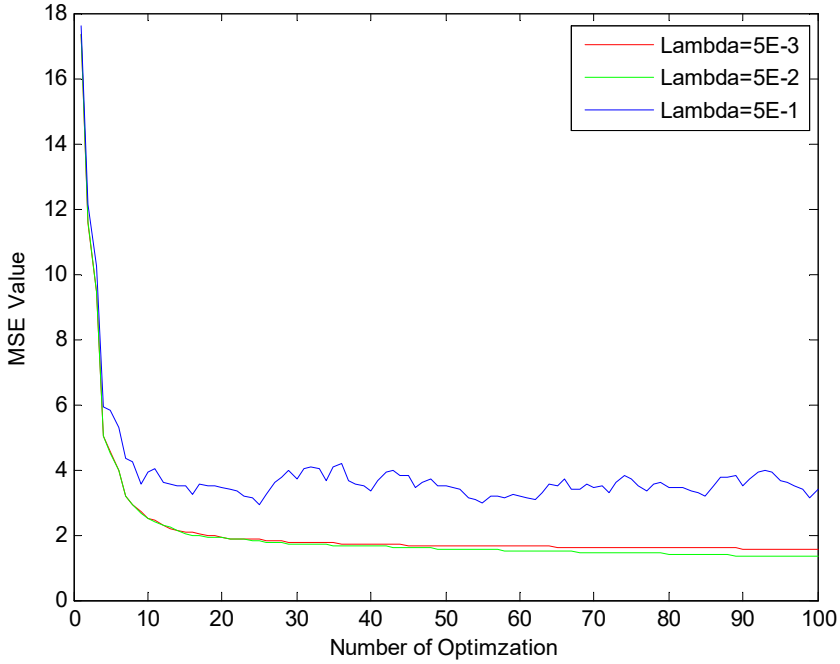

(a)

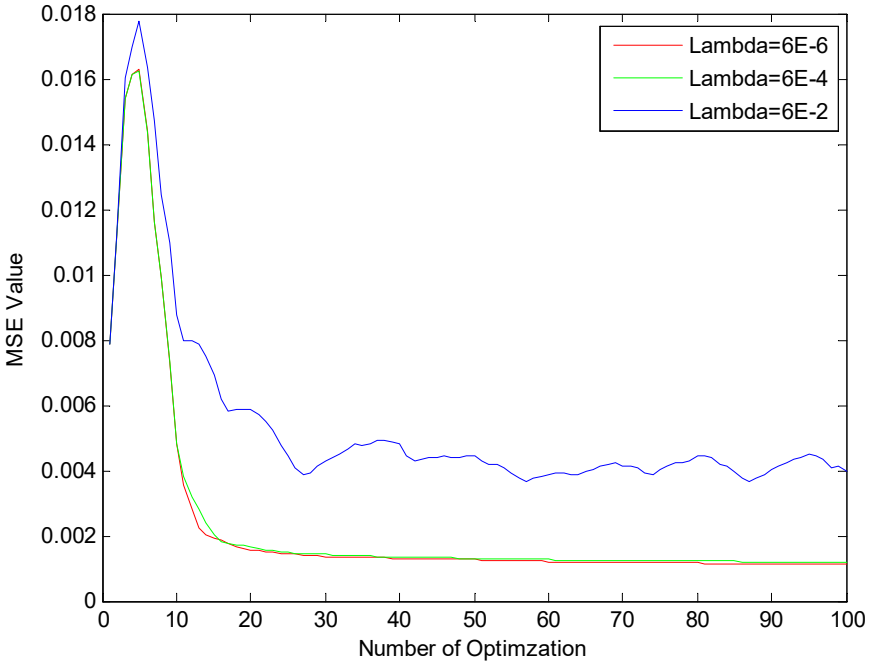

(b)

Figure 4.13: MSE calculation for reconstruction of (a) relative permittivity (b) conductivity (by using FBTS-TV regularization method) with different regularization parameter values versus number of iteration

MSE values for the reconstructions or relative permittivity and conductivity with different regularization parameter values as presented in Figure 4.13. Smaller MSE value yields less error hence more accurate reconstruction and vice versa. Based on Figure 4.13, it is proven that the selection of optimal lambda for relative permittivity, $\lambda_\sigma = 6 \times 10^{-4}$ and conductivity $\lambda_\sigma = 6 \times 10^{-6}$ give a better performance of FBTS-TV reconstruction because they give the smallest MSE value.

4.3 Reconstruction of a Simple Object in Free Space by FBTS-TV Regularization Method with Different Number of Antennas

This section focuses on the reconstruction of a simple object by FBTS-TV regularization utilizing the different number of antennas. The simulation setup applied as described in Section 4.2. A simple object of rectangular shape with the length of 40 mm and width of 16 mm embedded in the ROI. The object placed at the center of the ROI. The ROI is a circular shape with 80 mm in diameter. The test carried out in free space for 100 iterations. The actual profile of relative permittivity and conductivity are as shown in Figure 4.1. The different number of antennas located surrounding the ROI to investigate if the number of antennas will contribute to the effectiveness of the image reconstruction. Four different set of antenna configuration is applied in this section are 4, 8, 16 and 20 antennas setup. Figure 4.14 shows the antennas setup in the FDTD lattice. The coordinates for 4, 8, 16 and 20 antennas were summarize in Table 4.3 through Table 4.6.

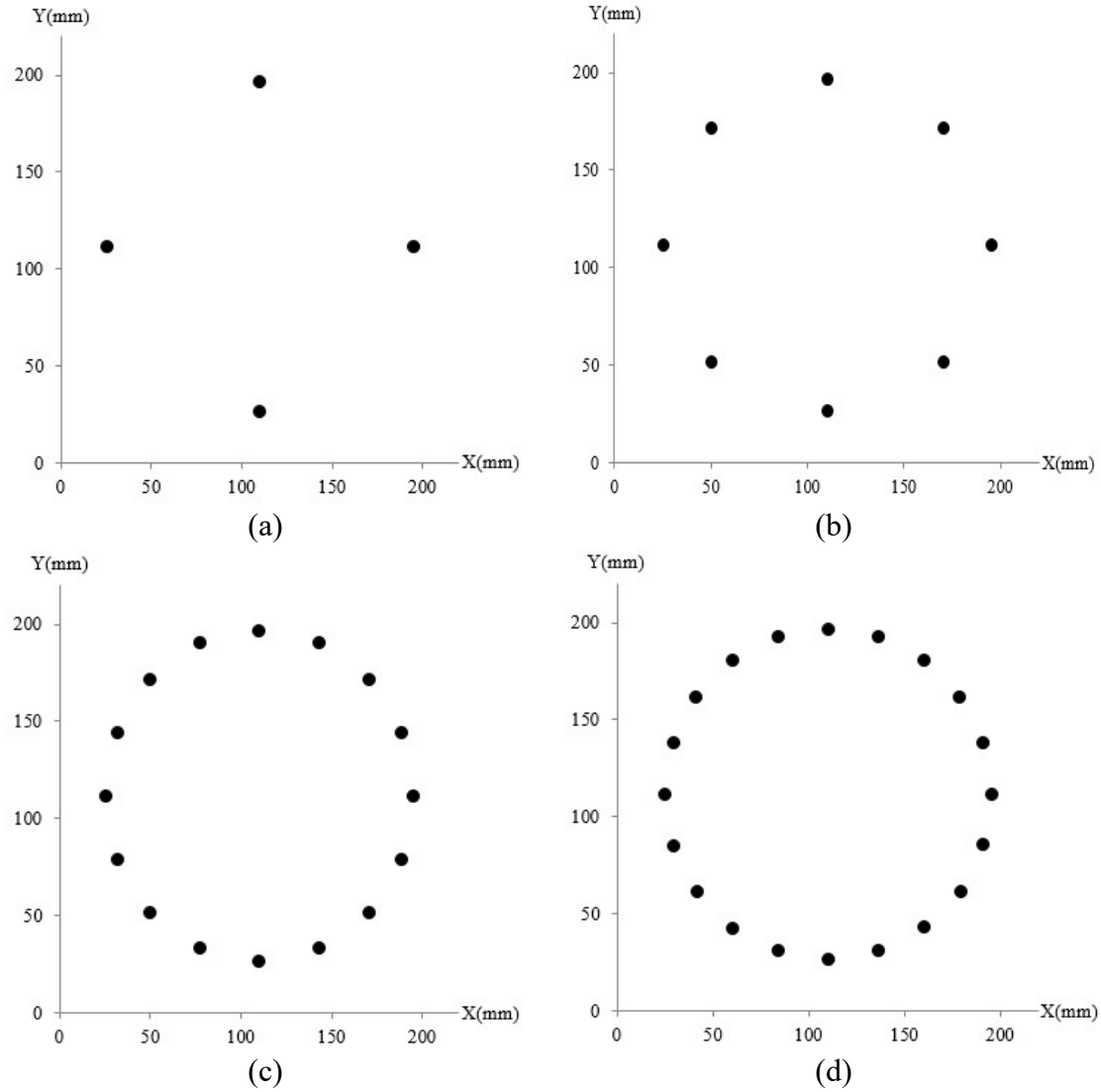

Figure 4.14: Antenna configurations of (a) 4 antenna (b) 8 antenna (c) 16 antenna (d) 20 antenna arrays

Table 4.3: Coordinate for 4 antenna arrays

Antenna	Coordinate	
	X	Y
1	26	111
2	111	26
3	196	111
4	111	196

Table 4.4: Coordinate for 8 antenna arrays

Antenna	Coordinate		Antenna	Coordinate	
	X	Y		X	Y
1	111	196	5	111	26
2	51	171	6	171	51
3	26	111	7	196	111
4	51	51	8	171	171

Table 4.5: Coordinate for 16 antenna arrays

Antenna	Coordinate		Antenna	Coordinate	
	X	Y		X	Y
1	171	171	9	51	51
2	144	190	10	79	32
3	111	196	11	111	26
4	78	190	12	144	32
5	51	171	13	171	51
6	32	144	14	190	79
7	26	111	15	196	111
8	32	78	16	190	144

Table 4.6: Coordinate for 20 antenna arrays

Antenna	Coordinate		Antenna	Coordinate	
	X	Y		X	Y
1	180	161	11	42	61
2	161	180	12	61	42
3	137	192	13	85	30
4	111	196	14	111	26
5	85	192	15	137	30
6	61	180	16	161	42
7	42	161	17	180	61
8	30	137	18	192	85
9	26	111	19	196	111
10	30	85	20	192	137

While one of the antennas acts as a transmitter, the other antennas remain as receiving antennas. The set of scattering calculation representing transmitter-receiver combinations is as shown in Table 4.7. Adding more antennas will increase the number of scattering calculations and provide more collection of the electric field data, hence will improve the reconstruction of the relative permittivity and conductivity. However, the addition of antenna will increase the computational time and data storage.

Table 4.7: Set of scattering calculation of transmitter-receiver combinations

	Array of Antenna Configuration			
	4	8	16	20
Set of scattering calculation	12	56	240	380

Figure 4.15 shows the reconstruction of the relative permittivity of FBTS-TV regularization method acquired by the different number of antenna configurations. The reconstruction of relative permittivity quality is progressing successfully as the number of antenna added. An addition of antenna will give more information of the unknown parameter and allowing a more accurate reconstruction of the object. There is a significant improvement of reconstruction obtained from 4 arrays to 16 antenna arrays configuration. There is a slight improvement obtained from 16 to 20 antenna arrays.

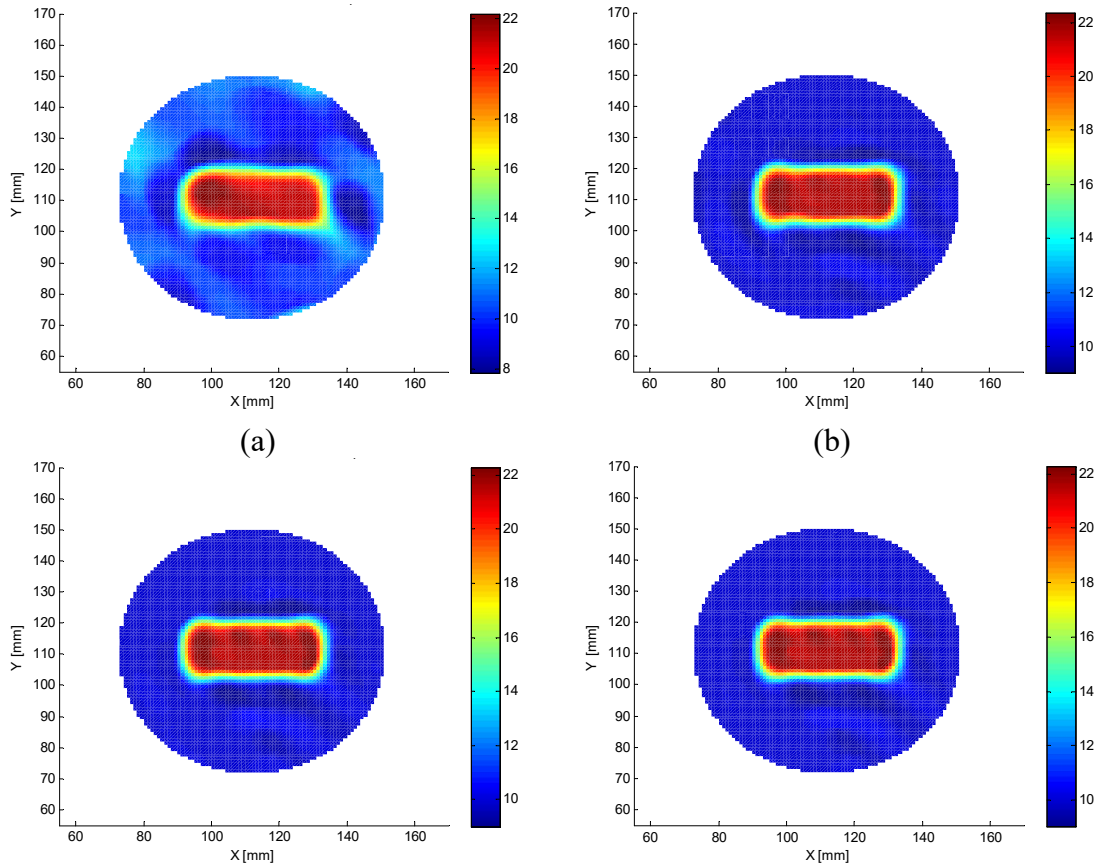

Figure 4.15: Reconstruction of relative permittivity (by using FBTS-TV regularization method) by (a) 4 antenna (b) 8 antenna (c) 16 antenna (d) 20 antenna arrays

The comparison of image reconstruction of relative permittivity obtained by the different number of antenna arrays at cross sectional y = 110 mm as shown in Figure 4.16. The detection and reconstruction of the embedded object is successful by all antenna arrays. The 4 antenna arrays showed the poorest reconstruction of the object and the best reconstruction of the object is obtained by 20 antenna arrays configuration.

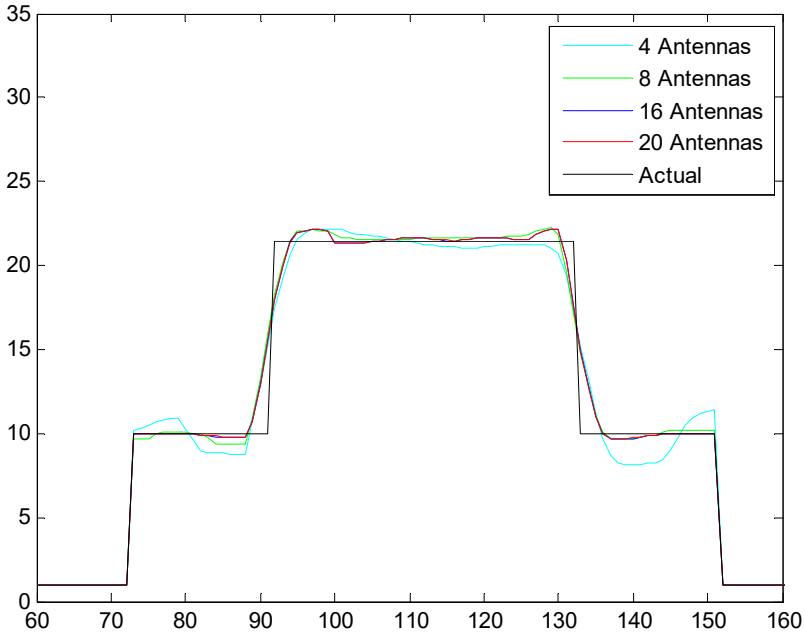

Figure 4.16: Reconstruction of relative permittivity (by using FBTS-TV regularization method) for different antenna arrays at cross sectional, y = 110 mm

The comparison of the relative permittivity reconstruction is also determined through calculation of MSE value as described in Equation (3.12). The MSE value obtained throughout the time of iterations for each antenna configuration represented in Figure 4.17. The MSE values for all simulation declining through 100 iterations. After the 100th iteration, the 4 antenna arrays configuration have the highest MSE value, 2.5937 while the lowest MSE value with the least error in relative permittivity reconstruction of the object is produced by the 20 antenna arrays configuration, 1.3152. There is a slight improvement of 1.3% for relative permittivity reconstruction by 20 over 16 antenna arrays.

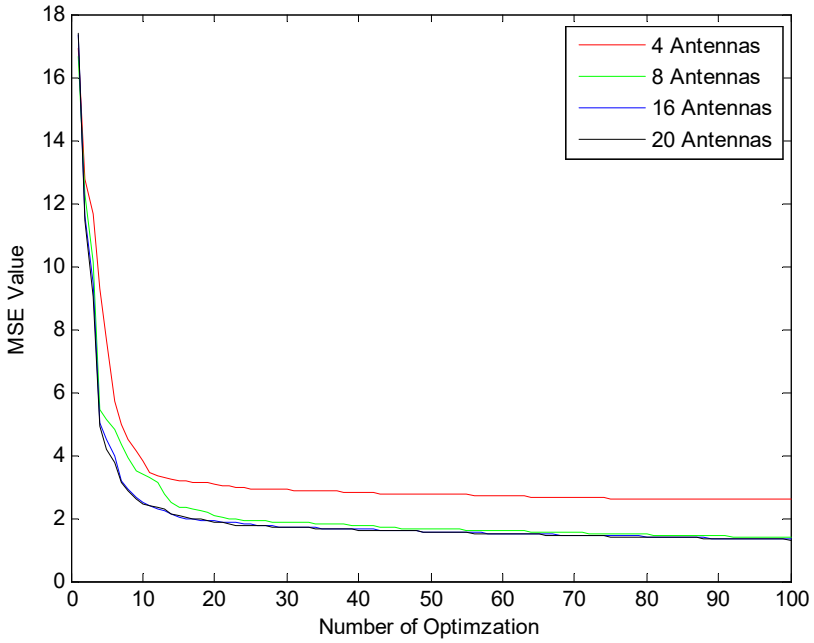

Figure 4.17: MSE calculation for reconstruction of relative permittivity (by using FBTS-TV regularization method) for different antenna arrays

Image reconstruction of a simple object for conductivity with FBTS-TV regularization method obtained by the different number of antenna configurations as illustrated in Figure 4.18. Through observation, increasing the number of antennas will produce more information about the object and therefore improve the quality of image reconstruction. The detection and reconstruction of the object can be achieved for all antenna configurations except for 4 antenna arrays. The reconstruction of conductivity using 4 antenna arrays is distorted and poorly reconstructed because of insufficient information about the scattering field gathered from the antennas. Image reconstruction of conductivity with 8 antenna arrays shown a noticeable object but has some vibrations. On the other hand, 16 and 20 antenna arrays configuration give a good quality of reconstruction and closer to the actual properties of the object.

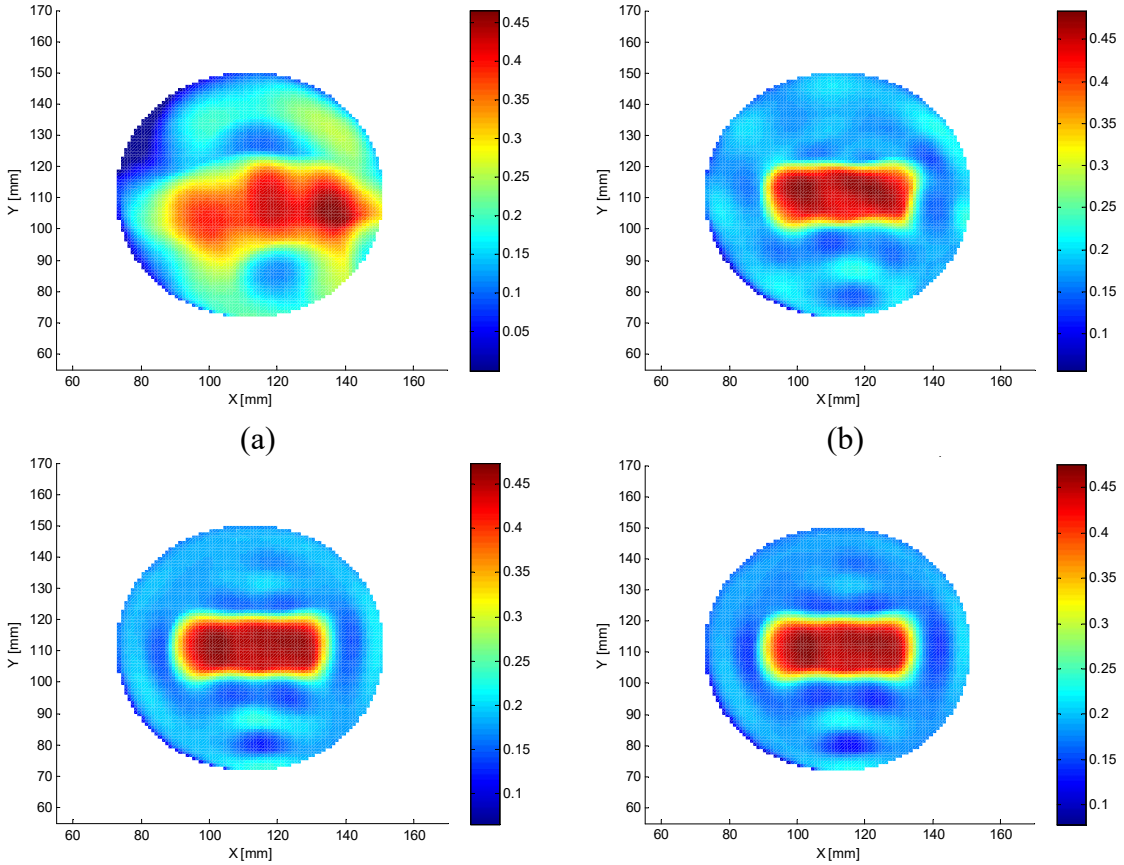

Figure 4.18: Reconstruction of conductivity (by using FBTS-TV regularization method) by (a) 4 antenna (b) 8 antenna (c) 16 antenna (d) 20 antenna arrays

Figure 4.19 shown the cross-sectional view taken at y = 110 mm the reconstruction of conductivity for all antenna configurations. Reconstruction of conductivity using 4 antenna arrays is distorted whereas the boundary of the object was poorly reconstructed, while the other reconstruction by 8, 16, and 20 antenna arrays configurations show a small scale of variances among them. Reconstruction by 16 and 20 antenna arrays were closer to actual object compare than using other antenna arrays.

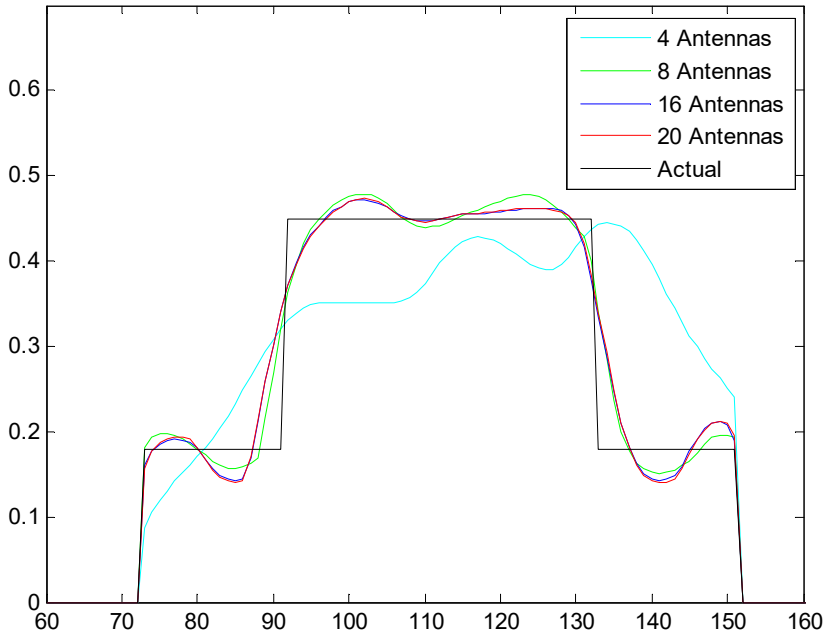

Figure 4.19: Reconstruction of conductivity (by using FBTS-TV regularization method) for different antenna arrays at cross sectional, y = 110 mm

Summary of MSE values for all antenna configurations for relative permittivity and conductivity reconstruction described in Table 4.8. From this table the MSE values of relative permittivity are declining as the number of antenna increased. Smaller MSE value means more accurate the reconstructed of the object. Increasing the number of antenna will provide more scattering data and improve the quality of reconstruction. The smallest MSE value in relative permittivity reconstruction is given by 20 antenna arrays, 1.3152 and the highest MSE value is given by 4 antenna arrays, 2.5937.

In the case of conductivity reconstruction, the value of MSE from 4 antenna to 16 antenna are declining. However, 16 and 20 antenna arrays showed the same MSE value in conductivity reconstruction. This indicated that the performance of conductivity is not improve, as the number of antenna arrays is more than 16. The smallest MSE value in

conductivity reconstruction is given by 16 and 20 antenna arrays, 0.0012 and the highest MSE value is given by 4 antenna arrays, 0.0077.

Table 4.8: Summary of MSE value for each antenna arrays after 100th iteration

Antenna Configurations	4 Arrays	8 Arrays	16 Arrays	20 Arrays
Relative Permittivity, ε_r	2.5937	1.3810	1.3221	1.3152
Conductivity, σ	0.0077	0.0013	0.0012	0.0012

MSE value for each antenna configuration for conductivity compared in a plot as shown in Figure 4.20 to further understanding of the reconstruction. From this figure, it is concluded that 4 antenna arrays could not be utilized for the reconstruction as the MSE value shows no sign of descending. The highest peak of MSE value is given by 8 antenna arrays. MSE values of 8, 16 and 20 antenna arrays configurations increase for the first five times of iterations before it declines rapidly.

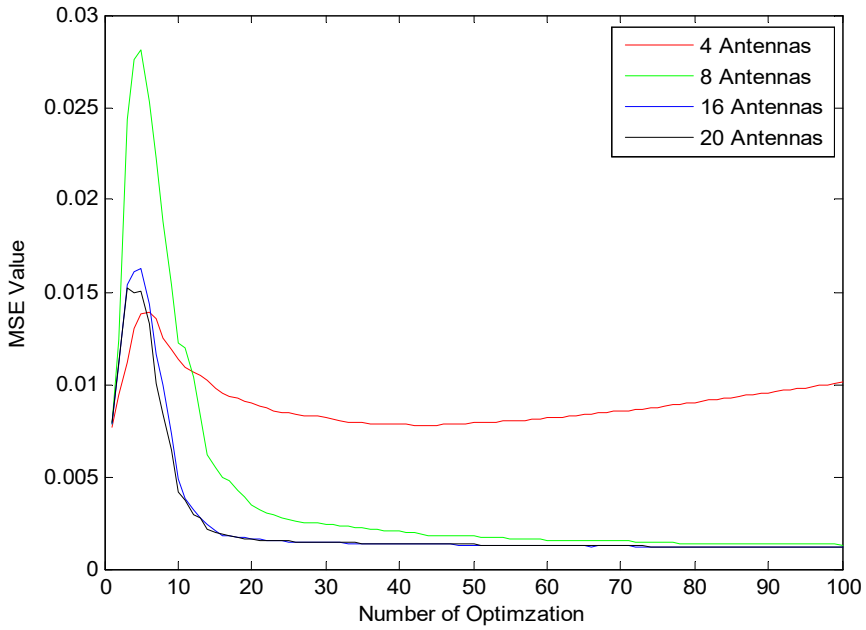

Figure 4.20: MSE calculation for reconstruction of conductivity (by using FBTS-TV regularization method) for different antenna arrays

Through observation, the value of MSE will continuously decrease as the number of antenna increased. However, in conductivity reconstruction, addition of antenna from 16 to 20 did not give a great difference or improvement in MSE value. The improvement using 20 antenna over 16 antenna for relative permittivity reconstruction is 0.5% while for reconstruction is no improvement. This behavior can be observe in Figure 4.17 and Figure 4.20 whereas the MSE value for conductivity reconstruction are becoming less differentiable toward increment of the number of antenna. Adding more antenna also increase the computational cost. Due to this reason, 16 antenna arrays is more preferable than 20 antenna arrays for both relative permittivity and conductivity reconstruction.

Figure 4.21 shows the FBTS-TV computational time when utilizing single computing with Intel® Core ™ i7-4510U CPU at 2 GHz processor and 16 GHz of RAM. The computational time increased as the number of antennas increased. The computational time utilizing 20 antenna arrays doubled than using 16 antenna arrays. Reconstructions utilizing 20 antenna arrays provide a slightly better improvement as compared to 16 antenna arrays. Nevertheless, in term of saving computational time, the 16 antenna arrays is preferred than 20 antenna arrays.

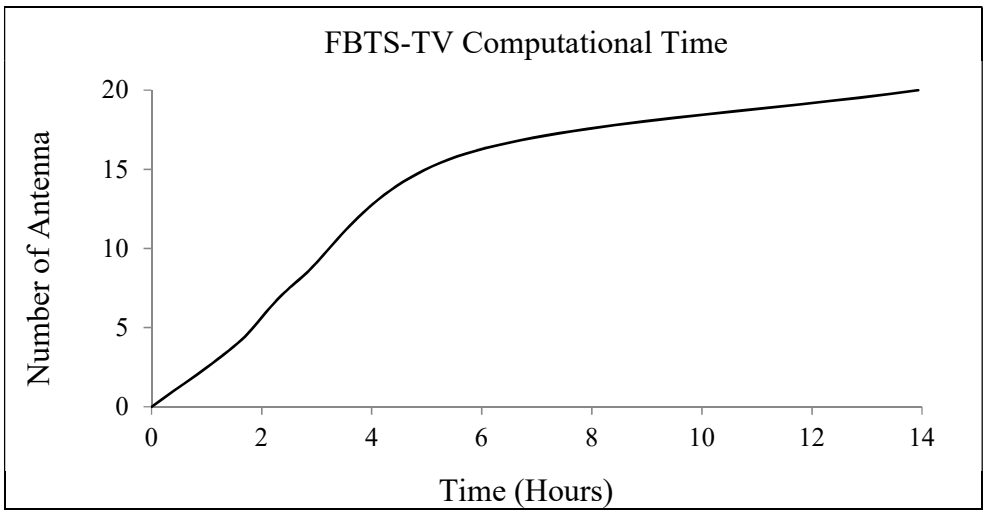

Figure 4.21: FBTS-TV Computational Time

4.4 Reconstruction of Multiple Objects in Free Space by FBTS-TV Regularization Method at Different Center Frequency

In this section, the research extended to reconstruction of multiple objects in free space utilizing FBTS-TV regularization method by varying center frequency. To investigate its effectiveness for the detection of objects with different sizes, three different center frequencies applied in the reconstruction; 1 GHz, 2 GHz and 3 GHz.

4.4.1 Reconstruction of Multiple Circular Objects in Free Space by FBTS-TV Regularization Method at Different Center Frequency

Three circular objects with different sizes added in the ROI with primary set up as mentioned in Section 4.2. The same object setting will be utilize for entire simulations with different center frequencies. The simulations carried out in free space for 100 iterations utilizing 16 antennas. Figure 4.22 shows the actual profile of relative permittivity and conductivity of the multiple objects. From the rightmost, the diameter of the object sized 6 mm, 14 mm, and 10 mm. The objects placed in series to ease observation at its cross-sectional view.

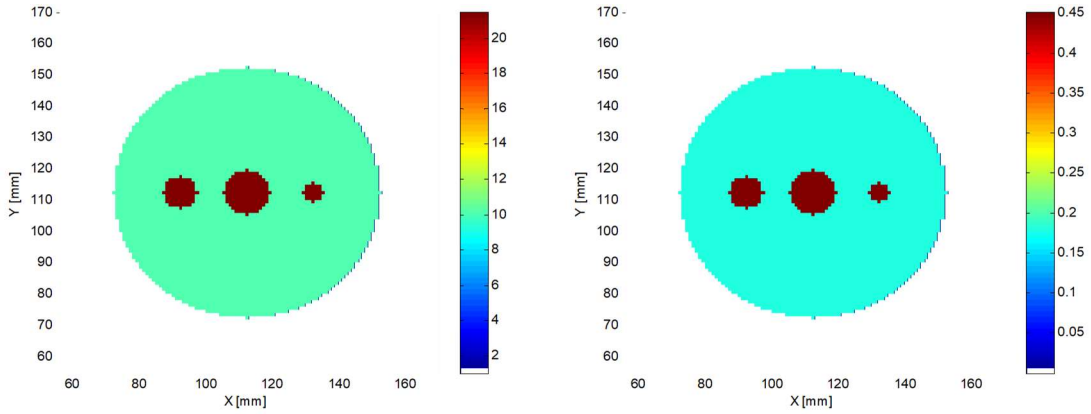

(a) (b)

Figure 4.22: Actual profile of the embedded objects (a) relative permittivity (b) conductivity

Figure 4.23 shows reconstruction of relative permittivity of multiple objects by FBTS-TV regularization method at different center frequencies of 1 GHz, 2 GHz and 3 GHz. FBTS-TV regularization method shows the ability to reconstruct and allocate multiple objects with different sizes but the performance is varied according to the center frequency.

At the center frequency of 1 GHz, the largest object, 14 mm diameter was successfully reconstructed while the other objects, 10 mm and 6 mm are unsuccessful. At 2 GHz, reconstruction for objects 14 mm and 10 mm are successful, and while for object 6 mm, the object is partially been reconstructed. At 3 GHz, reconstructions for all objects achieved, but the 6 mm object is been roughly reconstructed. Reconstruction of relative permittivity at 3 GHz has shown the best performance compared to center frequency of 1 GHz and 2 GHz because it had successfully detected and reconstructed all of the different sizes objects.

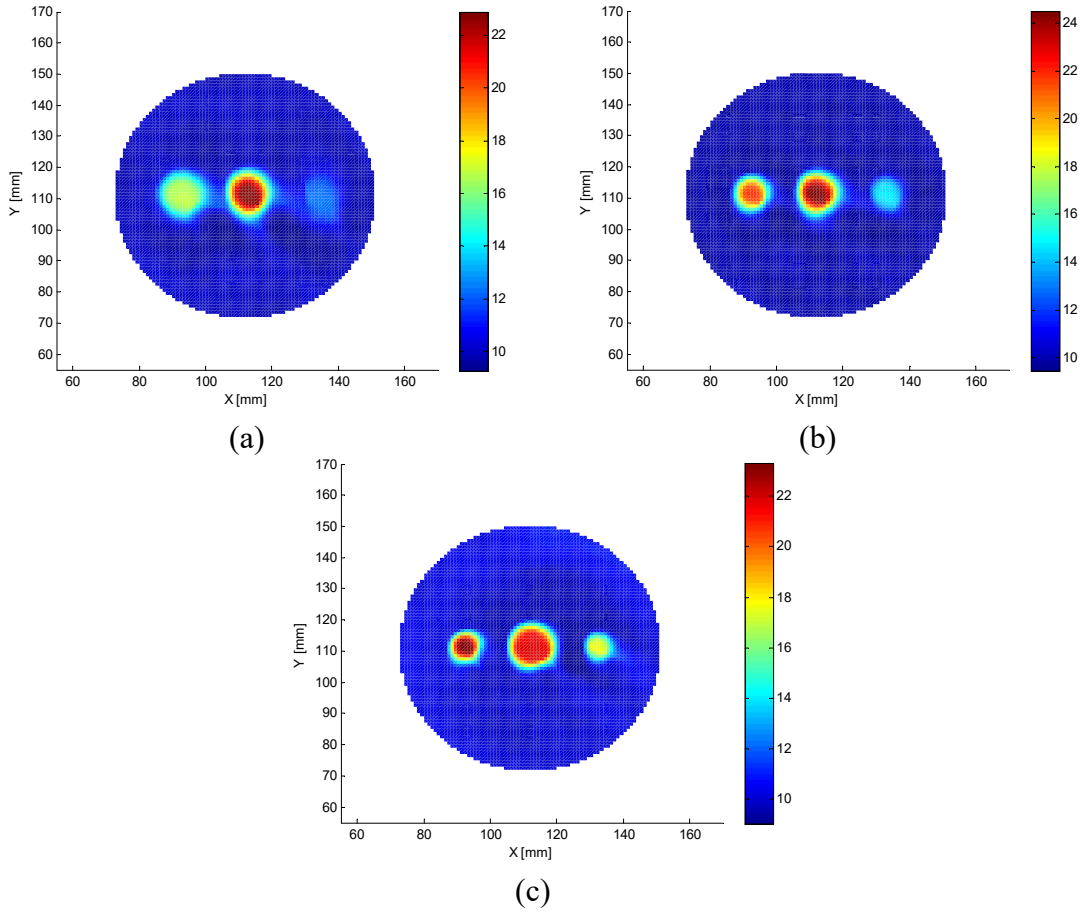

Figure 4.23: Reconstruction of relative permittivity (by using FBTS-TV regularization method) obtained at (a) 1 GHz (b) 2 GHz (c) 3 GHz center frequency

Figure 4.24 is the cross-sectional view at y = 110 mm shows the reconstruction of relative permittivity for different center frequency, 1 GHz, 2GHz and 3GHz. It is observed that reconstruction of multiple objects from 6 mm to 14 mm can be achieved by FBTS-TV regularization method at center frequency of 3 GHz. Reconstruction of relative permittivity at center frequency of 1 GHz showed the poorest quality and the objects are appeared to be widen that its actual size. The quality of reconstruction at 2 GHz is in between the performance of reconstruction at lower frequency, 1 GHz and the highest frequency, 3 GHz, indicates that the detection of small size object can be achieve at higher center frequency, while larger object can be accomplished by a lower center frequency.

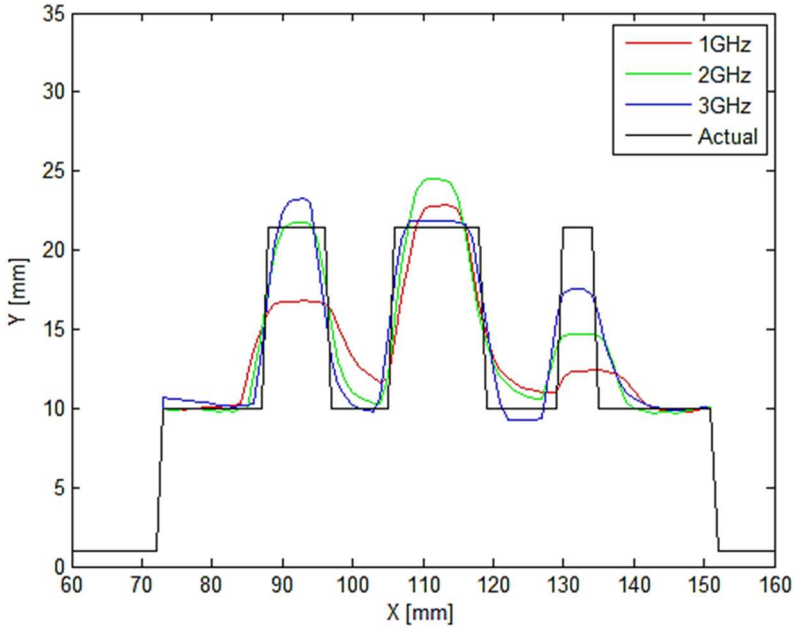

Figure 4.24: Reconstruction of relative permittivity (by using FBTS-TV regularization method) for different center frequency at cross sectional, y = 110 mm

The MSE value comparing the relative permittivity reconstruction at 1 GHz, 2 GHz, and 3 GHz as shown in Figure 4.25. The curve of the plot gradually decaying toward the number of iterations. The MSE value will decrease if the number of optimizing increased as explained in Section 4.2.2. At 100^{th} iteration, the reconstruction of relative permittivity at 1 GHz showed the highest MSE value while the lowest MSE value shown at 3 GHz.

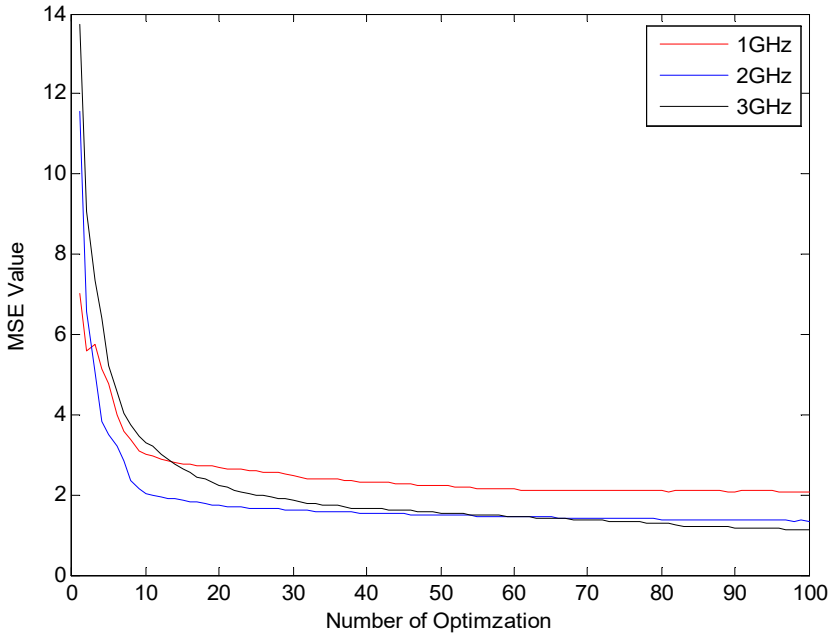

Figure 4.25: MSE calculation for reconstruction of relative permittivity (by using FBTS-TV regularization method) for different center frequency

Figure 4.26 shows reconstruction of conductivity of multiple objects by FBTS-TV regularization method at center frequency of 1 GHz, 2 GHz and 3 GHz. At center frequency of 1 GHz, the reconstruction of the 14 mm and 10 mm are achievable however for 6 mm is unsuccessful. At 2 GHz, the reconstructions for all objects achieved. However, at 3 GHz, the reconstruction of conductivity distorted, and the objects could not be distinguish. The best performance for conductivity reconstruction is at the center frequency of 2 GHz. Table 4.10 summarizes the MSE value for relative permittivity reconstruction at different center frequency.

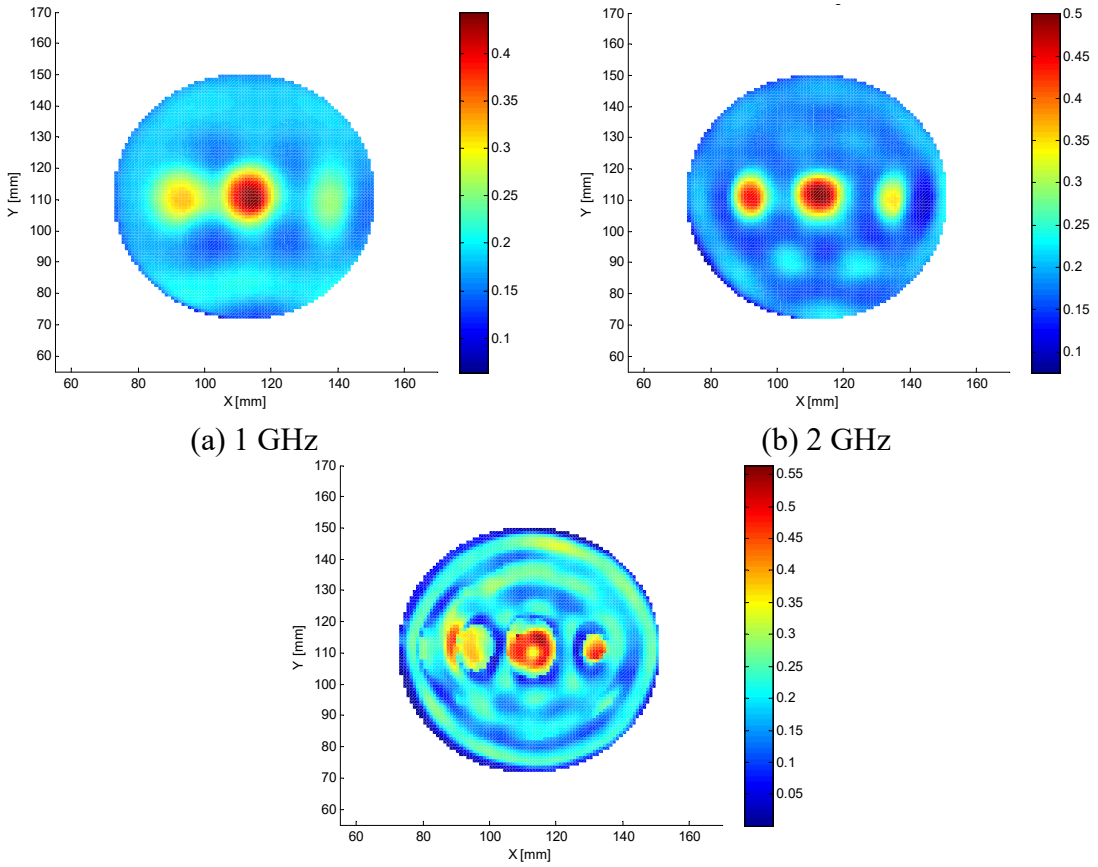

Figure 4.26: Reconstruction of conductivity (by using FBTS-TV regularization method) obtained at (a) 1 GHz (b) 2 GHz (c) 3 GHz center frequency

The reconstruction of conductivity at different center frequencies at a cross-sectional view of the reconstruction at y = 110 mm is shown in Figure 4.27. Reconstruction of the multiple object at 1 GHz appeared to be widen that its actual size, and at 3 GHz, the multiple objects is degraded severely. Center frequency of 2 GHz gave the best tradeoff of the reconstruction for both the smallest and the largest object.

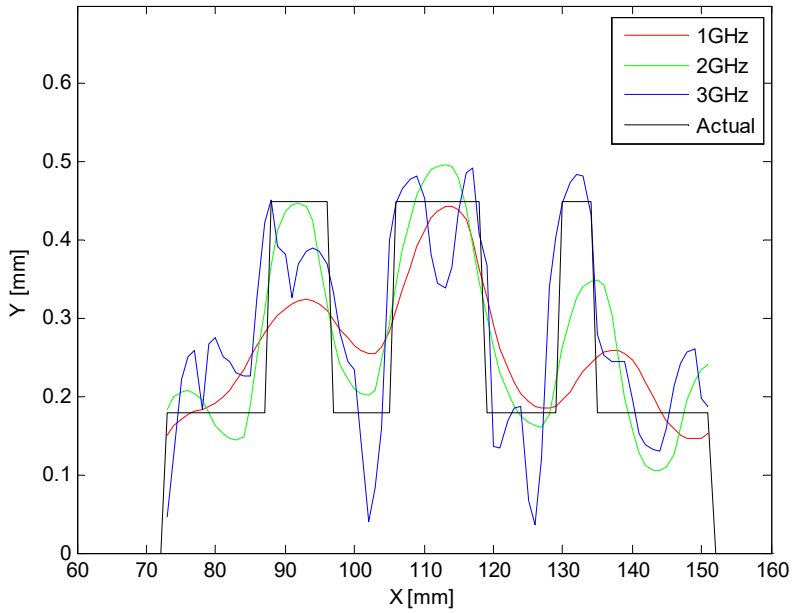

Figure 4.27: Reconstruction of conductivity (by using FBTS-TV regularization method) for different center frequency at cross sectional, y = 110 mm

Figure 4.28 shows the comparison of MSE value for each center frequency. At 100th iteration, the highest MSE value of conductivity is the reconstruction at 3 GHz while the smallest is the reconstruction at center frequency of 2 GHz.

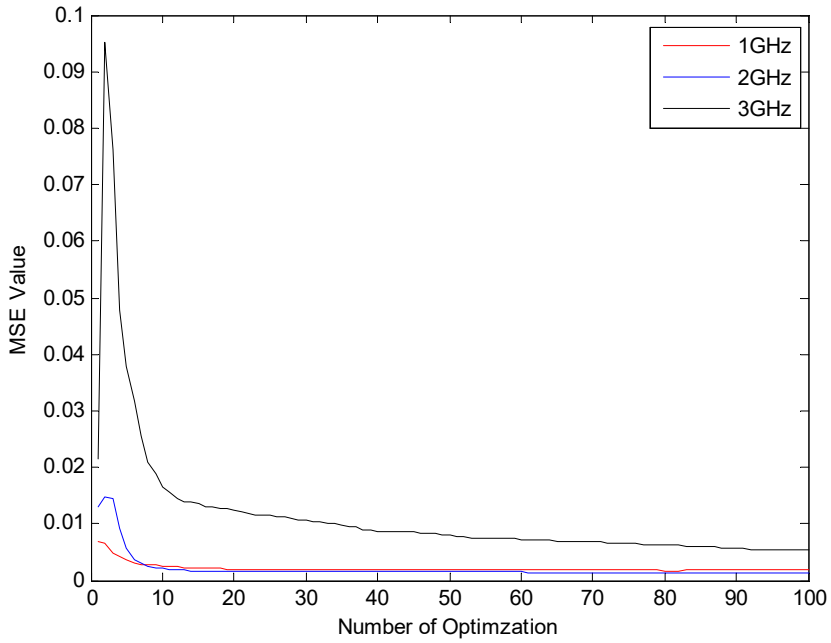

Figure 4.28: MSE calculation for reconstruction of conductivity (by using FBTS-TV regularization method) for different center frequency

Table 4.9 summarizes the MSE value for conductivity reconstruction at different center frequencies. For reconstruction of multiple objects in relative permittivity, the MSE value decreased as the central frequency increase from 1 GHz to 3 GHz, whereas the smallest value of MSE is 1.1249 (3 GHz), and the highest value is 2.0593 (1 GHz). For reconstruction of multiple objects in conductivity, the MSE value decreased as the central frequency increase from 1 GHz to 2 GHz, whereas the smallest value of MSE is 0.0014 (2 GHz), and the highest value is 0.0053 (3 GHz).

Table 4.9: The MSE value of reconstruction of relative permittivity and conductivity (by using FBTS-TV regularization method) with different center frequency

Center Frequency	1 GHz	2 GHz	3 GHz
Relative Permittivity, ε_r	2.0593	1.3487	1.1249
Conductivity, σ	0.0018	0.0014	0.0053

The best value of central frequency for FBTS-TV method is 2 GHz. The reconstruction of conductivity object is corresponding to reconstruction of relative permittivity object with the same size and location as searching for better estimation to improve the convergence of reconstruction. Consequently, to choose the best center frequency both reconstruction, relative permittivity and conductivity performance should be considered. Therefore, center frequency of 2 GHz is chosen because it give the best tradeoff in image reconstruction for both relative permittivity and conductivity.

4.4.2 Reconstruction of Multiple Square Shaped Objects in Free Space by FBTS-TV Regularization Method at Center Frequency of 2 GHz

Three objects of square shaped with different sizes added in the ROI with primary setup as mentioned in Section 3.1. The simulations carried out in free space for 100 iterations utilizing 16 antennas. The center frequency is at 2 GHz due to result of Section 4.4.1 that shown a great potential and feasibility in reconstruction by using center frequency of 2 GHz as compared to 1 GHz and 3 GHz.

Figure 4.29 shows the actual profile of relative permittivity and conductivity of the multiple objects, from the rightmost, the objects' sizes are 12 mm x 12 mm, 16 mm x 16 mm and 8 mm x 8 mm,. The objects placed in a series at its cross-sectional view, y = 110 mm. Square shape chosen to observe the efficacy of FBTS-TV regularization method to reconstruct the objects' edges.

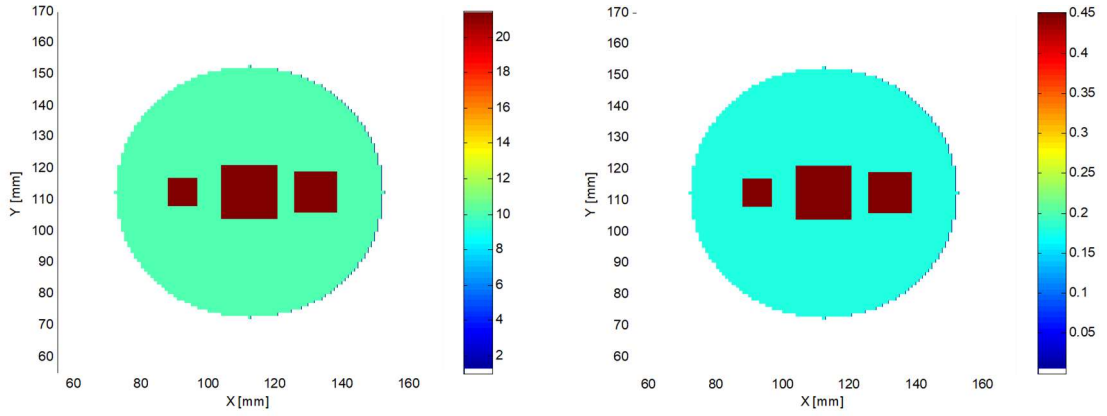

(a) (b)

Figure 4.29: Actual profile of the embedded objects (a) relative permittivity (b) conductivity

Figure 4.30 shows the reconstruction of relative permittivity and conductivity by FBTS-TV regularization method for three square objects with different sizes at center frequency of 2 GHz. It is observed that FBTS-TV regularization method capable to detect

and reconstruct multiple objects together with its location, shape and size. The reconstruction of the largest object, 16 mm x 16 mm square was rough, and for the reconstruction of 12 mm x 12 mm, and 8 mm x 8 mm, the shape of the objects is changed from square to circular. This occurs due to over-smoothing by the TV regularization method.

Though FBTS-TV regularization method able to sense and locate the multiple object, the edges of the object do not successfully reconstructed at 90 degree angle as perfectly as its original shape. This is due to the results are trapped in local minima during the optimization process. Therefore, the edges of the multiple square objects could not be successfully perfectly preserved.

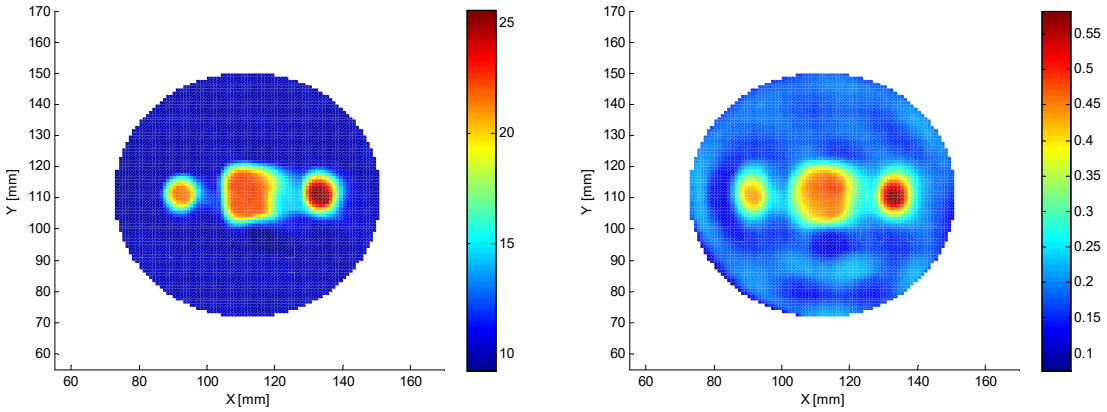

(a) (b)

Figure 4.30: Reconstruction of (a) relative permittivity (b) conductivity (by using FBTS-TV regularization method) at center frequency of 2 GHz

Figure 4.31 shows the cross-sectional view of the multiple square objects for relative permittivity and conductivity reconstruction along the x-axis at y = 110 mm. FBTS-TV regularization method shows the potential to reconstruct multiple object with different sizes. The reconstruction able to recover the location of the objects. Reconstruction of square objects was not accurate as the reconstruction of circular object. The square objects is

successfully detected and became widen, thus can successfully make separation of the three objects.

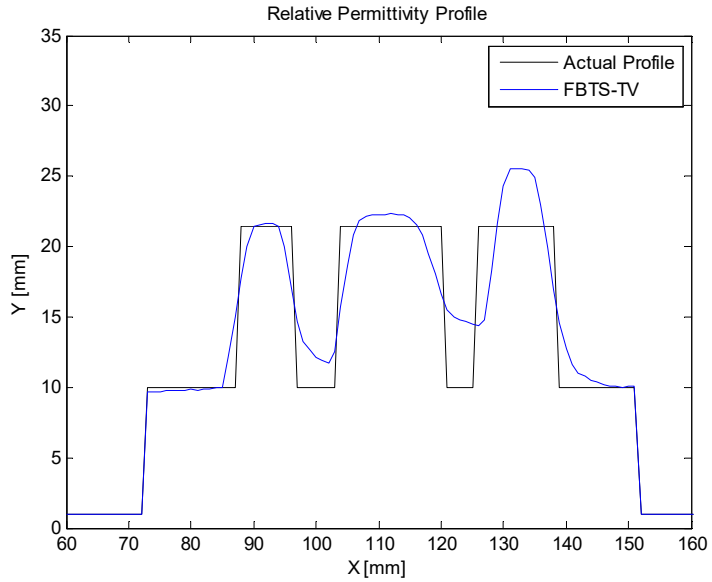

(a)

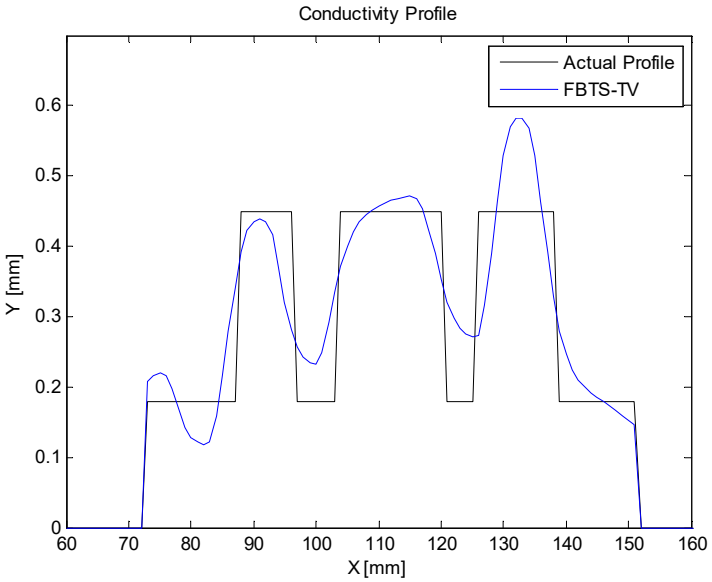

(b)

Figure 4.31: Reconstruction of (a) relative permittivity (b) conductivity (by using FBTS with and without TV regularization method) at cross sectional, y = 110 mm

The MSE value against the number of iterations for relative permittivity and conductivity as shown in Figure 4.32. The graph shows the MSE value were decreasing as

number of iteration increased. The MSE value at 100th iteration for relative permittivity is 2.3496 and for conductivity is 0.0020.

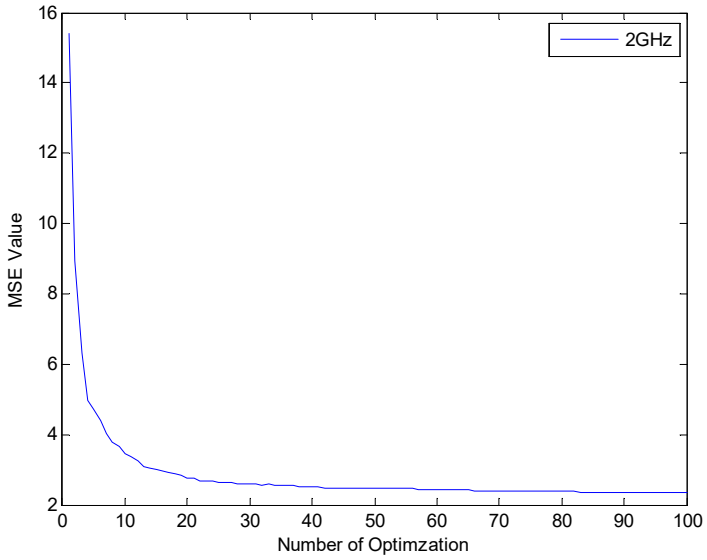

(a)

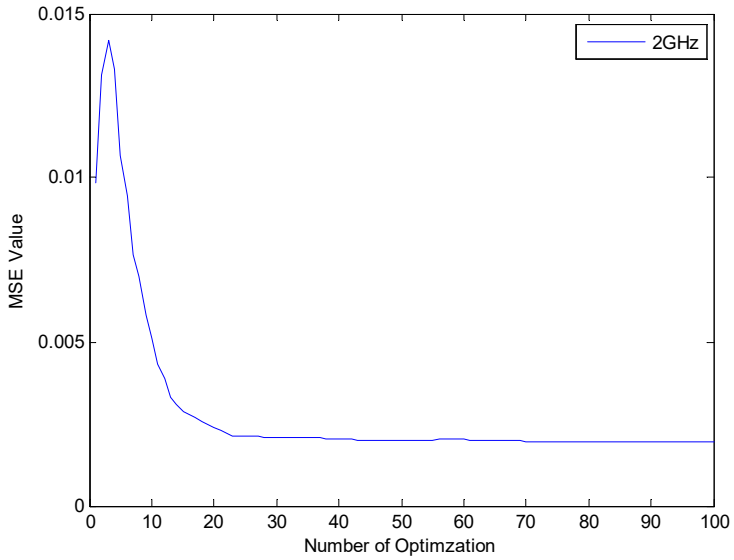

(b)

Figure 4.32: MSE calculation for reconstruction of (a) relative permittivity (b) conductivity (by using FBTS-TV regularization method)

4.5 Summary

Chapter 4 presents and discusses the findings of numerical experiments, which demonstrate the performance of the FBTS-TV regularization method. FBTS-TV has the good performance for reconstruction of a simple embedded object in dielectric properties with the knowledge of its size, shape and location. The reconstruction of relative permittivity is better quality than reconstruction of conductivity. The comparison of reconstruction of a simple object with and without regularization method shows improvement of 15% in reconstruction of relative permittivity. Optimal regularization parameter, lambda will dictate the performance of reconstruction in relative permittivity and conductivity. The optimal regularization for relative permittivity is 0.05 while conductivity is 0.0006. Increasing number of optimization and antenna will increase the quality of reconstruction but gain in more computational cost. Due to this reason, the number of optimization is 100 iterations, and number of antenna is 16 antenna. FBTS-TV shows a good potential in reconstructing multiple object. The smallest embedded object it can recover is 6 mm. It also proven that selecting the right center frequency for imaging will aid in reconstructing the size of the embedded object. The large object can be image by low center frequency, while small object can be image by high frequency.

CHAPTER 5

CONCLUSION AND RECOMMENDATIONS

5.1 Overview

This chapter assesses the conclusion of this research and its limitations. Recommendations for future improvement were proposed.

5.2 Conclusion

In this research, an image reconstruction based on a combination of an inverse scattering technique, Forward-Backward Time-Stepping (FBTS) and Total Variation (TV) regularization method in the two-dimensional transverse magnetic case has been described and presented. The effectiveness of the proposed method is confirmed by numerical simulations and presented through computational electromagnetic modeling. The FBTS-TV algorithm is developed in C++ language with a single computing.

The Forward-Backward Time-Stepping (FBTS) had proven its potential to reconstruct images that give information about the size, location, shape and the internal composition of the scatter or objects. By solving the inverse scattering problem in the time domain, FBTS will provide generous valuable quantitative information of the electromagnetic properties. Despite bearing a highly potential outcome, reconstruction of relative permittivity and conductivity by FBTS method have shown evident irregularities on the object surfaces and minor differences between the object's boundaries.

The TV regularization method is incorporated with the FBTS imaging algorithm to deal with the irregularities of the object's textures while retaining the edges of the reconstructions, henceforward increase the method accuracy and stability. TV regularization method is known to have a unique ability to enhance image reconstruction by smoothing irregular contours while preserved the boundaries. The results have demonstrated the potential of the FBTS-TV regularization method in image reconstruction of object detection in different size, shape and location.

The first objective of this research is to formulate edge preserving with Total Variation (TV) regularization method is achieved. The formulation of TV regularization method has been outline and described in Section 3.3.

The second objective is to analyze the effect of TV regularization method with different parameter setting such as regularization parameter, number of antenna, and center frequency is achieved. The results and findings are discussed and presented in Section 4.2.3, 4.3 and 4.4.

The third objective of this research is to incorporate Total Variation (TV) regularization method with the time-domain inverse scattering technique for edge-preserving image reconstruction is achieved. The integration of FBTS with TV regularization method as referred to FBTS-TV regularization has successfully achieved according to Equation 3.5. The reconstruction with TV regularization method is more accurate than without regularization method.

In Section 4.3.1, FBTS performance with and without TV regularization method has been compared and presented. Throughout the numerical simulations, adaptive of TV regularization method have shown a noticeable improvement in performance of FBTS

algorithm. It is proven that FBTS-TV regularization method capable to reconstruct images of relative permittivity and conductivity in free space medium with quantitative information about the size, location, and shape. The reconstructions were showing a good result, smoothing the uninterested textures and preserve the significant edges.

Reconstructions of relative permittivity with TV regularization method are more accurate and efficient. The efficacy of the reconstruction has been remarked with the small MSE calculation as shown in Table 4.1. After the 100^{th} iterations, the MSE value for relative permittivity is 1.3221 while for conductivity is 0.0012. Although conductivity reconstruction with FBTS-TV regularization method presented similarities with FBTS reconstruction, the differences between relative permittivity reconstruction with FBTS-TV and FBTS are pronounced. Improvement over reconstruction without applying regularization method is 15%.

In Section 4.3.2, the number of iteration was extended to 200 to investigate the efficacy of FBTS-TV regularization method with an increment of iteration. While there is a striking improvement in relative permittivity reconstruction, for the conductivity the reconstruction is stagnant. At 200^{th} iterations, the MSE values for relative permittivity is 0.9982 and for conductivity is remain as equal as at 100^{th} iteration, that is 0.0012.

In Section 4.3.3, the test shown that an appropriate value of the regularization parameter λ is highly important and affect the outcome of reconstruction. In FBTS-TV regularization method, the optimal value of the regularization parameter will give a tradeoff between the level of roughness and smoothness of the estimated image reconstruction. Reconstruction of relative permittivity and conductivity utilizing three selections of regularization parameters with the calculation of MSE is as shown in Table 4.3. In FBTS-

TV regularization method, a higher value of λ_{ε_r} will give more vibrations in relative permittivity reconstruction and a higher value of λ_{σ} will give more smoothing in conductivity reconstruction. The optimal value of relative permittivity is λ_{ε_r} = 0.05 and of conductivity is λ_{σ} = 0.0006. The optimal regularization parameter, lambda when are applied will give the smallest MSE value compared to other values.

In Section 4.4, the configuration of the antenna varies from 4, 8, 16 and 20 antenna arrays. The quality of reconstruction also depends on the number of antennas. The increment of antenna gave rise to the number of scattering calculation dataset and hence more information for reconstruction. Through the test, reconstruction with 20 antenna arrays gave the best performance, especially in relative permittivity reconstruction. Conductivity reconstruction did not show much improvement as the number of antennae increased. The MSE value for 100th iteration for relative permittivity reconstruction is 1.3152 while for conductivity is 0.0012. Although reconstruction with 20 antenna arrays bears remarkable reconstruction, it undergoes complexity and intensive computational cost compared to reconstruction with a lower number of antenna. Due to this reason, reconstruction by 16 antenna arrays configuration is preferred for FBTS-TV regularization method. Furthermore, the margin of improvement from 16 arrays to 20 arrays is rather small. Conversely, due to the very poor reconstruction of relative permittivity and conductivity, it is also concluded that reconstruction by 4 antenna arrays configuration is unusable and not recommended for FBTS-TV regularization method.

In Section 4.5.1 and Section 4.5.2, the FBTS-TV regularization method has shown its ability to sense multiple objects in the region of interest. The object with the diameter of 6 mm, 10 mm, and 14 mm was in the circular shape in Section 4.5.1 and square shape in Section 4.5.2. The reconstructed was carried out for three different center frequency, 1 GHz,

2 GHz and 3 GHz. The source for the FDTD is as explain in Section 3.3.1 is a sinusoidal Gaussian pulse is transmitted at different center frequency; 1 GHz, 2 GHz and 3 GHz into the FDTD lattice environment. The lowest center frequency (1 GHz) gave the best result for the largest object imaging (14 mm) while the highest center frequency (3 GHz) managed to resolve the smallest object imaging (6 mm). Despite the success of sensing the smallest object, the center frequency 3 GHz also produced a degraded image in term of the object's shape compared to other center frequencies. Hence, it is concluded that center frequency of 2 GHz is preferable to give an optimal tradeoff of the image's resolution and also the imaging performance of relative permittivity and conductivity in the reconstructed image. The reconstruction of the circular objects is found out to be more successful than the reconstruction of the square objects. The FBTS-TV is able to sense an object as small as 6 mm. Through this observation, it is shown that choosing the right central frequency is important to produce a better approximation of the reconstructed image and will dictate the minimum and maximum sizes of the reconstruction object.

5.3 Recommendations

TV regularization method was applied in FBTS and through the numerical simulations, the proposed method have shown a good performance of preserving image's boundaries for the reconstructed images, and hence improve the FBTS algorithm stability and accuracy.

Future studies on extending from two-dimensional to three-dimensional reconstruction cases are recommended. Due to scattering behavior, the microwaves are sensitive, and reconstruction in two-dimensional algorithm is habitually less accurate in real

world. Reconstruction in three-dimensional will increase the image's quality and accuracy together with the information about the shape, location, tissue structure identification of an unknown object through the measurement of the scattering field.

In future research work, the FBTS-TV regularization method can be utilized in medical imaging such as reconstruction of numerical model like breast composition reconstruction in [20, 26]. The reconstruction of breast composition is useful in breast cancer imaging. FBTS-TV regularization method can be applied to detect the presence of any malignancies in breast tissue due to the significant of the dielectric properties contrast. Besides medical imaging, FBTS-TV regularization method can be applied for buried object detection such as reconstruction of unknown objects in a certain search region with sufficient resolution [47].

REFERENCES

[1] Krieger, G., Hajnsek, I., Papathanassiou, K. P., Younis, M., & Moreira, A. (2010). Interferometric synthetic aperture radar missions employing formation flying. *Proceedings of the IEEE*, *98*(5), 816-843.

[2] Ouchi, K. (2013). Recent trend and advance of synthetic aperture radar with selected topics. *Remote Sensing, 5*(2), 716-807.

[3] Koo, V. C., Chan, Y. K., Vetharatnam, G., Chua, M. Y., Lim, C. H., Lim, C. S., ... & Bin Shahid, M. H. (2012). A new unmanned aerial vehicle synthetic aperture radar for environmental monitoring. *Progress in Electromagnetics Research*, *122*, 245-268.

[4] Koch, B. (2010). Status and future of laser scanning, synthetic aperture radar and hyperspectral remote sensing data for forest biomass assessment. *International Society for Photogrammetry and Remote Sensing Journal of Photogrammetry and Remote Sensing, 65*(6), 581-590.

[5] Jones, M. O., Jones, L. A., Kimball, J. S., & McDonald, K. C. (2011). Satellite passive microwave remote sensing for monitoring global land surface phenology. *Remote Sensing of Environment, 115*(4), 1102-1114.

[6] Joyce, K. E., Belliss, S. E., Samsonov, S. V., McNeill, S. J., & Glassey, P. J. (2009). A review of the status of satellite remote sensing and image processing techniques for mapping natural hazards and disasters. *Progress in Physical Geography, 33*(2), 183-207.

[7] He, Y., Pan, M., Luo, F., & Tian, G. (2011). Pulsed eddy current imaging and frequency spectrum analysis for hidden defect nondestructive testing and evaluation. *Non-Destructive Testing and Evaluation International, 44*(4), 344-352.

[8] He, Y., Luo, F., Pan, M., Weng, F., Hu, X., Gao, J., & Liu, B. (2010). Pulsed eddy current technique for defect detection in aircraft riveted structures. *Non-Destructive Testing and Evaluation International, 43*(2), 176-181.

[9] Zeng, X., Fhager, A., Linner, P., Persson, M., & Zirath, H. (2009, June). Accuracy evaluation of time domain measurement systems for microwave tomography. In *2009 IEEE Microwave Theory and Techniques Society International Microwave Symposium Digest* (pp. 1441-1444). IEEE.

[10] Rubdœk, T., Fhager, A., Jensen, P. D., Mohr, J. J., & Persson, M. (2011, August). Microwave imaging for breast cancer detection: Comparison of tomographic imaging algorithms using single-frequency and time-domain data. In *General Assembly and Scientific Symposium, 2011 XXXth URSI* (pp. 1-4). IEEE.

[11] Shea, J. D., Kosmas, P., Hagness, S. C., & Van Veen, B. D. (2010). Three-dimensional microwave imaging of realistic numerical breast phantoms via a multiple-frequency inverse scattering technique. *Medical physics, 37*(8), 4210-4226.

[12] Raghavan, S., & Ramaraj, M. (2012). An overview of microwave imaging towards for breast cancer diagnosis. *Progress in Electromagnetics Research Symposium Proceedings, Session 2A9, 338,* 627-630.

[13] Scapaticci, R., Kosmas, P., & Crocco, L. (2015). Wavelet-based regularization for robust microwave imaging in medical applications. *IEEE Transactions on Biomedical Engineering, 62*(4), 1195-1202.

[14] Grzegorczyk, T. M., Meaney, P. M., Kaufman, P. A., & Paulsen, K. D. (2012). Fast 3-D tomographic microwave imaging for breast cancer detection. *IEEE Transactions on Medical Imaging, 31*(8), 1584-1592.

[15] Winters, D. W., Shea, J. D., Kosmas, P., Van Veen, B. D., & Hagness, S. C. (2009). Three-dimensional microwave breast imaging: Dispersive dielectric properties

estimation using patient-specific basis functions. *IEEE Transactions on Medical Imaging, 28*(7), 969-981.

[16] Liu, Q. H., Zhang, Z. Q., Wang, T. T., Bryan, J. A., Ybarra, G. A., Nolte, L. W., & Joines, W. T. (2002). Active microwave imaging 2-D forward and inverse scattering methods. *IEEE Transactions on Microwave Theory and Techniques, 50*(1), 123-133.

[17] Donelli, M., Craddock, I. J., Gibbins, D., & Sarafianou, M. (2011). A three-dimensional time domain microwave imaging method for breast cancer detection based on an evolutionary algorithm. *Progress in Electromagnetics Research, 18*, 179-195.

[18] Takenaka, T., Jia, H., & Tanaka, T. (2000). Microwave imaging of electrical property distributions by a forward-backward time-stepping method. *Journal of Electromagnetic Waves and Applications, 14*(12), 1609-1626.

[19] Ping, K. A. H., Wei, N. S., Abidin, W. A. B. W. Z., bin Masri, T., bin Othman, A. K., Moriyama, T., & Takenaka, T. (2012, December). 2-D reconstruction of breast image using Forward-Backward Time-Stepping method for breast tumor detection. In *Applied Electromagnetics, 2012 IEEE Asia-Pacific Conference on* (pp. 70-73). IEEE.

[20] Johnson, J. E., Takenaka, T., Ping, K. A. H., Honda, S., & Tanaka, T. (2009). Advances in the 3-D forward–backward time-stepping inverse scattering technique for breast cancer detection. *IEEE Transactions on Biomedical Engineering*, *56*(9), 2232-2243.

[21] Moriyama, T., & Takenaka, T. (2015, November). Filtered forward-backward time-stepping method without information on incident field. In *Microwave Symposium, 2015 IEEE 15th Mediterranean* (pp. 1-4). IEEE.

[22] Kaltenbacher, B., Neubauer, A., & Scherzer, O. (2008). *Iterative regularization methods for nonlinear ill-posed problems (Vol. 6)*. Austria: Walter de Gruyter.

[23] Jha, S. K., & Yadava, R. D. S. (2011). Denoising by singular value decomposition and its application to electronic nose data processing. *IEEE Sensors Journal, 11*(1), 35-44.

[24] Demirel, H., Ozcinar, C., & Anbarjafari, G. (2010). Satellite image contrast enhancement using discrete wavelet transform and singular value decomposition. *IEEE Geoscience and remote sensing letters, 7*(2), 333-337.

[25] Rajwade, A., Rangarajan, A., & Banerjee, A. (2013). Image denoising using the higher order singular value decomposition. *IEEE Transactions on Pattern Analysis and Machine Intelligence, 35*(4), 849-862.

[26] Liu, G., & Zhang, Y. (2010, November). Three-dimensional microwave imaging for breast cancer detection based on forward-backward time-stepping and Tikhonov's regularization methods. In *Communication Technology, 2010 12th IEEE International Conference on* (pp. 845-848). IEEE.

[27] Jing, L., Liu, S., Zhihong, L., & Meng, S. (2009). An image reconstruction algorithm based on the extended Tikhonov regularization method for electrical capacitance tomography. *Measurement, 42*(3), 368-376.

[28] Rudin, L. I., Osher, S., & Fatemi, E. (1992). Nonlinear total variation based noise removal algorithms. *Physica D: nonlinear phenomena, 60*(1-4), 259-268.

[29] Hu, Y., & Jacob, M. (2011, March). Image recovery using improved total variation regularization. *Biomedical Imaging: From Nano to Macro, 2011 IEEE International Symposium on* (pp. 1154-1157). IEEE.

[30] Wohlberg, B., & Rodriguez, P. (2009, April). An ℓ 1-Total Variation algorithm for deconvolution with salt and pepper noise. In *Acoustics, Speech and Signal Processing, 2009. IEEE International Conference on* (pp. 1257-1260). IEEE.

[31] Afonso, M. V., & Sanches, J. M. R. (2015). Blind Inpainting Using and Total Variation Regularization. *IEEE Transactions on Image Processing, 24*(7), 2239-2253.

[32] Yoshikawa, A., Suzuki, S., Goto, T., Hirano, S., & Sakurai, M. (2010 September). Super resolution image reconstruction using total variation regularization and learning-based method. In IEEE *International Conference on Image Processing, 2010 17th IEEE International Conference on* (pp. 1993-1996). IEEE.

[33] Gholami, A., & Hosseini, S. M. (2013). A balanced combination of Tikhonov and total variation regularizations for reconstruction of piecewise-smooth signals. *Signal Processing, 93*(7), 1945-1960.

[34] Song, X., Xu, Y., & Dong, F. (2015). A hybrid regularization method combining Tikhonov with total variation for electrical resistance tomography. *Flow Measurement and Instrumentation, 46,* 268-275.

[35] Johnson, J. E., Takenaka, T., & Tanaka, T. (2008). Two-dimensional time-domain inverse scattering for quantitative analysis of breast composition. *IEEE Transactions on Biomedical Engineering, 55*(8), 1941-1945.

[36] Shah, P., Khankhoje, U. K., & Moghaddam, M. (2014, July). Joint L1-L2 regularization for inverse scattering. In *Antennas and Propagation Society International Symposium, 2014 IEEE* (pp. 868-869). IEEE.

[37] Mellors, R., Yang, X., White, J. A., Ramirez, A., Wagoner, J., & Camp, D. W. (2016). Advanced geophysical underground coal gasification monitoring. *Mitigation and Adaptation Strategies for Global Change, 21*(4), 487-500.

[38] Bardak, C., & Saed, M. (2013, July). Through the wall microwave imaging using Finite-Difference Time-Domain time reversal algorithm. In *Antennas and Propagation Society International Symposium, 2013 IEEE* (pp. 528-529). IEEE.

[39] Fallahpour, M., Case, J. T., Ghasr, M. T., & Zoughi, R. (2014). Piecewise and Wiener filter-based Synthetic Aperture Radar techniques for monostatic microwave imaging of layered structures. *IEEE Transactions on Antennas and Propagation, 62*(1), 282-294.

[40] Jung, S. H., Cho, Y. S., Park, R. S., Kim, J. M., Jung, H. K., & Chung, Y. S. (2017). High-resolution millimeter-wave ground-based SAR imaging via compressed sensing. *IEEE Transactions on Magnetics*, *54*(3), 1-4.

[41] Li, T., & Du, L. (2018). Target discrimination for SAR ATR based on scattering center feature and K-center one-class classification. *IEEE Sensors Journal*, *18*(6), 2453-2461.

[42] Zhurbenko, V. (2011). Challenges in the design of microwave imaging systems for breast cancer detection. *Advances in Electrical and Computer Engineering, 11*(1), 91-96.

[43] Kumar, A. T. N., Raymond, S. B., Bacskai, B. J., & Boas, D. A. (2008). Comparison of frequency-domain and time-domain fluorescence lifetime tomography. *Optics Letters, 33*(5), 470–472.

[44] Ning, K., Yufeng, H., Hongsen, W., & Guilan, L. (2017, October). The comparison of frequency domain method and time domain method in absorber reflectivity measurement. In *2017 IEEE 5th International Symposium on Electromagnetic Compatibility (EMC-Beijing)* (pp. 1-5). IEEE.

[45] Sarcevic, P., Pletl, S., & Kincses, Z. (2017, September). Comparison of time-and frequency-domain features for movement classification using data from wrist-worn

sensors. In *International Symposium on Intelligent Systems and Informatics, 2017 IEEE 15th International Symposium* (pp. 000261-000266). IEEE.

[46] Admin. (2019, May 22). Characteristics of Electromagnetic Wave - Properties, Wave Propagation. Retrieved from https://byjus.com/physics/characteristics-of-em-waves/.

[47] Sullivan, D. M. (2013). *Electromagnetic simulation using the Finite-Difference Time-Domain method*. New Jersey: John Wiley & Sons.

[48] Ping, K. A. H., Moriyama, T., Takenaka, T., & Tanaka, T. (2009, November). Two-dimensional Forward-Backward Time-Stepping method for tumor detection in dispersive breast tissues. In *Microwave Symposium, 2009 Mediterrannean* (pp. 1-4). IEEE.

[49] Takenaka, T., Jia, H., & Tanaka, T. (2000, December). An FDTD approach to the time-domain inverse scattering problem for a lossy cylindrical object. In *2000 Asia-Pacific Microwave Conference. Proceedings (Cat. No. 00TH8522)* (pp. 365-368). IEEE.

[50] Moriyama, T., Oliveri, G., Massa, A., & Takenaka, T. (2011, July). Iterative multiscaling strategy incorporated into time domain inverse scattering method for cross-borehole imaging. In *Geoscience and Remote Sensing Symposium*, *2011 IEEE International* (pp. 846-849). IEEE.

[51] Edwin, D. A., Sahrani, S., & Ping, K. H. (2017, November). Efficiency of scattering algorithm with overset grid generation for detection of buried object. In *Microwave Conference, 2017 IEEE Asia Pacific* (pp. 53-56). IEEE.

[52] Nawawi, J., Sahrani, S., Ping, K. A. H., Mat, D. A. A., & Zaidel, D. N. A. (2016, December). Iterative refinement in inverse scattering technique with median filter.

In *Asia-Pacific Conference on Applied Electromagnetics, 2016 IEEE Asia-Pacific Conference* (pp. 62-67). IEEE.

[53] Jamali, N. H., Ping, K. A. H., Sahrani, S., Mat, D. A. A., Marhaban, M. H., Saripan, M. I., ... & Takenaka, T. (2017). Image Reconstruction Based on Combination of Inverse Scattering Technique and Total Variation Regularization Method. *Indonesian Journal of Electrical Engineering and Computer Science, 5*(3), 569-576.

[54] Yong, G., Ping, K. A. H., Sahrani, S., Marhaban, M. H., Sariphn, M. I., Moriyama, T., & Takenaka, T. (2017). Profile Reconstruction Utilizing Forward-Backward Time-Stepping with the Integration of Automated Edge-Preserving Regularization Technique for Object Detection Applications. *Progress in Electromagnetics Research, 54,* 125-135.

[55] Wei, N. S., Ping, K. A. H., Yee, L. S., Abidin, W. Z., Moriyama, T., & Takenaka, T. (2015). Reconstruction of extremely dense breast composition utilizing inverse scattering technique integrated with frequency-hopping method. *Asian Research Publishing Network Journal of Engineering and Applied Sciences, 10*(18), 8479-8484.

[56] Manica, L., Oliveri, G., Takenaka, T., Hong Ping, K., Moriyama, T., & Massa, A. (2011). *Time-domain inversion with the Iterative Multi-Scaling approach with Forward-Backward Time-Stepping method*. University of Trento.

[57] Tanaka, T., Hiroshige, A., Moriyama, T., & Takenaka, T. (2016, August). Speed-up of Forward-Backward Time-Stepping method by using time-delay pulses. In *Progress in Electromagnetic Research Symposium* (pp. 3961-3961). IEEE.

[58] Qiu, D., Zhou, H., Takenaka, T., & Tanaka, T. (2006). Source-group method to speed up the reconstruction of objects from radar data by using the Forward-Backward Time-Stepping method. *Microwave and Optical Technology Letters, 48*(1), 67-71.

[59] Moriyama, T., Yamaguchi, Y., Hong Ping, K. A., Tanaka, T., & Takenaka, T. (2008). Parallel processing of Forward-Backward Time-Stepping method for time domain inverse scattering. *Electromagnetic Research Symposium Online, 4*(6), 695-700.

[60] Fhager, A., Hashemzadeh, P., & Persson, M. (2006). Reconstruction quality and spectral content of an electromagnetic time-domain inversion algorithm. *IEEE Transactions on Biomedical Engineering, 53*(8), 1594-1604.

[61] Fhager, A., & Persson, M. (2007). Using a priori data to improve the reconstruction of small objects in microwave tomography. *IEEE Transactions on Microwave Theory and Techniques, 55*(11), 2454-2462.

[62] Binajjaj, S., & Abdullah, M. Z. (2008, December). Single step microwave imaging in the time domain using FDTD based gradient minimization. In *Radio Frequency and Microwave Conference, 2008. RFM 2008. IEEE International* (pp. 55-59). IEEE.

[63] Chung, Y. S., Cheon, C., & Hahn, S. Y. (2000). Reconstruction of dielectric cylinders using FDTD and topology optimization technique. *IEEE Transactions on Magnetics, 36*(4), 956-959.

[64] Ireland, D., & Abbosh, A. (2013). Modeling human head at microwave frequencies using optimized Debye models and FDTD method. *IEEE Transactions on Antennas and Propagation, 61*(4), 2352-2355.

[65] Skubachevskii, A. A. (2016, August). Simulation of electromagnetic wave propagation in the medium using FDTD method. In *Progress in Electromagnetic Research Symposium* (pp. 338-343). IEEE.

[66] Zheng, F., Chen, Z., & Zhang, J. (1999). A finite-difference time-domain method without the Courant stability conditions. *IEEE Microwave and Guided Wave Letters, 9*(11), 441-443.

[67] Bardak, C., & Saed, M. (2013, July). Through the wall microwave imaging using FDTD time reversal algorithm. In *Antennas and Propagation Society International Symposium, 2013 IEEE* (pp. 528-529). IEEE.

[68] Azman, A., Sahrani, S., Ping, K. H., & Mat, D. A. A. (2017). A new method for solving inverse scattering problems with overset grid generation method. *Telecommunication, Computing, Electronics and Control, 15*(2), 820.

[69] Berenger, J. P. (1994). A perfectly matched layer for the absorption of electromagnetic waves. *Journal of Computational Physics, 114*(2), 185-200.

[70] Costen, F., Bérenger, J. P., & Brown, A. K. (2009). Comparison of FDTD hard source with FDTD soft source and accuracy assessment in Debye media. *IEEE Transactions on Antennas and Propagation, 57*(7), 2014-2022.

[71] Gedney, S. D. (2011). Introduction to the finite-difference time-domain (FDTD) method for electromagnetics. *Synthesis Lectures on Computational Electromagnetics, 6*(1), 1-250.

[72] Mansourabadi, M., & Pourkazemi, A. (2008). FDTD hard source and soft source reviews and modifications. *Progress in Electromagnetics Research, 3,* 143-160.

[73] Yu, X., & Sarris, C. D. (2012). A perfectly matched layer for subcell Finite-Difference Time-Domain and applications to the modeling of graphene structures. *IEEE Antennas and Wireless Propagation Letters, 11,* 1080-1083.

[74] Sung, S. Y., & Lee, Y. G. (2008). Trapping of a micro-bubble by non-paraxial Gaussian beam: computation using the Finite-Difference Time-Domain method. *Optics express, 16*(5), 3463-3473.

[75] Hadamard, J. (2003). *Lectures on Cauchy's problem in linear partial differential equations*. New York: Courier Corporation.

[76] Kabanikhin, S. I. (2008). Definitions and examples of inverse and ill-posed problems. *Journal of Inverse and Ill-Posed Problems, 16*(4), 317-357.

[77] Poggio, T., Torre, V., & Koch, C. (1987). Computational vision and regularization theory. In *Readings in Computer Vision* (pp. 638-643). Morgan Kaufmann.

[78] Poggio, T., & Koch, C. (1985). III-Posed problems early vision: from computational theory to analogue networks. *Proceedings of the Royal society of London. Series B. Biological sciences*, *226*(1244), 303-323.

[79] Torre, V., & Poggio, T. A. (1986). On edge detection. *IEEE Transactions on Pattern Analysis and Machine Intelligence, 2,* 147-163.

[80] Poggio, T., & Girosi, F. (1990). Networks for approximation and learning. *Proceedings of the IEEE, 78*(9)*,* 1481-1497.

[81] Chen, Z., & Haykin, S. (2002). On different facets of regularization theory. *Neural Computation, 14*(12), 2791-2846.

[82] Karl, W. C. (2005). Regularization in image restoration and reconstruction. In *Handbook of Image and Video Processing* (Second Edition) (pp. 183-V). United States of America: Academic Press.

[83] Hansen, P. C. (1987). The truncated singular value decomposition as a method for regularization. *Journal of Information Processing*, *27*(4), 534-553.

[84] Hansen, P. C. (1990). Truncated singular value decomposition solutions to discrete ill-posed problems with ill-determined numerical rank. *Society for Industrial and Applied Mathematics Journal on Scientific and Statistical Computing, 11*(3), 503-518.

[85] Noschese, S., & Reichel, L. (2014). A modified truncated singular value decomposition method for discrete ill-posed problems. *Numerical Linear Algebra with Applications, 21*(6), 813-822.

[86] Shea, J. D., Van Veen, B. D., & Hagness, S. C. (2012). A TSVD analysis of microwave inverse scattering for breast imaging. *IEEE Transactions on Biomedical Engineering, 59*(4), 936-945.

[87] Tikhonov, A. N., Goncharsky, A. V., Stepanov, V. V., & Yagola, A. G. (2013). *Numerical methods for the solution of ill-posed problems* (Vol. 328). Moscow: Springer Science & Business Media.

[88] Hansen, P. C. (1992). Analysis of Discrete Ill-Posed Problems by Means of the L-Curve. *Society for Industrial and Applied Mathematic Review, 34*(4), 561–580. http://doi.org/10.1137/1034115

[89] Kilmer, M. E., & O'Leary, D. P. (2001). Choosing regularization parameters in iterative methods for ill-posed problems. *Society for Industrial and Applied Mathematics Journal on matrix analysis and applications, 22*(4), 1204-1221.

[90] de Deus, H. P. A., S Jr, C. R. Á., Belo, I. M., & Beck, A. T. (2012). The Tikhonov regularization method in elastoplasticity. *Applied Mathematical Modelling, 36*(10), 4687-4707.

[91] Bouhamidi, A., Enkhbat, R., & Jbilou, K. (2014). Conditional gradient Tikhonov method for a convex optimization problem in image restoration. *Journal of Computational and Applied Mathematics, 255,* 580–592. http://doi.org/10.1016/j.cam.2013.06.011

[92] Pasadas, D. J., Ribeiro, A. L., Rocha, T., & Ramos, H. G. (2016). 2-D surface defect images applying Tikhonov regularized inversion and ECT. *Non-Destructive Testing and Evaluation International, 80,* 48–57. http://doi.org/10.1016/j.ndteint.2016.02.009

[93] Liu, D., Kamilov, U. S., & Boufounos, P. T. (2016, September). Compressive tomographic radar imaging with total variation regularization. In *2016 4th*

International Workshop on Compressed Sensing Theory and its Applications to Radar, Sonar and Remote Sensing (pp. 120-123). IEEE.

[94] Yaswanth, K., & Khankhoje, U. K. (2017, November). Two-dimensional non-linear microwave imaging with total variation regularization. In *2017 Progress in Electromagnetics Research Symposium-Fall* (pp. 1509-1513). IEEE.

[95] Getreuer, P. (2012). Rudin-Osher-Fatemi total variation denoising using split Bregman. *Image Processing On Line*, *2*, 74-95.

[96] Gunturk, B. K., & Li, X. (2012). *Image restoration: fundamentals and advances*. Florida: CRC Press.

[97] Puetter, R. C., Gosnell, T. R., & Yahil, A. (2005). Digital image reconstruction: deblurring and denoising. *Annual Review of Astronomy and Astrophysics, 43,* 139-194.

[98] Song, Y., Yang, C., Lin, Z., Li, H., Huang, Q., & Kuo, C. J. (2017). Image Inpainting using Multi-Scale Feature Image Translation. *ArXiv, abs/1711.08590*.

[99] Baig, M. H., Koltun, V., & Torresani, L. (2017, December). Learning to inpaint for image compression. In *Advances in Neural Information Processing Systems* (pp. 1246-1255).

[100] Zanetti, M., Ruggiero, V., & Miranda Jr, M. (2016). Numerical minimization of a second-order functional for image segmentation. *Communications in Nonlinear Science and Numerical Simulation, 36,* 528-548.

[101] Yong, G., Ping, K. A. H., Chie, A. S. C., Ng, S. W., & Masri, T. (2015, May). Preliminary study of Forward-Backward Time-Stepping technique with edge-preserving regularization for object detection applications. In *2015 International Conference on BioSignal Analysis, Processing and Systems (ICBAPS)* (pp. 77-81). IEEE.

[102] Elizabeth, M. A., K.A.H.,Rajaee, N.B., & Moriyama, T. (2015). Chebyshev filter applied to an inversion technique for breast tumour detection. *International Journal of Research in Engineering and Technology, 04*(06), 210-218.

APPENDIX

Journal

1. Jamali, N. H., Ping, K. A. H., Sahrani, S., Mat, D. A. A., Marhaban, M. H., Saripan, M. I., ... & Takenaka, T. (2017). Image Reconstruction Based on Combination of Inverse Scattering Technique and Total Variation Regularization Method. *Indonesian Journal of Electrical Engineering and Computer Science*, *5*(3), 569-576.

International Conference Proceeding

1. Jamali, N. H., Ping, K. A. H., Sahrani, S., Mat, D. A. A., Marhaban, M. H., Saripan, M. I., ... & Takenaka, T. Image Reconstruction Based on Combination of Inverse Scattering Technique and Total Variation Regularization Method. Proceeding of the International Conference on Electrical, Electronic, Communication and Control Engineering 2016, Universiti Teknologi Malaysia, Johor Bahru, Malaysia, December 2016.